The potential of

LOW & HIGH FIELD MRI

to diagnose pathologies
near orthopaedic
hardware

FEMKE SCHRÖDER

THE POTENTIAL OF LOW AND HIGH FIELD
MAGNETIC RESONANCE IMAGING TO DIAGNOSE
PATHOLOGIES NEAR ORTHOPAEDIC HARDWARE.

Femke Francisca Schröder

didici dixi defendi

THE POTENTIAL OF LOW AND HIGH FIELD MAGNETIC RESONANCE IMAGING TO DIAGNOSE PATHOLOGIES NEAR ORTHOPAEDIC HARDWARE.

PROEFSCHRIFT

ter verkrijging van
de graad van doctor aan de Universiteit Twente,
op gezag van de rector magnificus,
prof.dr.ir. A. Veldkamp,
volgens besluit van het College voor Promoties
in het openbaar te verdedigen
op donderdag 23 september 2021 om 16.45 uur

door

Femke Francisca Schröder

geboren op 30 december 1991
in Wierden, Nederland

Dit proefschrift is goedgekeurd door:

Promotor
prof. dr. ir. N.J.J. Verdonschot

Co-promotor
dr. M.H.A. Huis In 't Veld

Promotie commissie

Voorzitter/secretaris:
prof. dr. ir. H.F.J.M. Koopman

Promotor:
prof. dr. ir. N.J.J. Verdonschot

Co-promotor:
dr. M.H.A. Huis in't Veld

Leden:
prof. dr. ir. C.H. Slump, (Universiteit Twente)
prof. dr. ir. G.J. Verkerke, (Universiteit Twente)
prof. dr. L. Geris, (KU Leuven)
dr. J.M.H. Smolders, (Sint Maartenskliniek)
dr. A.J.H. Vochteloo, (Orthopedisch Centrum Oost Nederland)

Paranimfen:

drs. ing. A.N. Pattiasina-Hogenkamp

ir. C.E. Post

Contents

1

GENERAL INTRODUCTION AND OUTLINE OF THIS THESIS

1.1. Background

1.1.1. Diagnoses of pathologies near orthopaedic hardware

In orthopaedic practice, reconstructive surgery of the musculoskeletal (MSK) system is often required following a diagnosis of trauma, osteoarthritis or other MSK abnormality. During surgery orthopaedic hardware (e.g. prosthesis or osteosynthesis material (OSM) such as plates, suture anchors and screws) is inserted to optimise bone, joint or tendon function. The first internal screw and plate fixations were performed in the 19th century, followed in the 20th century by the first successful joint replacement procedures (1). If, after these procedures, patients have remaining or recurrent complaints, the diagnostic process to identify the cause of dissatisfaction is uncertain and often ineffective (2-4).

Traditionally, the diagnostic work-up in patients with orthopaedic hardware who experience complaints starts with the anamnesis, clinical examination and a conventional radiograph. Depending on the clinician's suspicion (e.g. ligament or tendon (re)tear, hardware migration, hardware malalignment, infection or other) additional imaging is required (5-7). Pre-operatively, magnetic resonance imaging (MRI) is often the imaging modality of choice for evaluating the bone and cartilage along with the surrounding muscles, tendons and ligaments (8) (Figure 1.1.a.). If metal implants are used, however, MRI images taken postoperatively are disturbed by susceptibility artefacts (Figure 1.1.b). Susceptibility artefacts appear when two materials with different magnetic susceptibility (such as soft tissues and a metal implant) are juxtaposed. This caused a local field distortion which results in a frequency shift and a local signal change (9). These metal-induced susceptibility artefacts result in a disturbed area
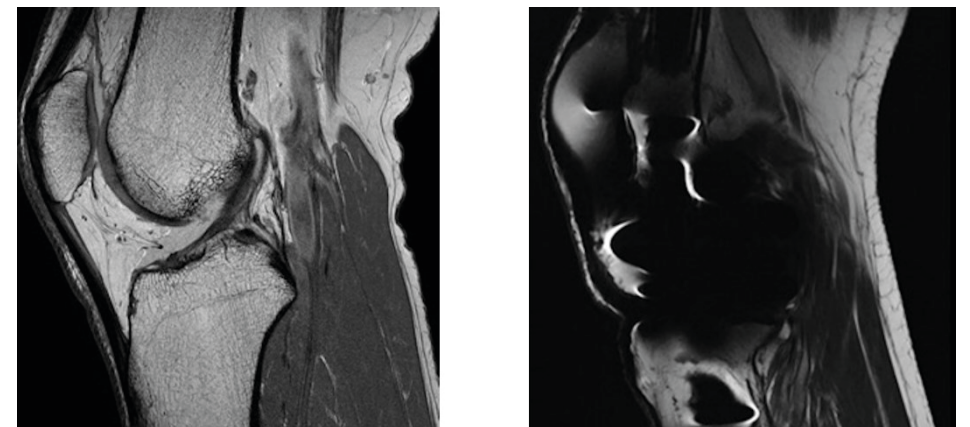

Figure 1.1. MRI of the native knee (A) and of the knee after total knee arthroplasty (B).

on the image near orthopaedic hardware (10), which reduces the image's diagnostic value (3, 11-13).

One example of a case in which post-operative imaging is important but may be hampered by metal artefacts is the evaluation of total knee arthroplasty (TKA). Although TKA is the most frequently executed total joint procedure (14), approximately 20% of TKA patients remain dissatisfied postoperatively, and, depending on the suspected cause of dissatisfaction, additional imaging is performed (15). Computed tomography (CT) is indicated when a patient is suffering from anterior knee pain and instability which is related to rotational or patellofemoral alignment problems (16). When another patellofemoral pathology is expected, then additional patellofemoral radiography, or sometimes single-photon emission computed tomography (SPECT), is performed as well (17, 18). If the tibial or femoral component of the prosthesis is suspected of loosening or migration, a CT is made (19). Furthermore, aspects such as alignment, migration and other pathologies such as infection, wear and instability could relate to the cause of complaints and be assessed on the images. Hence, clinicians may use a combination of imaging modalities, such as conventional radiographs, CT, stress radiographs, SPECT-CT or MRI (6, 20-24). Currently, there is not a single imaging modality with the ability to differentiate between the different causes of complaints.

Another, similar case is the evaluation of a painful shoulder after a rotator cuff repair with a titanium suture anchor. When a primary tear is suspected, ultrasound (US) and MRI are used to evaluate the cuff (25). After surgery, both MRI and US are disturbed by the presence of the metal anchor (26). This often results in additional invasive imaging, such as MR-arthrography (MRA) or CTA when a retear is suspected and the MRI is inconclusive (3). Taken together, evaluation of soft tissues such as muscles, ligaments and tendons after reparative surgery with orthopaedic hardware remains difficult.

Furthermore, all additional diagnostic imaging is performed in supine position. Given that, during the day, our limbs are usually in weight-bearing conditions, it seems important to image them in weight-bearing conditions. Recent research on the native knee shows that MRI scans made in upright weight-bearing position can contribute to diagnosing various patellofemoral parameters that are associated with knee pain and patellofemoral joint problems (27-31). However, it remains to be established how and whether the benefits of load-bearing examination also occur after implantation of orthopaedic hardware.

1.1.2. High- and low-field magnetic resonance imaging

Magnetic resonance imaging (MRI) – which exploits the response of atomic nuclei (typically hydrogen) to radiofrequency excitation in a strong magnetic field – is a relatively new imaging modality (32). In the 1970s the first MRI image, and consequently the first human MRI, was made (33), followed by the first commercial MRI system in 1980 (32). In the following decade, experience was gained with MRI of the musculoskeletal (MSK) system (34-36). The systems used in the early days of MRI were low-field systems (< 0.5 tesla (T)) with a permanent magnet (32). The use of superconducting magnets enabled imaging at high-field strengths, leading to the introduction of 1.5T in 1985 and of 3T in 1998 (32). Currently, 1.5T or sometimes 3T has become the standard in clinical practice (37).

However, an increased main magnetic field is correlated with increased susceptibility artefacts in the presence of orthopaedic hardware (38, 39). Traditional attempts to reduce metal artefacts primarily focus on the improvement of settings (e.g. shortening the echo time or increasing the bandwidth) and scan sequences (e.g. using metal artefact reducing sequences (MARS) such as slice encoding for Metal artefact correction (SEMAC), view angle tilting (VAT) or multi-acquisition variable-resonance image combination (MAVRIC)) (40-48). The development of MARS sequences has made MRI, which is a radiation-free technique preferable for imaging soft-tissue structures, a compelling alternative for imaging post-implantation of orthopaedic hardware (7, 49, 50).

However, reduction of the main magnetic field (low-field MRI < 0.5 T) might provide another option that would sufficiently diminish the susceptibility artefacts (38, 39). Since high-field MRI provides better spatial and contrast resolution, low-field MRI is seldom used (51). At the beginning of this century, it was stated that high-field MRI allows a more accurate interpretation of images than low-field MRI (51). However, the magnet construction, coil design, and sequence development are important for accurate imaging (52), and therefore it is currently doubtful whether high-field images are necessarily associated with greater diagnostic power (53). Recently, studies have actually shown that low-field MRI is highly suitable for parts of MSK imaging (39, 54). Moreover, it has low purchase and maintenance costs in comparison with high-field MRI, and no special room conditions are necessary for placement (55). All these factors make it interesting to evaluate the diagnostic potential of low-field MRI near orthopaedic hardware.

Additionally, some low-field MRI systems offer the possibility of scanning in upright weight-bearing conditions. As stated earlier, recent research shows that

there may be added value in scanning the native joint in weight-bearing conditions (27-31). If low-field MRI would offer the possibility of imaging near orthopaedic hardware, it might offer an opportunity to evaluate joints with orthopaedic hardware without the usual artefacts and in weight-bearing conditions.

1.2. Thesis objective

The aim of this thesis is two-fold. Firstly, it investigates the properties of MRI as a diagnostic modality for various pathologies near orthopaedic hardware. Secondly, the added value of weight-bearing low-field MRI to diagnose several pathologies post-TKA is explored.
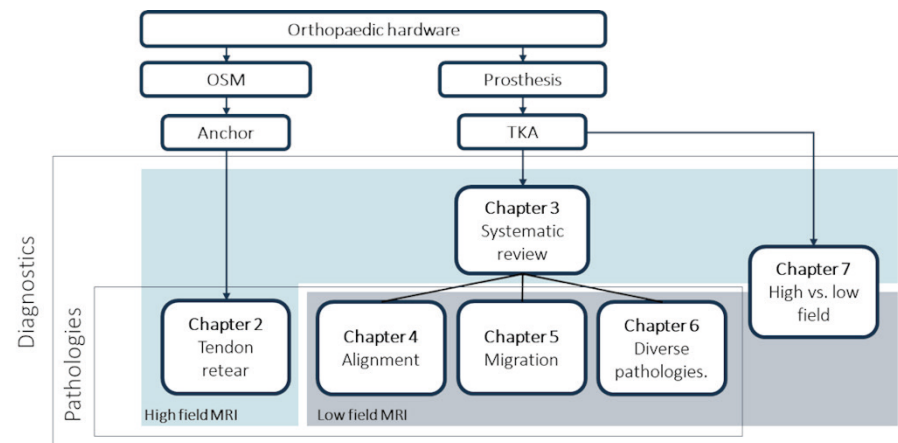
Figure 1.2. thesis outline. OSM = osteosynthesis material, TKA = total knee arthroplasty,

1.3. Thesis outline

In Figure 1.2 the thesis outline is summarized. In order to answer this two-fold research question, several aspects are investigated. To evaluate the diagnostic value of high-field MRI near orthopaedic hardware, **Chapter 2** evaluates the diagnostic value of high-field MRI to diagnose a rotator cuff tendon retear near titanium suture anchors. Subsequently, since the most often performed joint replacement procedure is the TKA, and 20% of patients remain dissatisfied after the procedure, **Chapter 3** aims to systematically review and critically appraise the literature on the diagnostic properties of high-field MRI in post-TKA patients.

The potential of using weight-bearing MRI in native joints to evaluate musculoskeletal disorders, together with the promising possibilities for

diagnosing infection, loosening and wear and malalignment with high-field MRI post-TKA, makes it interesting to evaluate the possibilities of weight-bearing low-field MRI after TKA. Firstly, **Chapter 4** aims to evaluate the effect of weight-bearing MRI on several patellofemoral alignment parameters. Moreover, the reliability of alignment measurements performed on low-field MRI is determined. Then, **Chapter 5** evaluates the potential of low-field MRI to measure prosthetic migration of the TKA. Finally, **Chapter 6** assesses the potential of low-field MRI to diagnose a range of pathologies including loosening and wear, component malalignment, instabilities and patellofemoral disorders after TKA is investigated.

Whereas Chapters 4–6 focus primarily on low-field MRI, in clinical practice high-field MRI is the standard (37). High-field MRI is suitable for imaging of almost all MSK parts of the human body and offers better overall image quality (51). Together with the recent developments in MARS sequences, it is interesting to compare the performance of low-field MRI with the more clinically available high-field MRI in imaging the knee post-TKA. Therefore, **Chapter 7** aims to compare the clinical value of low-field with high-field MRI for evaluating the knee post-TKA.

The findings and developments collected in this thesis are summarised in **Chapter 8**. Based on the discussion of these findings in relation to the research aims, conclusions are drawn and future perspectives are formulated.

2

Femke Schröder
Rianne Huis in 't Veld
Lydia den Otter
Sjoerd van Raak
Bennie ten Haken
Anne Vochteloo

METAL ARTEFACTS SEVERELY HAMPER MAGNETIC RESONANCE IMAGING

of the rotator cuff tendons
after rotator cuff
repair with titanium
suture anchors.

2.0 Abstract

Introduction: The rate of retear after rotator cuff surgery is 17%. Magnetic resonance imaging (MRI) scans are used for confirmative diagnosis of retear. However, because of the presence of titanium suture anchors, metal artefacts on the MRI are common. The present study evaluated the diagnostic value of MRI after rotator cuff tendon surgery with respect to assessing the integrity as well as the degeneration and atrophy of the rotator cuff tendons when titanium anchors are in place.

Methods: Twenty patients who underwent revision surgery of the rotator cuff as a result of a clinically suspected retear between 2013 and 2015 were included. The MRI scans of these patients were retrospectively analyzed by four specialized shoulder surgeons and compared with intra-operative findings (gold standard). Sensitivity and interobserver agreement among the surgeons in assessing retears as well as the Goutallier and Warner classification were examined.

Results: In 36% (range 15% to 50%) of the pre-operative MRI scans, the observers could not review the rotator cuff tendons. When the rotator cuff tendons were assessable, a diagnostic accuracy with a mean sensitivity of 0.84 (0.70 to 1.0) across the surgeons was found, with poor interobserver agreement (kappa = 0.12).

Conclusions: Metal artefacts prevented accurate diagnosis from MRI scans of rotator cuff retear in 36% of the patients studied.
Keywords: diagnostic value, interobserver agreement, metal artefacts, MRI, rotator cuff, shoulder

2.1 Introduction

Recurrent or persisting symptoms after rotator cuff surgery can be a result of retears or nonhealing of the repaired tendon(s). The mean rate of retear after rotator cuff surgery is reported to be 17%, with a wide range (11% to 94%).(56) A magnetic resonance imaging (MRI) scan is the preferred means of diagnosing retears and evaluating the muscle quality of the rotator cuff.(57) Many surgeons use metal (often titanium) suture anchors for cuff repair, which are placed at the rotator cuff footprint on the humeral head.(58-60) These titanium anchors cause metal artefacts on postoperative magnetic resonance images and therefore potentially limit the diagnostic value of the scan (Figure 2.1).(57-59, 61, 62)

Literature on the diagnostic accuracy of MRI after rotator cuff repair is scarce.(63-65) Only a few studies describe the diagnostic quality of these scans in detecting a retear (63, 64) or assess interobserver agreement in detecting retears.(65) None of the existing studies have investigated the degree to which metal artefacts reduce the diagnostic value of the postoperative MRI and thereby decrease interobserver agreement.

The present study aimed to determine the extent to which metal artefacts caused by titanium suture anchors inserted during the initial surgery hamper the MRI-based assessment of the rotator cuff tendon integrity and the degeneration and atrophy of the rotator muscles.
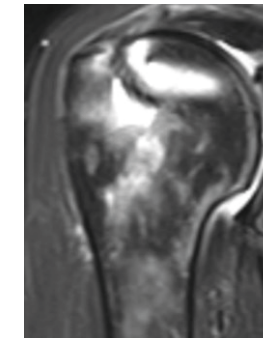
Figure 2.1. Magnetic resonance imaging of the shoulder. Coronal slice made with a T2 weighted fast spin echo sequence with clear metal artefacts after cuff repair with a titanium anchor

2.2 Materials and methods

A retrospective case cohort study was carried out. Between June 2013 and June 2015, 337 patients underwent rotator cuff surgery in our clinic. Based on

clinical symptoms, 24 (7%) of these patients underwent revision surgery of the rotator cuff. Four patients who had not undergone an MRI prior to the revision surgery were excluded. The study population consisted of 20 patients who underwent revision surgery of the rotator cuff and who had undergone a postoperative MRI scan after the primary cuff repair and before revision (Figure 2.2). The revision procedures were performed arthroscopically (45%) or using the mini-open technique (55%).

Figure 2.2. Flowchart of the study population.

The magnetic resonance images included sagittal, coronal and transversal oblique turbo spin echo sequences, T1, T2 and PD weighted (TR/TE 600-3670/12-93). Slice thicknesses ranged from 3 mm to 3.5 mm, with a gap of 1 mm. The field of view was 200 mm, with a matrix between 256 × 256 and 384 × 308. Images were acquired using a high field 1.5 Tesla (T) MRI (Magneto Avento; Siemens, Munich, Germany) with a dedicated shoulder coil.
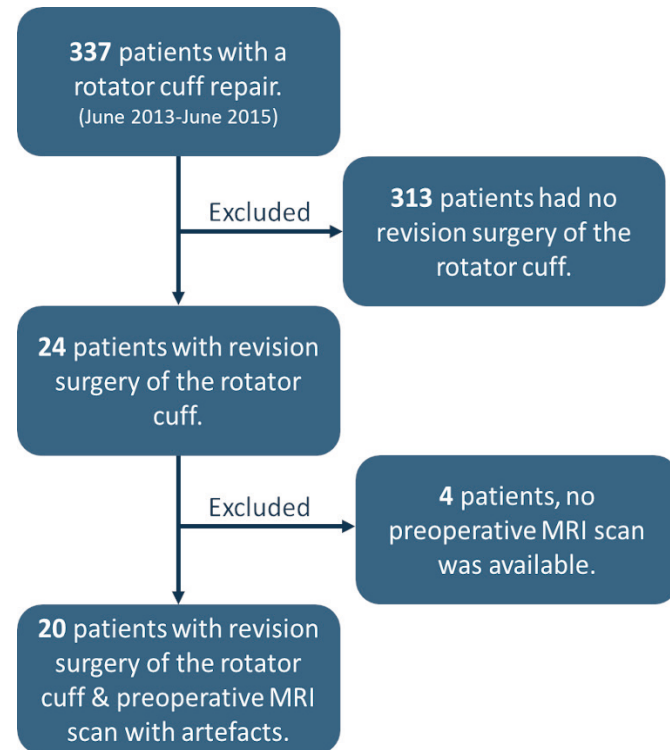
Data on patient characteristics (sex, age, side of the operation and surgical technique) were collected retrospectively. The intra-operative findings of the revision surgery were considered the gold standard; therefore, the surgical reports

were retrieved from the digital medical records (EZIS; ChipSoft, Amsterdam, The Netherlands). To assess the diagnostic utility of the MRI for evaluating the rotator cuff after surgery involving titanium suture anchors, the 20 anonymized scans were evaluated by four specialized shoulder surgeons. The surgeons were blinded for patient characteristics. The scans were scored as outlined below.

2.2.1 Scoring of scans

Retears: The rotator cuff was evaluated for the presence of retears. This was scored on a three-point grading scale, where 0 indicates 'no retear', 1 indicates 'retear' (partially or fully) and 2 indicates 'not assessable as a result of metal artefacts'.

Fatty degeneration and atrophy: Fatty degeneration and atrophy of the rotator cuff muscles using the Goutallier and Warner classification. (66, 67)The Goutallier classification quantifies the extent of fatty degeneration of the rotator cuff muscles, where 0 = normal muscle, 1 = some fatty streaks, 2 = more muscle than fat, 3 = equal amount of fat and muscle, and 4 = more fat than muscle.(66) The Warner classification is a grading scale for muscle atrophy ranging from 'no', 'mild' and 'moderate' atrophy to 'severe' atrophy.(67) The classification is based on the oblique sagittal-plane MRI, where an imaginary straight line connects the coracoid either to the scapular spine or to the tip of the scapula.

Hampering of metal artefacts: The extent to which metal artefacts reduce the visibility of the tendons and muscles of the rotator cuff was scored on a visual analogue scale (VAS) ranging from 0 = 'not assessable as a result of metal artefacts' to 10 = 'the anatomic structures were not obscured in any way by metal artefacts'.

2.2.2 Statistical analysis

Patient ages are presented as the mean (SD). Categorical data (sex, affected side/tendons) are summarized by frequency and percentage. The univariate association between continuous patient characteristic variables was assessed using a Student's independent t-test for continuous variables. Categorical variables were compared using Pearson's chi-squared test and Fisher's exact test. $p < 0.05$ was considered statistically significant.

To evaluate the interobserver agreement in identifying a rotator cuff tear, a linear weighted kappa was calculated between the four observers. The kappa statistic was categorized as indicating poor (< 0.50), good (0.51 to 0.75) or excellent (> 0.75) agreement.(68) As an indicator of the hampering of accurate assessment, the number (percentage and range) of postoperative MRI scans that the orthopaedic surgeons rated as 'not assessable as a result of metal artefacts' was

determined. These scans were excluded from the calculation of the MRI reassessments' sensitivity. The gold standard was the intra-operative findings (retear/intact).

A VAS scale was used to measure the extent to which metal artefacts reduce the visibility of the tendons and muscles. An average of the four surgeons' VAS ratings for the four tendons and muscles of the rotator cuff was calculated. For the degeneration and atrophy of the rotator cuff muscles, the intraclass correlation coefficient (ICC) for the Goutallier and Warner classification was determined. In the present study, the Goutallier and Warner classification served as the reference score for assessing interobserver reliability. Although we are aware that the tendon integrity score differs from the Goutallier and Warner classification, incorporating this scoring system provides information on the interobserver agreement of our sample of orthopaedic surgeons that is less subject to the metal artefacts' influence. As such, differences in interobserver agreement between these two scoring systems might serve as evidence of the metal artefacts' hampering effect on the MRI scan. All data were analyzed using SPSS, version 23 (IBM Corp., Armonk, NY, USA).

2.3 Results

Patient characteristics are summarized in Table 2.1. The study cohort consisted of 20 patients (65% male), with a mean (SD) age of 56 (8.8) years. The revision cuff repairs were performed either using the mini-open technique (55%) or arthroscopically (45%). There were no differences between the characteristics (sex, age, side of the operation and surgical technique) of the patients undergoing revision cuff surgery and those of the overall cuff repair group.

Intra-operatively, retears of the rotator cuff were found in 95% of cases. A combination of the supraspinatus, infraspinatus and subscapularis tendon was ruptured in 60% of the patients. There was an isolated tear of the supraspinatus tendon in 25% of the cases, infraspinatus tendon in 10% of the cases and subscapularis tendon in 5% of the cases.

As shown in Table 2.2, the shoulder surgeons judged approximately one-third (36%; range 15% to 50%) of the postoperative MRI scans of the rotator cuff to be 'not assessable' as a result of metal artefacts. The interobserver agreement for retears was poor, with a kappa of 0.12 (0.00 to 0.29). The mean sensitivity was 0.84 (0.70 to 1.00). High inconsistency in MRI assessments was found among the assessors: they were in complete agreement in only 2/20 (10%) of the MRI assessments, where one case concerned a retear and the other was judged as 'not assessable' by all four observers.

Table 2.1: Patients characteristics

	All cuff repairs (n = 337)	Re-repairs cuff (n = 20)	P-value
Factor			
Age, years, mean (SD)	59 (9.6)	56 (8.8)	0.54
Male, n(%)	179 (53.1)	13 (65.0)	0.36
Left shoulder, n(%)	124 (36.8)	7 (35.0)	0.53
Tendon(s) repaired, n(%)			
SSP	198 (58.8)	5 (25.0)	0.22
ISP	6 (1.8)	2 (10.0)	
SSC	4 (1.2)	0 (0.0)	
Combination	128 (37.9)	12 (60.0)	
Intact cuff	1 (0.3)	1(5.0)	

SD standard deviation, SSP Supraspinatus, ISP infraspinatus, SSC subscapularis.

Table 2.2: Interobserver agreement and sensitivity

Kappa	Surg. 2	Surg. 3	Surg. 4	Not assessable due to metal artefacts	Sensitivity (without missing)
Surg. 1	0.29	0.08	<0	15	75
Surg. 2		0.08	0.18	35	92
Surg. 3			0.07	45	70
Surg. 4				50	100
Mean			**0.12**	**36**	**84**

Figure 2.3 gives an overview of the extent to which metal artefacts hamper the visibility of the tendons and muscles of the rotator cuff. The supraspinatus tendon was most disturbed by the metal artefacts: it was completely unaffected by these in only 15% (3/20) of MRI assessments. Good agreement was found between

the assessors for the Goutallier and Warner classification (ICC of 0.67 and 0.73) (Table 2.3). Almost all muscles were given a VAS score of > 8, suggesting that diagnostics were not disturbed by metal artefacts.

Table 2.3: Goutallier and Warner

Goutallier	0	1	2	3	4
%	15	23	23	16	23
ICC	0.67				
Warner	None	Mild	Quite	Severe	
%	22	29	33	16	
ICC	0.73				
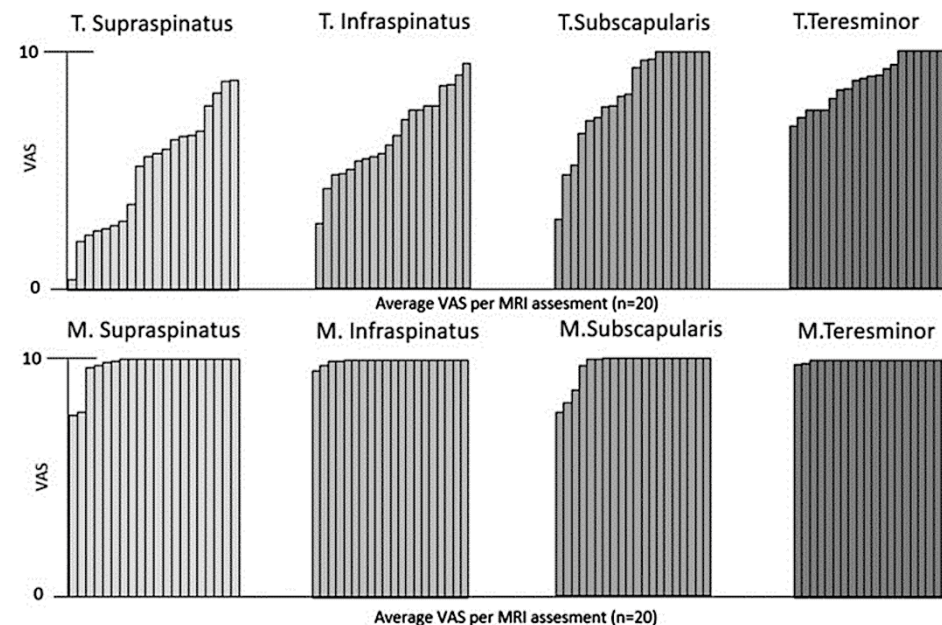
Figure 2.3. The extent metal artefacts hamper tendons and muscles to evaluate the rotator cuff. Tendons and muscles hampered as a result of metal artefacts (n = 20). Scoring was conducted on a visual analogue scale (VAS) scale by four specialized shoulder surgeons. 0 indicates that, as a result of metal artefacts, it was impossible to distinguish the anatomic structure, whereas 10 indicates that the anatomic structure was not obscured in any way by metal artefacts. MRI

2.4 Discussion

The present study has shown that metal artefacts caused by titanium suture anchors in rotator cuff surgery negatively affect MRI scans' diagnostic accuracy and interobserver agreement in detecting retears of the rotator cuff on MRI scans.

The sensitivity for diagnosing a retear after rotator cuff repair in our study was 84% (range 0.70 to 1.00). Motamedi et al.(64) report a similar sensitivity of 91%. In their study, the 37 MRI scans of the rotator cuff with titanium suture anchors were assessed by one observer (a musculoskeletal radiologist) compared to four (shoulder surgeons) in the present study.

In the present study, the interobserver agreement found for MRI scans after cuff repair was poor (kappa 0.12). Khazzam et al. (65)report a markedly higher interobserver agreement (kappa 0.60) for assessing retears on MRI scans after initial cuff repair. This can be explained by the type of suture anchors inserted during the initial surgery: Khazzam et al.(65) only included MRI scans of the rotator cuff after surgery with non-metal suture anchors, whereas, in the present study, titanium anchors were used. Because metal anchors cause larger artefacts than non-metal anchors, the presence of the former is likely to have resulted in poorer agreement in the present study. Heterogeneity of the assessors' diagnostic MRI imaging capabilities is less likely to have negatively affected agreement because all assessors in the present study were highly specialized, high-volume shoulder surgeons with a substantial amount of work experience.

To control for differences in assessors' capabilities independently of the disturbance of metal artefacts, the assessors' agreement on muscles that were not hampered by metal artefacts was assessed using the Goutallier and Warner classification. Results showed a good ICC (ICC of 0.67 and 0.73) amongst the observers with regard to fatty degeneration and muscle atrophy. Given this high agreement on the Goutallier and Warner classification, the low interobserver agreement found is more likely to be a result of the metal artefacts' hampering effect than to differences in the observers' capabilities.

2.4.1 Alternative anchor material

With the emergence of anchors made of bio-compatible materials, fewer titanium anchors might be used in the near future. Bio-anchors do not induce metal artefacts and appear to be as effective in secure tendon-to-bone repair as metal suture anchors.(69) Unfortunately, the use of some biodegradable anchors is also associated with complications, including foreign body reactions, cyst formation, fluid collection, osteolysis and chondral damage.(70) A promising

alternative is polyetheretherketone anchors, which are nonbiodegradable. These anchors act like metal implants without inducing the metal artefact and also do not cause the aforementioned complications. Future use of this anchor material will resolve the metal artefact problem. However, because titanium anchors are still often used during rotator cuff repairs, hampered medical decision-making as a result of metal artefacts on postoperative MRIs will remain a problem in the forthcoming time.

2.4.2 Improvement of or alternative imaging methods

If patients remain symptomatic (i.e. experiencing pain or malfunction after rotator cuff repair), imaging of the rotator cuff is important in order to determine possible treatment options. Limited imaging quality can result in invalid medical decision-making with consequences for the patient, such as unnecessary repeat surgery or conservative treatment. Given that metal artefacts hamper the adequate diagnosis of retears with conventional MRI scanning, the challenge is to find ways of overcoming this negative effect on MRI images. Technological improvement of scan sequences is one possibility to reduce metal artefacts. Ai et al.(71) show that metal artefact reduction sequences (MARS) yield up to 59% reduction compared to traditional fast spin echo sequences. However, at the time of this study, these MARS sequences were not available at our clinic and were also not widespread globally.

Ultrasound (US) is the preferred method for imaging rotator cuff tears. For detecting an initial rotator cuff tear, US and MRI are comparable in both sensitivity and specificity.(72) When assessing rotor cuff retears, US is less affected by metal artefacts than MRI or computerized tomography (CT). However, the postoperative rotator cuff can show altered morphology for years following the repair, which can manifest as loss of fibular architecture and abnormal echogenicity on US and make it difficult to diagnose a retear.(73) Furthermore, the reliability of US is highly dependent on the operator's experience, and a US is not easily re-assessable compared to CT or MRI images. Finally, the amount of muscle atrophy is yet not quantified with US, in contrast to CT and MRI.

Other imaging modalities such as MR arthrography (MRA) or CT arthrography (CTA) are expected to improve diagnostics when metal anchors are present. Compared to conventional MRI and CT scans, MRA and CTA have a comparable or slightly improved sensitivity and specificity for detecting initial rotator cuff tears in non-operated shoulders. However, these are invasive procedures.(74, 75) Furthermore, their accuracy decreases postoperatively. Scar tissue can act as a barrier that prevents contrast entering the subacromial space, therefore mimicking an intact cuff in case of a rupture. Furthermore, contrast in

the subacromial space on the postoperative MRA or CTA does not always indicate a (clinically relevant) retear.(59, 76)

Finally, it may be worth investigating the possibilities of reducing the main magnetic field. High field MRI (> 1 T) is currently used as a standard for musculoskeletal imaging.(77) Low field MRI (< 0.5 T), although rarely used at present, is hypothesized to be highly suitable for musculoskeletal imaging. (78, 79) Interestingly, Radzi et al.(80) found that decreasing the main magnetic field (from 3 T to 1.5 T) resulted in a 16% reduction of metal artefacts. It is expected that low field MRI (0.25 T) would further decrease metal artefacts. A comparison between metal artefact hampering in conventional and low field MRI scanning of the rotator cuff after repair with metal suture anchors should therefore be undertaken in the near future.

2.4.3 Strengths and limitations

The present study is among the first to evaluate the extent to which metal artefacts hamper MRI imaging of the rotator cuff after a repair using metal suture anchors and the clinical implications of this hampering. A unique aspect of the present study is that, in addition to the classical assessment of diagnostic accuracy, the extent to which metal artefacts hamper the quality of medical decision-making based on MRI scans was evaluated. Because no standardized method was available to measure the extent to which metal artefacts hamper MRI, we developed a measurement based on proven classifications such as Warner's and Goutallier's. Future research could benefit from further validation of this method.

An important limitation of the present study was that only one patient in our dataset underwent revision surgery without having a retear (i.e. there was only one true negative). With only one 'negative' cuff tear, calculating specificity accurately was impossible because more true negatives are required to do so. However, because clinical practice attempts to avoid true negatives, the prevalence of true negatives for study purposes will remain low.

Second, the shoulder surgeons knew that the patients in the present study had undergone revision surgery because of suspected retears after rotator cuff surgery, which might have influenced the sensitivity that was measured.

The present study has shown that metal artefacts hamper the diagnostic accuracy of postoperative MRIs and that these artefacts also cause poor interobserver agreement. Potential methods to overcome this hampering are the use of MR/CT arthrography or low field MRI for imaging of the rotator cuff tendons in patients with recurrent or persisting symptoms after rotator cuff surgery with metal suture anchors.

3

Magnetic resonance imaging

AS DIAGNOSTIC MODALITY FOR ANALYSING THE PROBLEMATIC KNEE ARTHROPLASTY:

a systematic review.

Femke Schröder
Corine Post
Frank-Christiaan Wagenaar
Nico Verdonschot
Rianne Huis in't Veld

3.0 Abstract

Introduction: Various diagnostic modalities are available to assess the problematic knee arthroplasty. Visualization of soft tissue structures in relation to the arthroplasty and bone remains difficult. Recent developments in MRI sequences could make MRI a viable addition to the diagnostic arsenal. Therefore, the purpose of this study is to review the diagnostic properties of MRI, to identify certain causes of complaints that may be directly related to implant failure of total (TKA) or unicompartmental knee arthroplasty (UKA); infection, loosening and wear, instability, malalignment, arthrofibrosis, or patellofemoral problems.

Methods: Twenty-three studies were included;16 TKA, 4 UKA, and 3 cadaveric studies. Causes of knee arthroplasty complaints analyzed were; infection (3), loosening and wear (11), malalignment (5) and instability (4). PubMed, SCOPUS and EMBASE were searched. Risk of bias was assessed using the COnsensus-based Standards for the selection of health Measurement Instruments (COSMIN) and the QUality Assessment of Diagnostic Accuracy Studies-2 (QUADAS-2) .

Results: Fifteen studies assessed the reproducibility of analyzing infection, loosening and wear, and malalignment. Fourteen of 15 studies were deemed as adequate to good quality. Results showed a moderate to excellent agreement (ICC/K 0.55–0.97). Fourteen studies addressed the accuracy. For infection, and loosening and wear the sensitivity and specificity estimates varied between 0.85-0.97 and 0.70-1.00 respectively. The accuracy for malalignment was excellent (r≥0.81). For these studies QUADAS-2 analysis suggested few risks of bias. A meta-analysis was not possible due to the heterogeneity of the data.

Conclusion: This study supports that MRI can be used with overall reproducible and accurate results for diagnosing infection, loosening and wear, and malalignment after knee arthroplasty. Nonetheless, studies regarding the diagnosis of instability, arthrofibrosis or patellofemoral complaints using MRI are limited and inconclusive.

3.1 Introduction

Unicompartmental knee arthroplasty (UKA) and total knee arthroplasty (TKA) are widely accepted treatment options for end-stage osteoarthritis (81). The number of UKA and TKA procedures performed is growing annually due to the aging of the population; as well as the increased incidence of osteoarthritis in younger patients, amongst whom there is increased demand for and acceptance of these procedures (82). Consequently, the number of revision surgeries is also increasing and likely will increase further in the coming decades (83). An important aspect that influences the success rate of revision surgery is identification of the underlying cause(s) of the failure of the problematic knee arthroplasty (83). The most common causes of a problematic knee arthroplasty for which revision surgery may offer benefits are infection, loosening and wear, instability, malalignment and, less frequently, arthrofibrosis (6, 7). In addition to these causes, there are various problems that revision surgery cannot solve, such as peri-articular causes (e.g. tendinopathies or local and/or diffuse neuropathic pain) or extra-articular causes (e.g. hip osteoarthritis) (84).

To differentiate amongst the potential causative factor(s), various imaging techniques are available after the basic work-up, which involves extensive history, physical examination, radiographs (including long leg view) and lab tests. The imaging techniques utilized include combinations of radiographic views, stress radiographs, computed tomography (CT), magnetic resonance imaging (MRI), planar bone scintigraphy with or without single photon emission computed tomography (SPECT), and fluorodeoxyglucose (FDG)-positron emission tomography (PET)/CT (5, 85). It would be valuable if one imaging technique could offer the same diagnostic power as two or more other imaging techniques for identifying the cause(s) of failure.

In recent decades, MRI has become the standard for the evaluation of joints and soft tissues in the native knee (8). However, MRI is considered to have limited diagnostic properties for TKA patients, due to artefacts caused by the prosthetic implant (86, 87). Interestingly, a literature study conducted by Fritz et al. (7) discussed strategies for MRI around knee arthroplasty implants and demonstrated the imaging appearances of common causes of complaints. That study suggested that MRI with optimized sequences and advanced metal artefact reduction techniques could be applied to evaluate the underlying causes of failed knee arthroplasty. However, the additional diagnostic properties of MRI for diagnosing the knee after arthroplasty were not assessed.

Therefore, the aim of the current study was to critically appraise, summarize, and compare the literature on the diagnostic properties of MRI, to

identify the causes of complaints that are directly related to implant failure. Hence, this systematic review focused on MRI studies that examined implant-related issues of infection, loosening and wear, instability, malalignment, arthrofibrosis and patellofemoral complaints after TKA or UKA.

3.2 Materials and methods

This systematic review was performed in accordance with the Preferred Reporting Items for Systematic review and Meta-Analyses (PRISMA) (88).

3.2.1 Eligibility Criteria

Studies were included that reported on:

- The ability of MRI to diagnose (one of the) probable causes of complaints (for definitions, see Table 3.1) after primary TKA or UKA.
- Patients or cadaveric studies.
- Studies were excluded if they were:
- Written in a language other than English.
- Letters to the editor.
- Review articles.

Table 3.1: Probable causes of complaints after knee arthroplasty and their MRI manifestations

Infection	Loosening and wear	Instability	Malalignment	Arthrofibrosis	Patellofemoral
Lamellated hyperintense synovitis, extracapsular soft-tissue oedema, extracapsular collections and reactive lymphadenopathy (23).	Fibrous membrane formation between the bone and the implant or cement (7). Cytokine-mediated inflammatory reaction due to polyethylene wear (89).	Tendon abnormalities, tendinosis or tendon rupture of the quadriceps or patellar tendon. Deficiency of the posteromedial or lateral stabilizers (7).	Increased internal-external or varus-valgus rotation of the femoral or tibial component (90, 91).	Fibrous tissue i.e. thickening along the synovial lining (7, 92).	Patellar problems, as patellar clunk, patella baja, patella alta (7).

3.2.2 Search Strategy

The search included studies published between January 1st 2003 and February 28th 2019. The reference lists were imported to Endnote 8.1 (Thompson Reuters, CA) and duplicate articles were removed. A literature search was conducted using the following electronic databases: PubMed, SCOPUS and EMBASE. The search terms used were 'knee prosthesis' and all synonyms thereof and 'MRI' and all synonyms thereof. The detailed search strategies for each database are given in Table 3.2.

Table 3.2: Search strategy

Database	Search strategy	Results
PubMed	1. ((((MRI[Title/Abstract]) OR MR imaging[Title/Abstract]) OR magnetic resonance imaging[Title/Abstract])) 2. AND ((((((((knee prosthesis[Title/Abstract]) OR knee replacement[Title/Abstract]) OR knee arthroplasty[Title/Abstract]) OR tibial component[Title/Abstract]) OR femur component[Title/Abstract]) OR TKA[Title/Abstract]) OR TKR[Title/Abstract]) OR UKA[Title/Abstract]) 3. AND ("2003/01/01"[Date - Publication] : "3000"[Date - Publication]))	490
SCOPUS	1. (TITLE-ABS-KEY (((mri) OR mr AND imaging) OR magnetic AND resonance AND imaging) 2. AND TITLE-ABS-KEY ((((((((knee AND prosthesis) OR knee AND replacement) OR knee AND arthroplasty) OR tibial AND component) OR femur AND component) OR tka) OR tkr) OR uka)) 3. AND PUBYEAR > 2002	681
EMBASE	1. ('(((((((knee prosthesis)':ab OR 'knee replacement)':ab, OR 'knee arthroplasty)':ab OR 'tibial component)':ab OR 'femur component)':ab OR 'tka)':abOR 'tkr)':ab OR 'uka':ab) 2. AND ('((mri)':ab OR 'mr imaging)':ab OR 'magnetic resonance imaging':ab) 3. AND [2003-2019]/py	840

3.2.3 Study Selection & Data Collection

Two independent observers (C.P. and F.S. , respectively 2 and 4 years of research experience) selected eligible studies and extracted the data. First, titles and abstracts were screened. Studies that were identified as potentially relevant by at least one reader were retrieved and the full texts were evaluated. Any disagreement between the two readers was resolved through discussion. In case of remaining disagreement, the dispute was resolved with the help of a third reviewer (R.H. with 18 years of research experience). Additionally, the references of all considered articles were hand-searched to identify any relevant studies that may have been overlooked by the search strategy.

Study characteristics were extracted as: year of publication, study design, causes of complaints, number of subjects, number of controls, mean age, type of prosthesis (UKA or TKA), and MRI settings. It was noted when the prosthesis was made out of zirconium, because zirconium prostheses are known for their reduced metal artefacts, which may influence study results (93).
The included studies were divided into three groups —TKA, UKA and cadaveric studies— and sorted by their reported causes of complaints.

3.2.4 Critical Appraisal & Analysis

The included studies assessed the diagnostic properties of MRI to identify probable causes of complaints. Some studies achieved this by evaluating the reproducibility of measurements, and others assessed diagnostic accuracy. To evaluate these studies, two different critical appraisal tools were chosen.

The methodological quality of the reproducibility studies was assessed by evaluating reliability with the reliability box of the Consensus-based Standards for the selection of health status Measurement Instruments (COSMIN) (94). Reliability is a measure of the consistency between or within observers. The questions in the reliability box can be answered with 'very good', 'adequate', 'doubtful' or 'inadequate'. The total score for reliability is based on the lowest rating given for any of the questions (94).

Moreover, outcome measures for the reproducibility of the MRI measurements, such as the intraclass correlation coefficient (ICC) or kappa, were collected from these studies. The ICC values were defined as follows: ICC values lower than 0.5 indicate poor reliability, values between 0.5–0.75 moderate reliability, values between 0.75–0.9 good reliability, and values greater than 0.90 excellent reliability (95). Kappa values were defined as follows: 0.01–0.20 no agreement, 0.21–0.40 fair agreement, 0.41–0.60 moderate agreement, 0.61–0.80 good agreement, and 0.81–1.00 almost excellent agreement (96).

Diagnostic accuracy was assessed in terms of validity using the Quality Assessment of Diagnostic Accuracy Studies 2 (QUADAS-2) tool (97). Validity indicates that MRI is able to accurately identify complaints compared to the reference standard (criterion validity) or compared to another standard (construct validity). The QUADAS questions can be answered with 'low', 'high', or 'unclear'. Included studies with outcome measures reporting the diagnostic accuracy for one or more of the possible causes of complaints expressed in sensitivity, specificity, p-values, and correlations were collected. p-values < 0.05 were considered to be significant. Studies that assessed both reproducibility and accuracy were evaluated using both critical appraisal tools.
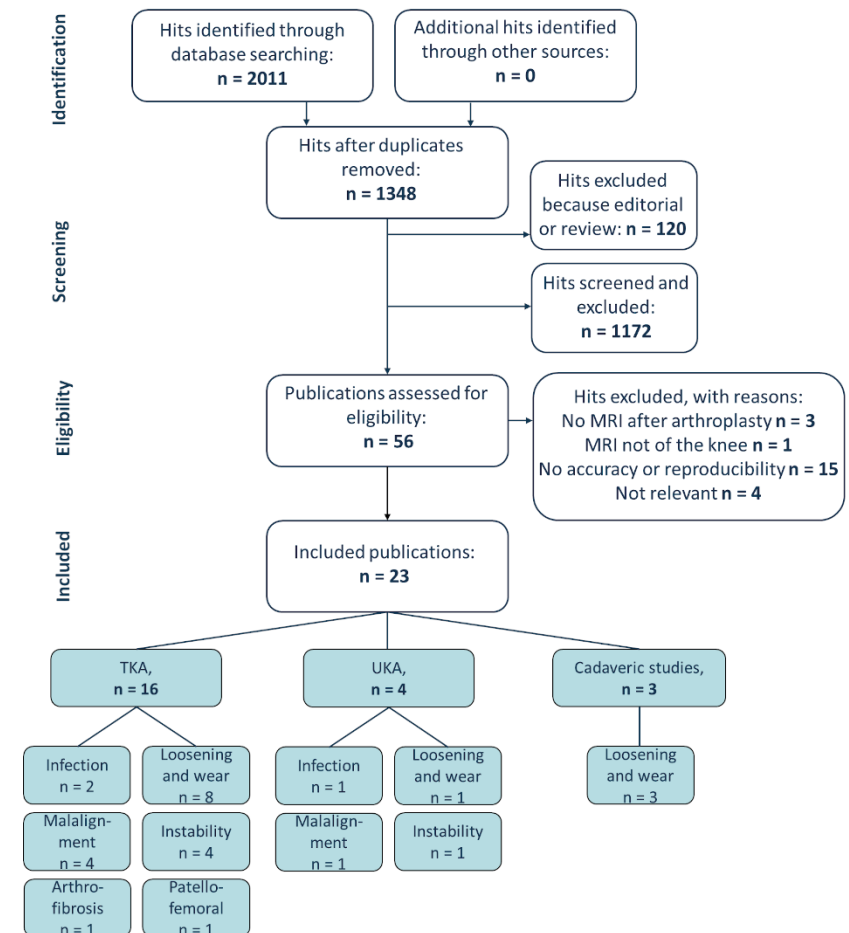

Figure 3.1. Flowchart of the study selection.

3.3 Results

3.3.1 Study Selection

The search initially returned 2,011 hits (Figure 3.1 shows the flowchart of the study selection process). After the removal of duplicates, 1,348 citations remained. After titles and abstracts were screened, a total of 56 full-text articles remained. Of these, a total of 23 publications met the eligibility criteria. Reference checking did not yield additional relevant publications.

3.3.2 Study Characteristics

Of the 23 included studies described in Table 3.3, 16 publications concerning diagnostic MRI after TKA were retrieved, with a total number of 650 patients. Four publications (58 patients) were found concerning diagnostic MRI after UKA. Three remaining publications concerned cadaveric studies (18 human or porcine cadaveric specimens) and tried to determine the added value of MRI in diagnosing the underlying causes of loosening after arthroplasty.

3.3.3 Reproducibility

The reproducibility of MRI for diagnosing one or more of the probable causes of complaints was examined in 11 out of the 16 TKA studies, 3 out of the 4 UKA studies, and 1 out of the 3 cadaveric studies (Table 3.4). All studies except one (98) scored adequate to very good for reliability, by the COSMIN. However, despite their adequate to very good methodological quality, these studies typically failed to indicate the time between repeated measurements (87, 90, 99-107).

Periprosthetic joint infections were associated with signs of lamellated hyperintense synovitis on MRI. Almost excellent reproducibility results were found regarding lamellated hyperintense synovitis, with an inter-rater reproducibility of (K = 0.82 and K = 0.82) and intra-rater reproducibility of (K = 0.83 and K = 0.89) (23, 99). Loosening was evaluated in two studies by assessing the implant–bone interface. These studies reported inter-rater reproducibilities that were almost excellent (K ≥ 0.80) (101) and moderate (K ≥ 0.60) (107). One study scored frondlike hypertrophied synovitis, associated with loosening due to wear, and concluded that inter-rater reproducibility was good (K = 0.72) (105).

In contrast, when soft tissue structures, which are associated with instability, were assessed, the inter-rater reproducibility ranged between poor and excellent (ICC between 0.24–0.85; kappa between 0.59–1.00) (100, 106). However, these wide ranges could be explained by the fact that these studies assessed diverse soft tissue structures, which were visualized with multiple sequences around different prosthetic materials.

Table 3.3: Study characteristics

Study (year published)	Design	Subjects (n)	Controls (n)	Mean age (years)	Investigated cause of complaints	Prosthesis	MRI (tesla; sequence)
Total knee arthroplasty							
A. Li et al. (2016) (99)	Retrospective, cross-sectional	73	-	65	Infection, instability, loosening and wear	TKA	1,5T; FSE + IR + MAVRIC
A. Plodkowski et al. (2013) (23)	Retrospective, case control	28	28	64	Infection	TKA	1,5T; FSE + IR
B. Raphael et al. (2006) (100)	Retrospective	21	-	57	Instability	TKA, 14 Zirconium	1,5T; FSE + IR
A. Jawhar (2018) (106)	Retrospective	15	-	76	Instability	TKA	1,5T; TSE + VAT + SEMAC
T. Heyse et al. (2011)(101)	Retrospective	55	-	59	Loosening and wear	TKA, 27 Zirconium	1,5T; FSE + IR
A. Li et al. (2016) (21)	Retrospective, observational	96	-	64	Loosening and wear	TKA	1,5T; FSE + IR + MAVRIC
A. Li et al. (2017)(105)	Prospective, longitudinal	61	-	66	Loosening and wear	TKA	1,5T; FSE + IR + MAVRIC
M. Meftah et al. (2013) (109)	Retrospective	24	-	63	Loosening and wear	TKA	1,5T; FSE + MAVRIC
C. Sofka et al. (2003) (86)	Retrospective	41	-	n/a	Loosening and wear, instability, arthrofibrosis	TKA	1,5T; FSE + IR
R. Sutter et al. (2003) (110)	Prospective	42	29	66	Loosening and wear	TKA	1,5T; TSE + IR + SEMAC
M. Vessely et al. (2006) (111)	Retrospective	10	-	67	Loosening and wear	TKA	1,5T; FSE + IR
T. Heyse et al. (2012) (98)	Retrospective	55	-	59	Malalignment	TKA, 27 Zirconium	1,5T; FSE + IR
T. Heyse et al. (2015) (104)	Retrospective	55	-	65	Malalignment	TKA	1,5T; FSE
A. Murakami et al. (2012) (90)	Retrospective, case-control	50	16	69	Malalignment	TKA	1,5T; FSE
M. Sgroi et al. (2015) (108)	Prospective, cohort	12	12	70	Malalignment	TKA	1,5T; TSE
T. Heyse et al. (2012) (102)	Retrospective	12	-	63	Patellofemoral	TKA, 1 Zirconium	1,5T; FSE + IR
Unicompartmental knee arthroplasty							
C. Park et al. (2015) (112)	Retrospective	28	-	57	Infection and others	UKA	1,5T; FSE + IR
T. Heyse et al. (2012) (87)	Retrospective	10	-	65	Instability	UKA, 10 Zirconium	1,5T; TSE
D. Malcherczyk et al. (2015) (107)	Retrospective	10	-	65	Loosening and wear	UKA, 10 Zirconium	1,5T; TSE
T. Heyse et al. (2013) (103)	Retrospective	10	-	65	Malalignment	UKA, 10 Zirconium	1,5T; TSE
Cadaveric studies							
Y. Minoda et al. (2014) (113)	Proof of concept	6 pc	-	-	Loosening and wear	FC	1,5T
Y. Minoda et al. (2017) (114)	Proof of concept	6 pc	-	-	Loosening and wear	FC, Zirconium	1,5T
L. Solomon et al. (2012) (115)	Proof of concept	6 hc	-	-	Loosening and wear	TKA	1,5T; FSE + IR

TKA = total knee arthroplasty, UKA = unicompartmental knee arthroplasty, pc = porcine cadaver, hc = human cadaver, TSE = turbo spin echo, FSE = fast spin echo, VAT = view angle tilting, IR = inversion recovery, SEMAC = Slice Encoding for Metal Artifact Correction, MAVRIC = Multi-Acquisition Variable Resonance Image Combination

Table 3.4: Reproducibility of MRI measurements to diagnose probable causes of complaints after knee arthroplasty, sorted by pathology with their statistic results and the results of the critical appraisal (COSMIN) for the reliabilitybox.

Author (year)	Pathology	Measurement	Inter-rater reliability	95% CI	Intra-rater reliability	95% CI	COSMIN Reliability box
Total knee arthroplasty							
A. Li et al. (2016) (99)	Infection,	Lamellated hyperintense synovitis	K= 0.82	0.72-0.91	K = 0.83	0.74-0.93	++
	loosening and wear	Frond like hypertrophied synovitis					
	instability and other	Homogeneous effusion					
A. Plodkowski et al. (2013) (23)	Infection	Synovitis	K = 0.82	0.72-0.93	K = 0.89	0.78-1.00	++
B. Raphael et al. (2006) (100)	Instability	Medial collateral ligament	ICC > 0.77	n/a	n/a	n/a	++
		Lateral collateral ligament	ICC > 0.74				
		Joint effusion	ICC > 0.24				
		Quadriceps tendon	ICC > 0.71				
		Patellar tendon	ICC > 0.83				
		Tibial component	ICC > 0.65				
		Femoral component	ICC > 0.53				
		Patellar component	ICC > 0.45				
A. Jawhar (2018) (106)	Instability	Posterior cruciate ligament	ICC > 0.90	n/a	n/a	n/a	+
		Medial collateral ligament	ICC > 0.34				
		Lateral collateral ligament	ICC > 0.37				
		Patella tendon	ICC > 0.68				
		Popliteal vessels	ICC > 0.83				
		Periprosthetic bone	ICC > 0.80				
T. Heyse et al. (2011) (101)	Loosening and wear	Implant bone interface tibial	K > 0.95	n/a	n/a	n/a	++
		Implant bone interface femoral	K > 0.80				
		Implant bone interface patellar	K > 0.94				
A. Li et al. (2017) (105)	Loosening and wear	Synovitis	K = 0.72	0.65-0.80	n/a	n/a	+
T. Heyse et al. (2012) (98)	Malalignment	Femoral component rotation	α = 0.82	n/a	α = 0.95	n/a	-
		Tibial component rotation	α = 0.89		α = 0.91		
T. Heyse et al. (2015) (104)	Malalignment	Tibial component rotation	ICC = 0.63-0.97	n/a	ICC = 0.53-0.96	n/a	++
A. Murakami et al. (2012) (90)	Malalignment	Femoral component rotation	ICC = 0.75	0.63-0.84	n/a	n/a	++
		Tibial component rotation	ICC = 0.75	0.62-0.84			
M. Sgroi et al. (2015) (108)	Malalignment	Femoral component rotation	ICC = 0.55	n/a	ICC = 0.92	n/a	+
		Tibial component rotation	ICC = 0.89		ICC = 0.95		
T.Heyse et al. (2012) (102)	Patellofemoral	Patella clunk	ICC = 0.75-0.93	n/a	n/a	n/a	++
Unicompartmental knee arthroplasty							
T.Heyse et al. (2012) (87)	Instability	Anterior cruciate ligament	K = 1.0	n/a	n/a	n/a	++
		Posterior cruciate ligament	K = 0.76				
		Lateral collateral ligament	K = 0.81				
		Medial collateral ligament	K = 1.0				
		Meniscus	K = 1.0				
		Cartilage	K = 0.84				
		Effusion	K = 1.0				
		Patellar tendon	K = 1.0				
		Quadriceps tendon	K = 1.0				
D. Malcherczyk et al. (2015) (107)	Loosening and wear	Implant bone interface	K = 0.60-1.00	n/a	n/a	n/a	++
T. Heyse et al. (2013) (103)	Malalignment	Femoral component rotation	ICC = 0.96	n/a	ICC = 0.99	n/a	++
		Tibial component rotation	ICC ≥ 0.56		ICC ≥ 0.88		
Cadaveric studies							
L. Solomon et al. (2012) (115)	Loosening and wear	Periprosthetic osteolysis	K = 0.61	n/a	K = 0.80-0.86	n/a	+

K = Cohen's Kappa, ICC = intra class correlation coefficient, α = Cronbach's alpha, n/a = not applicable, ++ = very good, + = adequate, -- = doubtful, - = inadequate.

Regarding prosthetic malalignment, five studies (90, 98, 103, 104, 108) assessed the femoral component rotation (FCR) and/or tibial component rotation (TCR). For FCR and TCR, the inter-rater reproducibility ranged between moderate and excellent (for FCR, an ICC between 0.55–0.96 (90, 103, 108), and for TCR, an ICC between 0.56–0.97 (90, 103, 104, 108)).

3.3.4 Accuracy

The accuracy of MRI in diagnosing one or more of the probable causes of complaints was examined in 10 out of the 16 TKA publications, 1 out of the 4 UKA publications, and 3 out of the 3 cadaveric studies (Table 3.5). The methodological quality of the accuracy studies assessed with QUADAS-2 varied from a high risk of bias (21, 86, 112, 113) to a few risk of bias (23, 99, 105, 108, 110). Criterion validity was assessed by comparing MRI findings with perioperative findings (21, 23, 86, 99, 105, 111-115). Construct validity was determined by using different standards as comparators, as CT (108, 110), knee pain (109) and healthy controls (90). Due to the retrospective designs of the included studies, which is thought to increase susceptibility to selection bias, none of the retrospective studies scored 'low risk' for the patient selection bias by the QUADAS-2. In addition, concerns were raised regarding the applicability of patient selection, because some studies did not describe patient selection clearly (21, 86, 109, 111, 112).

The sensitivity and specificity for diagnosing infection by the signs of lamellated hyperintense synovitis on MRI when taking culture results of perioperativy obtained tissue as the reference standard for periprosthetic joint infections varied between 0.89 (0.750–0.970, 95%CI) (23) and 0.85-0.92 (0.537-0.996, 95%CI) (99) for sensitivity and between 0.89 (0.559–1.00, 95%CI) (23) and 1.00 (0.93–1.00) (99) for specificity.

A relation was found between the presence of frondlike hypertrophied synovitis on MRI and perioperative findings of loosening due to wear (105). When these MRI findings were compared with the reference standard perioperative findings, the sensitivity and specificity of the diagnoses varied between 0.94–0.97 and 0.70-0.73 (99).

Diagnosing aseptic loosening by signs of periprosthetic osteolysis on MRI compared with perioperative findings was evaluated in one good-quality study, with sensitivity and specificity of 0.93 and 1.00 (110).
Malalignment measurement on MRI and CT showed an excellent correlation for FCR (r = 0.81) and TCR (r = 0.91) (108). Strikingly, one of the malalignment studies also included healthy controls and found significant differences between patients after TKA and healthy controls for FCR, p < 0.03 (90).

Table 3.5: Accuracy of MRI to diagnose probable causes of complaints after knee arthroplasty, sorted by pathology for different comparators (measurements on MRI compared with the reference standard or other) with their statistic results and the results of the critical appraisal (QUADAS-2) for the risk of bias and the applicability of concerns.

Author (year)	Pathology	Comparator	Statistics	QUADAS-2 Risk of Bias: Patient selection	Index test	Reference standard	Flow and timing	Applicability Concerns: Patients selection	Index test	Reference standard
Total knee arthroplasty										
A. Li et al. (2016) (99)	Infection	Lamellated hyperintense synovitis	se = 0.89, sp = 1.00							
	Loosening and wear	Frond like hypertrophied synovitis	se = 0.96, sp = 0.71							
	Instability and other	Homogeneous effusion	se = 0.63, sp = 0.97							
A. Plodkowski et al. (2013) (23)	Infection	Lamellated hyperintense synovitis	se = 0.89, sp = 0.89							
A. Li et al. (2016) (21)	Loosening and wear	Appearance of the liner on MRI	n/a							
A. Li et al. (2017) (105)	Loosening and wear	Synovitis and total liner wear	r = 0.46, p < 0.001							
M. Meftah et al. (2013) (109)	Loosening and wear	Synovitis and pain	r = 0.03, p = 0.8							
		Osteolysis and pain	r = 0.5, p = 0.15							
		Synovitis and thickness of fibrous membrane	r = 0.58, p = 0.003							
		Osteolysis and thickness of fibrous membrane	r = 0.47, p = 0.022							
C. Sofka et al. (2003) (86)	All	MRI findings and operative findings	n/a							
R. Sutter et al. (2013) (110)	Loosening and wear	Periprosthetic osteolysis	se = 0.93, sp = 1.00							
M. Vessely et al. (2006) (111)	Loosening and wear	Periprosthetic osteolysis	n/a							
A. Murakami et al. (2012) (90)	Malalignment	Femoral component rotation and complaints	p ≤ 0.03							
		Tibial component rotation and complaints	p ≤ 0.60							
M. Sgroi et al. (2015) (108)	Malalignment	Femoral component rotation MRI and CT	r > 0.8, p < 0.001							
		Tibial component rotation MRI and CT	r > 0.91, p < 0.001							
Unicompartmental knee arthroplasty										
C. Park et al. (2015) (112)	All	MRI findings and operative findings	n/a							
Cadaveric studies										
Y. Minoda et al. (2014) (113)	Loosening and wear	Periprosthetic osteolysis	se = 0.00, sp = 0.00							
Y. Minoda et al. (2017) (114)	Loosening and wear	Periprosthetic osteolysis	se = 0.84, sp = 0.87							
L. Solomon et al. (2012) (115)	Loosening and wear	Periprosthetic osteolysis	se = 0.89, sp = 0.90							

se = sensitivity, sp = specificity, n/a = not applicable, + low, ▮ high, ? unclear.

3.4 Discussion

The aim of this study was to critically appraise, summarize, and compare the literature on the diagnostic properties of MRI for identifying the causes of complaints in patients or cadaveric studies in terms of infection, loosening and wear, instability, malalignment, arthrofibrosis, and patellofemoral complaints after TKA or UKA. The available good-quality studies showed good to excellent reproducibility for MRI for diagnosing infection, loosening and wear, or malalignment after TKA. Studies in which accuracy was assessed were highly varied in terms of methodological quality.

The MRI properties to assess various arthroplasty failure causations were evaluated in this systematic review. First, MRI to identify periprosthetic joint infection based on MRI findings of hypertrophied synovitis compared with the reference standard was evaluated by two studies of adequate quality. Diagnostic properties were found in terms of sensitivity and specificity (0.89 and 0.89; 0.96 and 0.71) with 'almost excellent' reliability (23, 99). Nonetheless, it should be noted that both TKA studies were conducted by the same research group. Currently, the reference standard to diagnose infection is the diagnosis of a pathogen via multiple intraoperative cultures (116). In the literature, numerous preoperative and intraoperative tests for diagnosing periprosthetic joint infection were evaluated, as were several imaging modalities. Unfortunately, no test or modality has perfect sensitivity and specificity (117). Overall, MRI may be considered as a possible preoperative imaging technique that can contribute to diagnosing infection.

Second, regarding loosening due to liner wear, results showed that osteolysis can be recognized on MRI (110), and wear can be diagnosed based on synovitis patterns (99). Moreover, there is a significant relation between synovitis on MRI and liner wear (105). These findings are analogous to literature regarding the diagnostic properties of MRI for diagnosing liner wear in total hip arthroplasty (118). In clinical practice, early loosening is very difficult to diagnose on X-ray, and diagnosis usually becomes clearer only upon follow-up x-rays (119). When X-ray is inconclusive, other imaging modalities may be used (119), and based on these results, MRI may be considered as a possible modality.

Third, femoral and tibial component malalignment measurements can reliably be performed based on MRI after TKA or UKA (90, 103, 104, 108). At present, a combination of the imaging modalities of long leg view and CT is preferred for evaluating malalignment (120). However, CT scanning results in radiation load for the patient. Fortunately, MRI and CT show an excellent correlation regarding malalignment measurements in TKA (108). Moreover, a significant relation between complaints and internal rotation of the femur component on MRI was found (90). This was confirmed by the recent research of Panni et al. (91) which concluded that excessive internal rotation of the tibial TKA component represents an important risk factor for pain and inferior functional outcomes.

Fourth, regarding the other probable causes of complaints, the number of studies or their methodological quality was limited. Results regarding instability were inconsistent (87, 100, 106), probably due to the material of the scanned prostheses. Some of the instability studies that were included used a femoral component made from zirconium (87, 100). Soft tissue structures surrounding a zirconium prosthesis are more visible on MRI, because zirconium is non-ferromagnetic and therefore less hampered by metal artefacts (93). This may be the reason for the inconclusive results of the instability studies. Moreover, all the instability studies that were included only evaluated reproducibility and not accuracy.

Fifth, arthrofibrosis was only assessed in the more explorative studies, together with all other probable causes of complaints. In clinical practice, arthrofibrosis is diagnosed when patients experience stiffness and a restricted range of motion following knee arthroplasty (121). If other possible causes are not suspected, there is no need for additional diagnostic images such as MRI. However, the two studies included in this review that also evaluated MRI-based diagnoses of arthrofibrosis suggest that MRI performs well in this domain (86, 112).

Sixth, patellofemoral problems can be evaluated by several patellofemoral parameters, and MRI can be used in the native knee to assess the patellofemoral joint (27). However, studies that used MRI to evaluate patellofemoral complaints after TKA were not available. Only one of the included studies assessed the reproducibility of diagnosing patellar clunk and reported good results (102). However, patella clunk is a rare finding in modern-day TKA designs.

This review included studies published after 2002. It is notable that MRI after TKA is a young field of research: 19 of the 23 studies were published in 2012 or thereafter. This can be explained by the fact that traditional MRI is not capable of adequately imaging the structures, bone and soft tissue that surround metal implants (122). In recent decades, MRI sequences have greatly improved, partly due to the introduction of metal artefact reducing sequences (MARS) such as Slice Encoding for Metal Artefact Correction (SEMAC) and Multi-Acquisition Variable Resonance Image Combination (MAVRIC) (123, 124). The literature shows that when SEMAC is used, distortions caused by metal artefacts are significantly

reduced, resulting in more reliable evaluation of soft tissue structures (106, 110). Similarly, increased sensitivity and specificity values are found for diagnosing loosening based on periprosthetic osteolysis (110). Therefore, it is conceivable that use of MARS sequences may further improve the diagnostic properties of MRI after arthroplasty and resolve the inconclusiveness regarding MRI diagnoses of soft tissue and patellofemoral problems.

Many issues in the design and conduct of diagnostic studies can lead to bias or variation. The results of the critical appraisal revealed some interesting methodological challenges related to examining the diagnostic properties of MRI for identifying the causes of complaints after TKA or UKA. When evaluating criterion validity, it is noticeable that the studies' retrospective design (21, 23, 86, 99, 105, 111, 112) made them susceptible to selection bias. Due to the retrospective design, the study inclusion criteria occasionally only allowed revision surgery patients who had had a pre-operative MRI to be included, with a lack of healthy controls. This made evaluation with the reference standard possible. However, it induces selection bias, and leads to the possibility that sensitivity and specificity values were overestimated (99, 105). Moreover, if image observers had known that there was always some pathology to find on the MRI, this certainty may have led them to overestimate the inter- and intra- reproducibility values.

Therefore, the optimal study design should be prospective, and the spectrum of patients should include individuals who are likely to undergo imaging to diagnose complaints after knee arthroplasty. However, it is not ethical to evaluate MRI findings with the reference standard perioperative findings when surgery is not indicated. The tension between using a study design that reduces patient selection bias and the possibility of assessing criterion validity justifies the selection of a retrospective design to assess criterion validity. Other general methodological limitations of the studies that were reviewed included insufficient descriptions of sample size determination.

We performed a systematic review to focus on the diagnostic properties of MRI after knee arthroplasty to identify probable causes of complaints (including infection, loosening and wear, instability, malalignment, arthrofibrosis, and patellofemoral complaints). However, the study has some inherent limitations. First, the heterogeneity of the studies included made it impossible to conduct a meta-analysis. Moreover, this heterogeneity made it difficult to compare the study results and to categorize them according to probable causes of complaints. Second, this study included and compared various types of studies: patient studies, cadaveric studies, TKA studies, and UKA studies. Hence, this review is among the first to systematically present this heterogeneity by categorizing the availability of MRI knowledge per pathology associated with

complaints after knee arthroplasty. We believe this study presents a systematic and practical indication of the properties of MRI for diagnosing various causes of complaints after knee replacement.

In conclusion, this study supports that MRI can be used with overall reproducible and accurate results for diagnosing infection, loosening and wear, and malalignment after knee arthroplasty. Nonetheless, definitive conclusions cannot be drawn regarding the diagnostic properties of MRI for diagnosing all probable causes of complaints after knee arthroplasty. Studies regarding the diagnosis of instability, arthrofibrosis or patellofemoral complaints using MRI are limited and inconclusive. When comparing MRI to other diagnostic modalities that asses a problematic TKA, MRI is non-invasive and does not expose the patient to harmful radiation. This makes MRI a promising alternative for assessing a problematic TKA in clinical practice and for further research. Future research should focus on the diagnostic accuracy of MRI for diagnosing complaints after knee arthroplasty in a prospective cohort study using state-of-the-art MRI sequences.
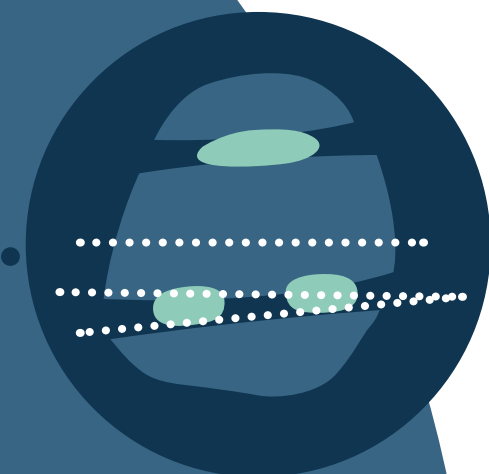
Femke Schröder
Corine Post
Frank Simonis
Frank-Christiaan Wagenaar
Rianne Huis in 't Veld
Nico Verdonschot

Under review.

4

Reproducibility of

PATELLOFEMORAL AND ROTATIONAL COMPONENT ALIGNMENT MEASUREMENTS IN POST- TKA PATIENTS

under weight-bearing and non-weight bearing conditions using low field MRI.

4.0 Abstract

Introduction: Patellofemoral joint problems and/or malalignment belong to the potential causes of dissatisfaction after total knee arthroplasty (TKA). MRI is preferable to evaluate the native knee. Post-TKA, metal artefacts disturb MRI, using low-field MRI these should be reduced. The knee is a loaded joint, evaluating the knee during weight-bearing (WB) seems relevant. This explorative study aims to evaluate the reproducibility of patellofemoral and component alignment parameters in TKA using low field (WB)-MRI. Secondary, is evaluated whether there are differences in patellofemoral parameters across the WB and non-WB conditions.

Method: Eight patients without complaints after primary TKA were scanned in a low field MRI scanner in WB and non-WB conditions. Patellofemoral parameters and rotational component alignment parameters were measured by two independent observers. Inter- and intra-observer reliability were determined with the intraclass correlation coefficient (ICC). Differences in parameters between WB and non-WB were calculated using the Wilcoxon rank test.

Results: The Insall-Salvati and Cation-Descamps ratios could be measured with excellent inter- and intra-observer reproducibility (ICC > 0.94), whereas the other parameters were measured with good reproducibility (ICC > 0.85). Small, but not significant differences between the WB and non-WB conditions were observed for the TT-TG and the PTA.

Conclusion: Patellofemoral and alignment can be reproducibly measured after TKA using low field MRI. The differences between the WB and non-WB conditions were relatively small. The ability to take reproducible measurements after TKA using low field WB MRI illustrates the potential of low field MRI for evaluating post-TKA patients with (patellofemoral) complaints.

4.1 Introduction

Approximately 20% of patients remain dissatisfied after total knee arthroplasty (TKA) (15, 125, 126). This dissatisfaction often relates to anterior knee pain, which is associated with patellofemoral joint problems and/or rotational component malalignment that contribute to a substantial proportion (20–30%) of revision procedures (127, 128).

Patellofemoral problems and rotational component malalignment are usually analysed using plain radiography (129) and CT (130, 131). However, recent research has suggested that MRI is a suitable alternative to measure patellofemoral parameters in the native knee (29, 132, 133) and rotational alignment parameters after TKA (16, 90), with results showing moderate to excellent reproducibility (16, 29, 90).

In the native knee, MRI is the imaging modality of choice to evaluate musculoskeletal tissues (8). However, following TKA, susceptibility artefacts caused by the metal TKA hamper visualization and subsequent interpretation (86). The introduction of new metal-artefact-reducing MRI sequences (110) prompts a re-evaluation of the possibility of using MRI to visualize the knee after TKA. Furthermore, low field MRI (0.25T) systems, which have traditionally been known for their reduced image quality, have improved (53). Lowering the main magnetic field reduces susceptibility artefacts near metal hardware compared with traditional MRI (11). Low field MRI also allows for scanning under upright weight-bearing (WB) conditions and is considerably less expensive than traditional MRI (37).

Currently, imaging of the knee before and after TKA is performed in a supine non-weight-bearing (NWB) position, except in the case of plain radiography. However, as the knee is a load-bearing joint, it may be more relevant to perform imaging under a loading condition in order to improve understanding of the normal and abnormal kinematic behaviour of the knee joint after TKA (134).

Recent research has shown that, in the native knee, WB MRI can contribute to diagnosing various patellofemoral parameters that are associated with knee pain and patellofemoral joint problems (27-31). For example, research in the native knee in the WB position (27, 29) has identified deviated patellar height, which has been suggested to be positively associated with lateral displacement and patellar tilt (30). Moreover, diagnosis of patellar maltracking is most effective at the patellar tilt angle in the WB condition (27), and the tibial tubercle-trochlear groove distance seems lower in the WB than the NWB position (28). It remains to be established whether these observations also apply after TKA.

Taken together, the issue of post-TKA patellofemoral and rotational problems and the developments in MRI call for an evaluation of whether patellofemoral and rotational alignment parameters can be measured reproducibly after TKA using low field MRI. Therefore, the primary aim of this explorative pilot study is to evaluate the inter- and intra-observer reproducibility of several patellofemoral and component alignment parameters in TKA using low field MRI. Furthermore, WB MRI research in the native knee suggests that there may be differences between the WB and NWB positions after TKA, which may be taken into consideration in the diagnosis of anterior knee pain in future. A secondary aim of this study is therefore to evaluate whether there are differences in the patellofemoral parameters across the WB and NWB positions.

## 4.2 Materials and Methods

4.2.1 Patient selection criteria

An exploratory pilot study was conducted between June 2018 and November 2018. Eight patients were included during their regular one-year postoperative TKA check-up at the '*clinic name*'. The number of eight patients was chosen since it has been found to be the minimum number of subjects to be included in both public and industry-funded explorative pilot and feasibility trials (135). Inclusion criteria were that patients had had a TKA (NexGen, posterior stabilized, BiometZimmer) and did not have any post-TKA complaints. Exclusion criteria were a body mass index (BMI) of over 35 kg/m², implanted devices that could interact with the magnetic field, and the inability to stand for the duration of the MR imaging. The study was approved by the medical ethics research committee of Twente (national trial register, NTR7207). Informed consent was obtained from all patients. Patient characteristics (gender, age, side of TKA, length of implantations) were obtained from their electronic medical records.

4.2.2 Image acquisition

Patients were scanned on a low field 0.25 tesla MRI system (G-scan brio; Esaote SpA, Genova, Italy) in the WB and NWB positions using a dedicated knee coil, with the knee fixated in extension (0-5 degrees of rotation). Spin echo (SE), fast spin echo (FSE), and X-MAR sequences (based on the view angle tilt (VAT) technique) were performed. A detailed outline of the MRI scan protocol is provided in Table 4.1. The WB examinations were performed first, with the patient table at an angle of 81⁰. Both knees were under physiological load during the WB examination (Figure 4.1). The total duration of the imaging protocol was approximately 30 minutes (five minutes for positioning and rotation, 12 minutes for WB MRI, one minute for rotation and repositioning, 12 minutes for NWB MRI).
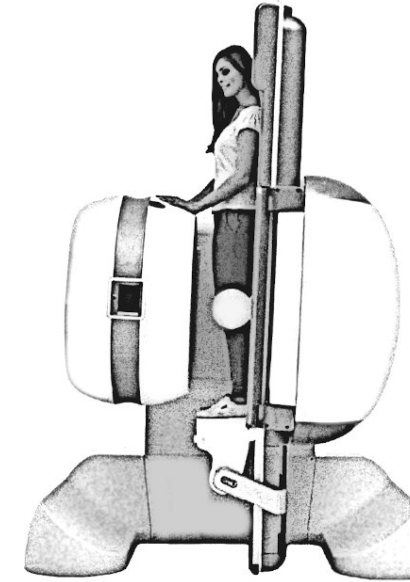
Figure 4.1. Low field MRI of the knee in weight-bearing upright condition. *Adapted with permission from Esaote (esaote.com)*

Table 4.1: MRI protocol

Position	Sequence	Plane	TR (ms)	TE (ms)	ST (mm)	FOV (mm²)	Time (min:sec)	Matrix
WB and NWB	Spin Echo PD-weighted	Sagittal	1160	18	4.0	200 x 200	03:22	512 x 512
	Fast Spin Echo PD-weighted X-MAR	Transversal	7060	12	4.0	260 x 260	03:31	256 x 256
	Fast Spin Echo T₂-weighted X-MAR	Coronal	6500	72	4.0	260 x 260	03:15	256 x 256

PD = proton density, X-MAR = metal artefact reduction, TR = repetition time, TE= echo time, ST = slice thickness, FOV = field of view.

4.2.3 Measurements

MRI scans in the WB and NWB conditions were evaluated for the parameters listed below by two independent MRI imaging experts, who were blinded for patient characteristics. Additionally, to enable an evaluation of the intra-observer reproducibility, one of the researchers assessed the images three times with an interval of two weeks between assessments. The patellofemoral joint was evaluated based on four patellofemoral parameters and two alignment parameters.

Patellar height was evaluated by the Insall-Salvati ratio (IS, normal 0.8–1.2 (27)) and the Caton-Deschamps ratio (CD, normal 0.6–1.2 (129)). These normal values are based on plain radiography measurements in the native knee (27, 129). The IS was determined on the sagittal MRI slice where the patella was most prone by dividing the length of the patellar tendon by the diagonal length of the patella (136) (Figure 4.2.a). The same sagittal MRI slice was used to determine the CD by dividing the distance between the distal pole of the patella and the anterosuperior border of the tibial plateau by the length of the articular surface of the patella (137) (Figure 4.2.b).
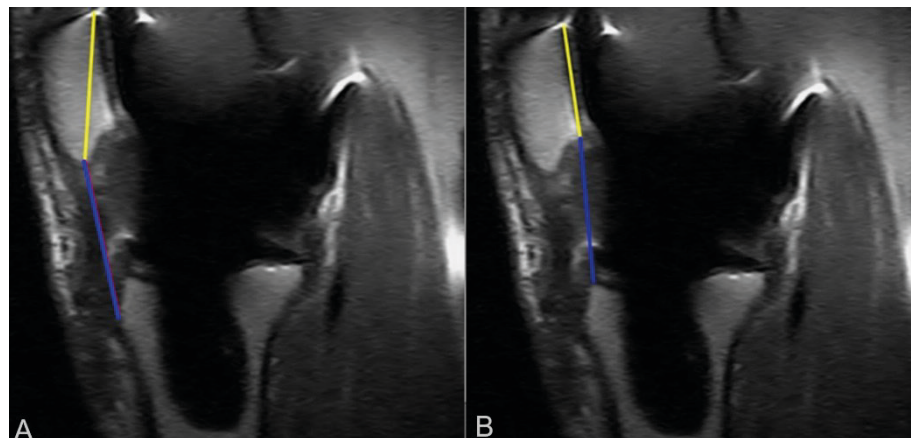

Figure 4.2. Patellar height measurements. 2.a Insall-Salvati ratio, the length of the patellar tendon (blue line) is divided by the diagonal length of the patella (yellow line) 2.b Caton-Deschamps ratio, the distance between the distal pole of the patella and the tibial plateau (blue line) is divided by the posterior length of the patella (yellow line)

Patellar tilt was evaluated based on the patellar tilt angle (PTA, normal 3^0–7^0, values based on CT images of the native knee (27)). The PTA was measured in the transversal MRI and defined as the angle between the posterior condylar axis and the maximal width of the patella.(138) . The posterior condylar angle was measured on the transversal slice where the posterior condyles were most prone and the line was projected on the slice where the patella had the greatest length in mediolateral dimension and the patellar width could be measured. (Figure 4.3).
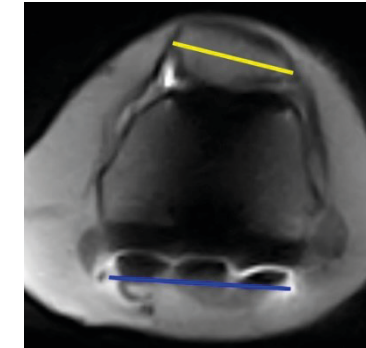

Figure 4.3. Patellar tilt angle, the angle between the maximum width of the patella (yellow line) and the posterior condylar axis (blue line).

The tibial tubercle-trochlear groove distance (TT-TG)) was measured on the appropriate transversal MRI slices as the distance between the deepest point of the trochlear groove perpendicular to the posterior condylar axis and the centre of the tibia tuberosity (132) (Figure 4.4). The normal TT-TG range in the native knee has been described as 10–15 mm (130).
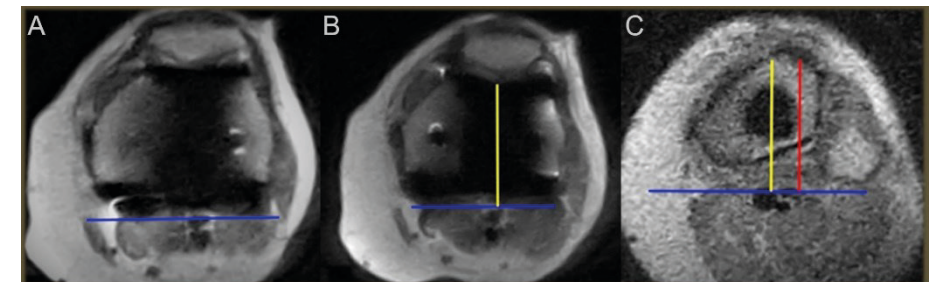
Figure 4.4. The tibial tubercle- trochlear groove distance. 4.a A line through the posterior epicondyle (blue) is drawn. 4.b. A line through the deepest point of the trochlear groove (yellow) perpendicular to the posterior epicondyle is drawn. 4.c A second line (red) through the most anterior portion of the tibial tuberosity is drawn. The distance between the two lines is the TT-TG distance.

Rotational component alignment was evaluated using two parameters, as described by Berger (139). Tibial component rotation (TCR) was determined using the Berger angle, i.e. using the geometric centre of the proximal tibial plateau, the distal level of the tibial tubercle and the posterior axis of the tibial plate (normal 18^0 internal rotation (139)) (Figure 4.5). Femoral component rotation (FCR) was determined by measuring the posterior condylar angle (PCA), i.e. the angle between the posterior condylar line and the surgical epicondylar axis (normal 3.5 ± 1.2° for males or 0.3 ± 1.2° for females when measured on CT (131)) (Figure 4.6). The images were evaluated semi-automatically using Matlab software that was developed in house (R2018a, The Mathworks, Natick, USA).
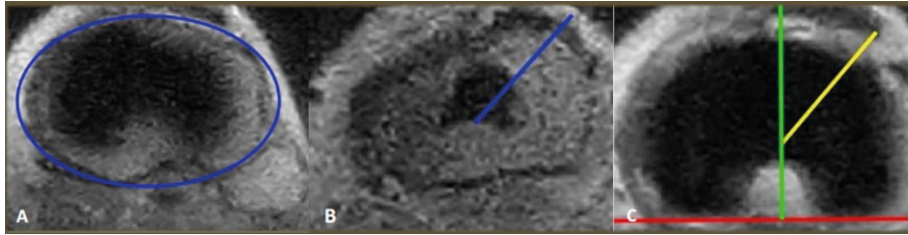
Figure 4.5. Berger protocol; Tibial component rotation. 5.a The centre of the tibia is determined, 5.b The centre of the tibia is connected to the top of the tibial tuberosity (blue line), 5.c The angle between this line (blue) and the line perpendicular on the tangent of the tibia plateau of the tibial component (red) is calculated.
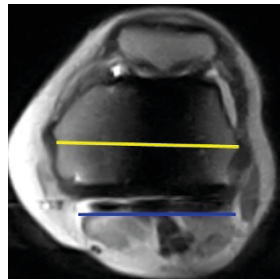
Figure 4.6. Berger protocol; Femoral component rotation. Angle between the posterior condylar axis (blue line) and the surgical transepicondylar axis (yellow line).

4.2.4 Statistical analysis

Subject characteristics were summarized using descriptive statistics. To determine the inter- and intra-observer reproducibility, the intra-class correlation coefficient (ICC) was calculated between the two observers and between the three within-observer measurements using a two-way mixed model with absolute agreement for single measurements for all measured parameters. The ICC values were interpreted as follows: below 0.50 was considered to indicate poor reliability, between 0.50 and 0.75 moderate reliability, between 0.75 and 0.90 good reliability and above 0.90 excellent reliability (95).

The results of the parameter measurements per image expert are presented for the WB-MRI and NWB-MRI conditions with the medians and interquartile ranges. Of image expert one, who measured the images three times, the average of the three measurements was presented. For the patellofemoral parameters, each patient's WB and NWB average values between the MRI experts are plotted together with the normal range reported in the literature for the native knee.

Statistical differences in each patient's average patellofemoral parameters in the WB-MRI and NWB-MRI conditions were evaluated by means of the Wilcoxon signed-rank test. The statistical analyses were performed using SPSS (version 25, IBM Corp., Armonk, NY, USA). Since four parameters were evaluated the level of significance was set at < 0.0125 after a Bonferroni correction for all analyses.

4.3 Results

4.3.1 Patient characteristics

Patellofemoral and alignment parameters were measured in the WB and NWB conditions in eight patients (50% male) with a median age of 64 years (IQR 59.5–75). The MRI scans were taken 15.6 months (IQR 13.5–18.6) after surgery. The data set included three left and five right knees.

4.3.2 Reproducibility

The patellofemoral height parameters, i.e. the IS and CD ratios, were measured with excellent inter- and intra-observer agreement (ICC > 0.94). The PTA, TT-TG, TCR and FCR were measured with good-inter and intra-observer agreement (ICC > 0.85). All reproducibility results are presented per image expert in Table 4.2, together with the median patellofemoral parameters, the median alignment parameters.

4.3.3 Weight-bearing vs. non-weight-bearing

Figure 4.7 illustrates the average measured patellofemoral parameters per patient per condition, together with the ranges reported in the literature for the native knee. The TT-TG distance decreased in the WB condition. This difference between the WB and NWB conditions tends towards statistical significance (p = 0.02). Furthermore, the PTA decreased in the WB condition in seven out of eight patients. However, this decrease was not statistically significant (p = 0.12). The IS and CD ratios remained similar or changed only slightly in the WB condition.

4.4 Discussion

This pilot study explored the possibility of using low field MRI to image the knee after TKA by assessing the inter- and intra-observer reproducibility of several patellofemoral and rotational component alignment parameters. Because differences in patellofemoral parameters across WB and NWB conditions in the native knee are associated with patellofemoral joint complaints (27-31), the study

also evaluated whether there are differences in the patellofemoral parameters after TKA (IS, CD, PTA, TT-TG) between the WB and NWB positions.

Table 4.2: Median, interquartile range and Inter and Intra observer agreement for patellofemoral parameters and alignment parameters measured in non-weight bearing and weight-bearing condition.

Parameters	Non-weight-bearing		Weight-bearing		Inter and intra observer agreement.	
	Imaging expert 1 median (IQR)	Imaging expert 2 median (IQR)	Imaging expert 1 median (IQR)	Imaging expert 2 median (IQR)	Inter ICC (95% CI)	Intra ICC (95% CI)
IS (ratio)	1.20 (0.26)	1.22 (0.32)	1.01 (0.50)	0.97 (0.52)	0.94 (0.83-0.98)	0.97 (0.93-0.99)
CD (ratio)	1.27 (0.79)	1.22 (0.60)	1.13 (0.93)	0.97 (0.77)	0.94 (0.76-0.98)	0.99 (0.98-1.00)
PTA (⁰)	5.95 (9.52)	5.62 (7.71)	4.22 (3.95)	6.68 (5.70)	0.89 (0.73-0.96)	0.85 (0.70-0.94)
TT-TG (mm)	13.78 (5.18)	12.10 (4.10)	10.13 (10.86)	11.35 (8.12)	0.87 (0.59-0.96)	0.94 (0.87-0.98)
TCR (⁰)	33.60 (13.49)	29.92 (11.08)	31.39 (18.97)	29.87 (15.64)	0.89 (0.72-0.96)	0.89 (0.77-0.96)
FCR (⁰)	0.53 (5.16)	0.65 (6.43)	1.81 (3.64)	1.58 (6.43)	0.89 (0.71-0.96)	0.87 (0.74-0.95)

IQR = inter quartile range, WB = WB, NWB = NWB, ICC = inter(/intra) class correlation coefficient, IS = Insall Salvati, CD = Caton Deschamps, PTA = Patellar Tilt Angle, TT-TG = Tibial Tubercle-Trochlear Groove distance, TCR = Tibial Component Rotation, FCR = Femoral Component Rotation.
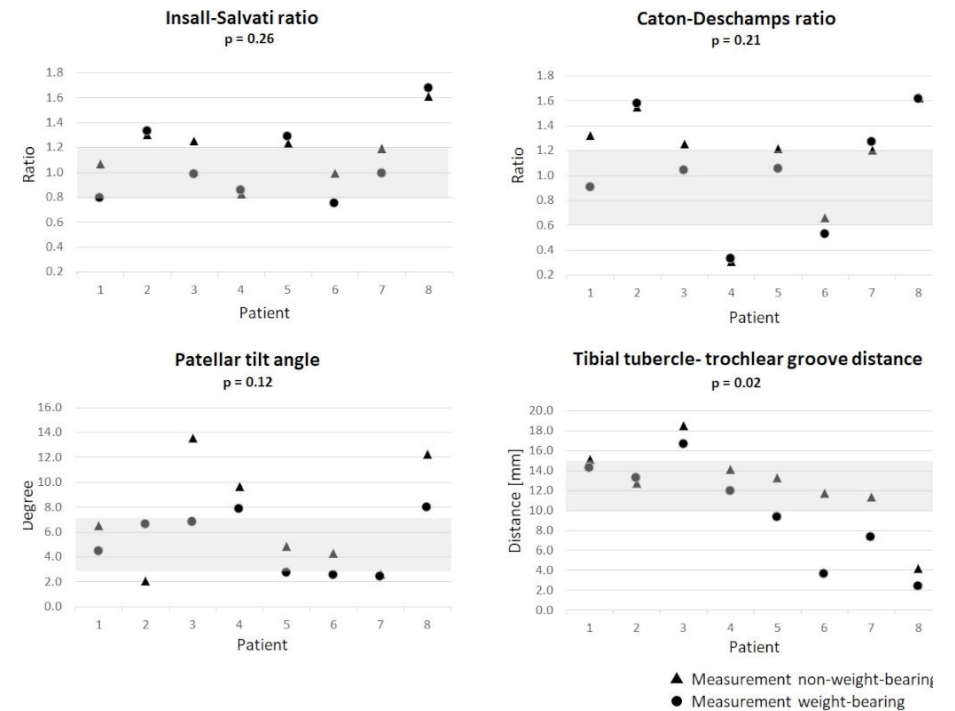
Figure 4.7. Results of the patellofemoral measurements. Average measurements for eight patients after TKA scanned in WB and NWB conditions using low field MRI for the IS and CD ratios, the PTA and the TT-TG distance are presented. The grey areas are the ranges given in the literature for the native knee.

The reproducibility results showed good to excellent inter- and intra-observer agreement for all patellofemoral and rotational component alignment measurements. The differences for the measured patellofemoral parameters between the WB and non-WB conditions were relatively small.

Regarding reproducibility, good to excellent inter- and intra-observer agreement was found for all patellofemoral parameters (ICC = 0.85–0.99). For the patellar height measurements IS and CD, the reproducibility scores were excellent (ICC ≥ 0.94), potentially because these measurements were performed on one slice rather than several slices, as was required for the other measurements.

Good inter- and intra-observer reproducibility scores were obtained for the rotational component alignment parameters, i.e. TCR (inter ICC = 0.893, intra ICC = 0.887) and FCR (inter ICC = 0.889 and intra ICC = 0.874). The reproducibility values for TCR are comparable with values found in the study of Sgroi et al.(16) who measured the TCR with high-field MRI and CT and found an excellent correlation between MRI and CT. Our reproducibility values for FCR are

higher than those provided in studies that used high-field MRI or CT to measure component rotation. Several studies that have reported FCR found only moderate reproducibility (ICC < 0.75) (16, 90, 104). This relatively low reproducibility has been suggested to be due to artefact formation around the femoral component (16). In our study, the main magnetic field was six times lower than in high-field MRI, and we used metal-artefact-reducing sequences, which could have contributed to our good reproducibility results. Moreover, we used semiautomatic software (in-house developed Matlab algorithm) to assess the MRI scans. This software might make the analysis more reproducible by remembering lines between the slices and always drawing a line perpendicular, orthogonal or central on the first point/line. Becher et al. (29) have evaluated the effects of using WB MRI to measure patellofemoral parameters (IS, CD, PTA and TT-TG) in the native knee in patients with and without patellofemoral complaints. They found good to excellent inter- and intra-observer results (ICC = 0.72–0.96). We found slightly higher levels of agreement. Becher et al. (29) also found differences in patellofemoral parameters between the control and complaint group (29). In light of these findings, a future study should compare post-TKA patients with and without patellofemoral complaints.

Another notable finding was that the PTA measurement showed a broader range than is considered normal in the native knee. In the native knee, PTA values typically range between 3^0 and 7^0 (27, 31). Our findings showed a wider range, between 2° and 14°, which is comparable to Carpenter el al. (140), who also examined PTA in TKA patients (posterior cruciate retaining and posterior stabilized TKA). The wider range found might be typical for post-TKA knees or due to the relatively small sample sizes studied. Therefore, it is recommended to replicate this study in a larger patient cohort, preferably including patients with and without complaints.

In the comparison of patellofemoral parameters across the WB and NWB conditions none of the parameters showed a significant difference between WB and NWB. Given the small sample size a limited value should be given to the results of the Wilcoxon signed-rank test. The TT-TG tends towards significance between WB and NWB.and seem to decrease in the WB conditions. This is analogous to findings for the native knee (3). The decrease can be explained with reference to the effect of the activation of the quadriceps muscle during WB. This quadriceps loading causes a slight internal rotation of the lower limb, resulting in a decrease of the TT-TG (141). Regarding the PTA, the current study found no significant differences between the WB and NWB conditions. Literature on this topic is scarce, and only available for the native knee (27, 29). In line with our findings, Mariani et al. (27) also did not find significant differences in the native

knee in patients without complaints. Interestingly, in the group of patients with complaints, these authors found WB-MRI to have high diagnostic value for unmasking PF-maltracking and to have the best predictive value for patellar maltracking of the PTA measurement (27). The literature regarding patellar height has reported differences between WB and NWB conditions (27, 29). However, this literature is not clear about the direction of these differences. In our study subtle differences between the WB and NWB conditions for patellar height (NWB vs. WB ratio differences between 0.14 and 0.25) were observed. However, these differences were not statistically significant.

Our study population only included patients without complaints, and the differences between the WB and NWB conditions were relatively small for the patellofemoral parameters. The difference between measurements in the WB and NWB conditions may increase for patients with patellofemoral complaints after TKA. This is in line with comparable literature on patellofemoral complaints in the native knee (27, 29).

The current study is subject to several limitations. First, as a pilot study, its sample size is limited, but it indicates the potential of low field MRI for determining future reference values and evaluating the knee after TKA. Second, it turned out to be challenging to run a short MRI protocol with metal-artefact-reduction sequences. A scan time of approximately 15 minutes was necessary during the WB condition. To reduce the scan time, the slice thickness was increased to 4 mm, which reduced the resolution perpendicular to the image plane. This slice thickness made it important to properly align the MRI in the sagittal direction on the slice where the patella is most prone. However, this trade-off between scan time and image quality is unavoidable when using MR imaging and did not appear to affect the inter-rater reproducibility of the measurements evaluated in the current study. Third, the knee was evaluated under static upright WB conditions, which do not reflect the dynamic flexion kinematics of the knee.

Anterior knee pain after TKA is a complex issue that is generally reported during WB activities, including climbing stairs, rising from a chair and walking. Consequently, imaging the TKA in a WB position may offer important information for the diagnostic process. This study evaluated the patellofemoral structures and prosthetic component positions in a WB condition and showed that patellofemoral and alignment measurements can be reproducibly obtained in NWB and WB conditions. For the patellofemoral parameters, small differences between the NWB and WB conditions were observed. However, to determine the clinical relevance of these differences, further research is required. Future studies

should include larger patient groups and evaluate the diagnostic capacity of MRI in patients with and without complaints after TKA.

Interestingly, other research has suggested that MRI is excellently suited for the general evaluation of soft tissue signs of periprosthetic joint infection and polyethylene wear (20). Furthermore, a proof-of-concept paper has suggested that component migration can be measured using low field MRI (142). Taken together, the findings of the current study and the available literature suggest that MRI might offer possibilities as an imaging modality to evaluate problematic TKAs. In the future, (low field) MRI may be used to evaluate other probable causes of complaints, such as infection, loosening and wear or instability in (problematic) TKA.

In conclusion, this pilot study showed that patellofemoral and rotational component alignment parameters, which are associated with patellofemoral joint problems and anterior knee pain, can be measured reproducibly after TKA using low field MRI in WB and NWB conditions. In our measured population, which consisted of patients without complaints after TKA, differences between the WB and NWB conditions for the patellofemoral parameters were relatively small. Further research should focus on evaluating whether these parameters differ in patients with and without patellofemoral complaints after TKA.

4

4

Low-field magnetic resonance imaging

OFFERS POTENTIAL FOR MEASURING TIBIAL COMPONENT MIGRATION.

5

Femke Schröder
Nico Verdonschot
Bennie ten Haken
Anil Peters
Dean Pakvis
Rianne Huis in 't Veld

5.0 Abstract

Introduction: Roentgen stereophotogrammetric analysis (RSA) is used to measure early prosthetic migration and to predict future implant failure. RSA has several disadvantages, such as the need for perioperatively inserted tantalum markers. Therefore, this study evaluates low-field MRI as an alternative to RSA. The use of traditional MRI with prostheses induces disturbing metal artefacts which are reduced by low-field MRI. The purpose of this study is to assess the feasibility to use low-field (0.25 Tesla) MRI for measuring the precision of zero motion. This was assessed by calculating the virtual prosthetic motion of a zero-motion prosthetic reconstruction in multiple scanning sessions. Furthermore, the effects of different registration methods on these virtual motions were tested.

Results: The precision of zero motion for low-field MRI was between 0.584 mm and 1.974 mm for translation and 0.884° and 3.774° for rotation. The manual registration method seemed most accurate, with $\mu \leq 0.13$ mm ($\sigma \leq 0.931$ mm) for translation and $\mu \leq 0.15°$ ($\sigma \leq 1.63°$) for rotation.

Conclusion: Low-field MRI is not yet as precise as today's golden standard (marker based RSA) as reported in the literature. However, low-field MRI is feasible of measuring the relative position of bone and implant with comparable precision as obtained with marker-free RSA techniques. Of the three registration methods tested, manual registration was most accurate. Before starting clinical validation further research is necessary and should focus on improving scan sequences and registration algorithms.

5.1 Introduction

Early prosthetic migration is associated with future aseptic loosening. (143) Roentgen stereophotogrammetric analysis (RSA) is the golden standard in measuring early component migration. (144-146) Currently, the clinically obtained accuracy of conventional RSA varies between 0.05 and 0.5 mm for translation and 0.15° to 1.15° for rotation (95% confidence intervals (CI)). This accuracy level is considered clinically relevant for diagnosing early prosthetic migration. (143, 147)

Clinical application of the RSA technique is limited because of the extended operation time due to the requirement of perioperative insertion of tantalum markers, the use of calibration cages and specific radiological facilities with two X-ray machines, the availability of specialized software and trained personnel, and the fact that patients are exposed to additional radiation during longitudinal RSA studies. (148, 149)

Improvements have focused on "marker-free" RSA methods. However, these are less accurate when compared to conventional RSA, and additional CT models are needed. (147, 150) Previous attempts to use MRI models instead of CT have failed, because MRI models interfere with the used X-ray shape-matching procedure which is based on Hounsfield units. (151)

MRI has some characteristics that make it less suitable for bone and prosthetic imaging: it provides lower bone contrast than CT; it suffers from spatial and geometric distortions, field inhomogeneity, and metal artefacts. (62, 151, 152) (Figure 5.1.a) Disadvantages of MRI may be partly overcome by the use of low-field MRI. (Figure 5.1.b) A lower magnetic field reduces spatial and geometric distortions, increases the field homogeneity and bone contrast, and decreases metal artefacts. (78) Furthermore, MRI offers imaging of soft tissues, which provides clinicians with additional diagnostic information. Although low-field MRI (< 0.5 T) is rarely used in clinical practice, it is considered to be highly suitable for musculoskeletal imaging. (78, 79)

In order to determine the potential of low-field MRI as an alternative, its precision in measuring position of implant and bone must be calculated. The precision of low-field MRI for measuring zero motion depends partly on the imaging technique and partly on the analysis process, which consists of segmentation and registration. It is important to quantify the precision of low-field MRI first, since this is prerequisite before implementing the method in clinical practice.

Segmentation can be performed manually or (semi-)automatically and provides 3D models to be used in subsequent registration steps. In order to

calculate prosthetic migration, model matching which is called registration between 3D models is necessary.

A **B**
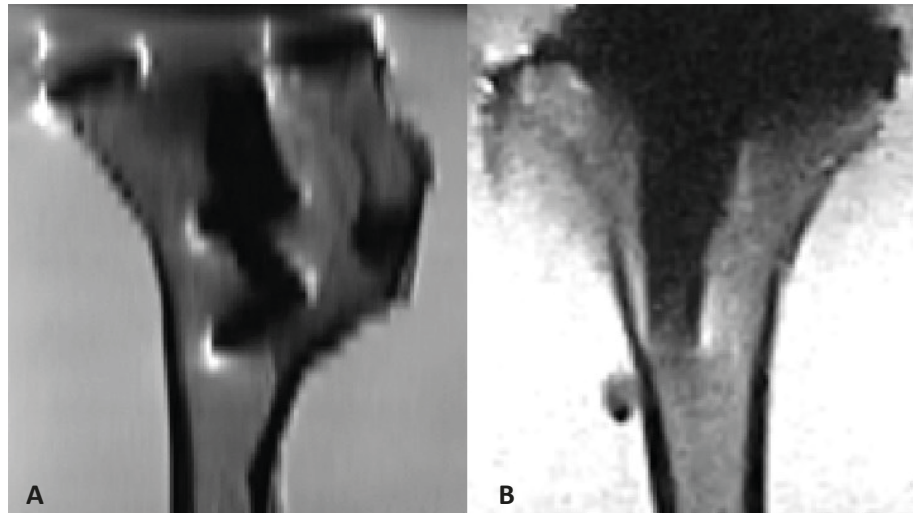
Figure 5.1.a. MRI slices of the tibial component of a total knee prosthesis made with high field MRI with a TSE PD sequence in the sagittal direction. **b.** MRI slices of the tibial component of a total knee prosthesis made with low-field MRI made with a TSE/FSE PD sequence in the sagittal direction.

An accurate, fully automatic segmentation and registration procedure is more standardized and time-effective than manual registration. However, manual registration may be more precise and visual feed-back can be interpreted while performing the segmentations steps. In order to determine which registration method is most suitable three methods: manual, semi-automatic with the use of 3D reference models and semi-automatic without the use of 3D reference models were compared.

The primary goal of this study was to assess the feasibility to use low-field (0.25 Tesla) MRI for measuring the precision of zero motion, using a tibial component of a total knee prosthesis in a phantom.

Additionally, the type of registration method most suitable for measuring the position of the tibial component was assessed.

5.2 Method

The aim of the following study was to determine the feasibility of low-field MRI to measure the precision of zero motion, several steps were taken (Figure 5.2).

1. Acquisition of the 3D models of the prosthesis and the porcine tibia.

2. Preparation of the phantom.

3. Acquisition of 12 MRI scans with repositioning between.

4. Segmentation of the 12 MRI scans for the bone and prosthesis.

5. Registration of earlier obtained 3D models on the segmentations; manual (M), automatic (A) and without using 3D models (W).

6. Determination of the accuracy of zero motion of these registration methods.

Figure 5.2. Study design.

5.2.1 Creating 3D reference models

In order to determine the position of the tibial component (Genesis II, Smith & Nephew Inc. Memphis USA) with respect to the surrounding bone, 3D geometrical models of both the prosthesis and the bone were made. The study focused on the tibial component of a total knee arthroplasty because according to the Swedish arthroplasty register their failure of the tibial component (6.8%) is much more frequent than that of the femoral component (1.1%).(153) The outer surface of the prosthesis was created using a 3D optical scanner (Konica Minolta Vivid 910). The 3D model of the porcine tibial bone was created by scanning the bone (without containing the implant) on a low-field MRI (0.25 T) (Esaote G-scan brio) with a 3D SHARC sequence (TR/TE 25/12.5, slice thickness 0.4 mm, acquisition time 5:38, field of view 200 mm with a matrix of 512x512). In order to obtain the 3D surface model of the bone, an imaging expert semi-automatically segmented the cortical bone of both the tibia and fibula with Mimics (Mimics Research 18.0, Materialise NV), resulting in an inner and outer surface of the porcine tibial bone just distal from the site where the future prosthesis would be positioned.

5.2.2 MRI acquisitions

Subsequently, a phantom was created by implanting the tibial component of the knee prosthesis into a porcine tibial bone and placing this bone in a gelatine solution (2%). Gelatine was chosen for its properties such as relaxation time and elasticity in order to mimic the soft tissue of the knee. (154)

In this phantom study, it was ensured that the prosthesis did not migrate with respect to the surrounding bone (zero motion) during the various scanning sessions. The phantom was relocated 12 times, the relocation varied between maximal 25 degrees rotation left and right from the supine position. The differences in translation and rotations of the tibial plate with respect to the position of the bone measured across the 12 acquisitions were defined as the precision of zero-motion for low-field MRI. Similarly as described in ISO guideline for RSA studies. (155) During each of the 12 acquisitions, the phantom was scanned in a transverse direction on a low-field MRI with a 2D PD-weighted metal artefact reduction sequence (MARS) PD-XMAR (TR/TE 1020/10, slice thickness 3mm, acquisition time 5:08 minutes, field of view 180 mm with a matrix of 224x224). This particular sequence was chosen because it reduces metal artefacts, provides good contrast between bone and surrounding soft tissue, and is capable of adequately imaging the human knee. During all acquisitions, the temperatures of the room and the phantom were kept constant (21 degrees Centigrade).

5.2.3 Segmentation and 3D model reconstruction

The prosthesis and the cortical bone of the tibia and fibula distal to the prosthesis on the 12 MR-acquisitions obtained were semi-automatically segmented by an imaging expert in approximate 30 min per acquisition using Mimics. The segmentations included the following steps:

1. A suitable threshold was determined by applying a profile line in Mimics.
2. A region growing algorithm was applied to collect the connected voxels.
3. Abundant voxels were erased manually.
4. Missing voxels in the segmented region were filled with the morphology operation ("closing").
5. All slices were checked manually, abundant voxels were erased, and missing voxels were filled.
6. A 3D model (the segmentation model) was constructed from the connected voxels.

This resulted in 12 segmentation models of the bone and 12 of the prosthesis.

5.2.4 Analysis

The segmentation models of the bone and prosthesis were registered to the 3D reference models constructed earlier. Registration was performed to transform all segmented datasets into the reference coordinate system in order to facilitate future calculations. Registration was performed in three different ways in order to determine which method is most accurate. The three methods are described below.

1. Marker-free MRI manual registration (MMRI-M): The segmentation of the bone was registered to the 3D reference model of the bone with the automatic registration algorithm available in Mimics (global registration followed by local registration). The 3D reference model of the prosthesis was manually fit to the segmentation of the prosthesis by an imaging expert in approximately 5 minutes. Several landmarks of the prosthetic model, e.g. the posterior edge and the distal notch, were precisely matched on the segmentation.
2. Marker-free MRI automatic registration, fully automatic registration with the use of 3D reference models (MMRI-A): The automatic registration algorithm available in Mimics was used to register the prosthetic and bone segmentations to the 3D reference models of the prosthetic and the bone.
3. Marker-free MRI automatic registration, fully automatic without the use of 3D reference models (MMRI-W): The segmentations of the prosthesis and the bone based on the MRI scans of acquisition number one were

taken as a reference model instead of the 3D reference models. Using the automatic registration algorithm available in Mimics, these were registered to the segmentations of the prosthesis and bone based on the remaining acquisitions.

During registration, all 3D segmentations were matched to a 3D reference model and transformed to the reference coordinate system. Subsequently, using a procrustes algorithm in Matlab (R2015b, Mathworks©), the position (3-D translations and rotations) of the prosthesis with respect to the bone was calculated across two acquisitions (one with two, two with three, etc.) with all three registration methods enlisted before.

Results are presented for all three registration methods. The translation and rotation for all six degrees of freedom of the prosthesis calculated from the midpoint are presented for the 12 acquisitions, with the mean (μ) and standard deviation (σ), which defined the precision of zero motion. In order to compare the different registration algorithms, three distance plot presenting the migration of the tibial component calculated par point were compiled. Boxplots were constructed to calculate the precision of zero motion per degree of freedom per registration method at 95% CI; μ ± 1.96 σ. The boxplots also visualize the current golden standard, i.e. 0.5 mm for translation and 1.15° for rotation (95% CI) (143, 147).

5.3 Results

In Table 5.1, each row represents a calculated zero-motion result, which indicates the difference between two acquisitions for each of the three registration methods applied (MMRI-M, MMRI-A, and MMRI-W). Of the three registration methods, MMRI-M measured the precision of zero motion most precise, with a maximal mean error of 0.128 mm for translation (maximal σ 0.931 mm) and of 0.152° for rotation (maximal σ 1.630°). External internal migration was fully within the range considered clinically relevant. For MMRI-A and MMRI-W, maximal errors for translation and rotation were 0.147 mm for translation (σ 1.974 mm) and 0.033° for rotation (σ 3.774°); and 0.136 mm for translation (σ 1.518 mm) and 0.068° for rotation (σ 2.527°), respectively.

Figure 5.3 shows the distance plots of the tibial component. In this figure, the difference between the calculated value (error) and the real migration (zero) is visualized on the surface of the tibial component. The smallest error was seen in the distal part of the stem of the tibial component. Of the proximal plate, the posterior area had the smallest error.

The boxplots in Figure 5.4 display the calculated values per registration method with the ranges of the golden standard. As is evident, the results are mostly out of range for all degrees of freedom, regardless of the registration method used. The distal-proximal direction shows the largest translation error.
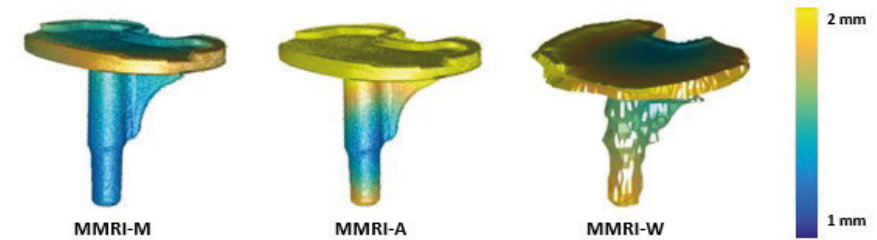
Figure 5.3. Distance plots for translation of the prosthesis with respect to the bone for the three types of registration methods used. (MMRI-M, MMRI-A and MMRI-W)

Table 5.1:
MRI images of the phantom of 12 different acquisitions have been registered with three different methods.

MMRI-M

Acquisition (Reference acquisition)	medial-lateral migration (mm)	distal-proximal migration(mm)	posterior-anterior migration(mm)	flexion-extension migration (deg)	external-internal migration (deg)	varus-valgus migration (deg)
1 (2)	-0.367	1.657	0.129	-1.460	0.984	0.557
2 (3)	0.241	-1.313	-0.446	0.682	0.681	1.846
3 (4)	-0.158	0.711	-0.535	0.829	-0.107	-0.960
4 (5)	0.857	-0.209	0.359	-1.183	0.386	-0.952
5 (6)	-0.258	-0.116	-0.424	1.623	-0.080	2.125
6 (7)	0.912	0.426	-0.428	2.272	1.039	-0.748
7 (8)	-0.724	-0.525	0.885	-3.657	-0.109	-1.624
8 (9)	-0.146	1.334	-0.699	0.518	0.570	0.456
9 (10)	-0.084	-1.207	-0.295	-1.197	-1.780	-0.821
10 (11)	1.231	-0.372	0.985	0.775	0.712	0.291
11 (12)	0.135	0.516	-0.118	0.465	0.781	0.301
12 (1)	-0.105	-0.642	-0.833	0.939	-1.252	-0.398
μ(σ)	**0.128 (0.584)**	**0.022 (0.931)**	**-0.118 (0.593)**	**0.050 (1.630)**	**0.152 (0.884)**	**0.006 (1.147)**

MMRI-A

Acquisition (Reference acquisition)	medial-lateral migration (mm)	distal-proximal migration (mm)	posterior-anterior migration (mm)	flexion-extension migration (deg)	external-internal migration (deg)	varus-valgus migration (deg)
1 (2)	0.288	-0.561	1.836	1.506	0.936	-1.022
2 (3)	1.571	-2.674	-2.178	2.964	0.900	6.187
3 (4)	-0.738	3.648	0.381	-2.857	0.298	-3.799
4 (5)	-0.040	-2.650	-0.001	0.952	-0.840	1.247
5 (6)	-1.006	-1.651	-1.670	-4.091	-0.321	3.394
6 (7)	1.210	0.226	1.094	1.968	1.573	-3.264
7 (8)	1.489	0.986	0.597	2.472	1.206	-1.856
8 (9)	-2.071	0.131	-0.667	-5.606	-1.682	0.943
9 (10)	-0.568	2.232	-0.203	1.584	-4.138	2.737
10 (11)	0.535	0.079	0.495	0.628	1.160	-0.290
11 (12)	1.565	-1.566	-1.880	2.888	0.125	3.453
12 (1)	-0.470	1.964	1.167	-2.522	0.393	-7.439
$\mu(\sigma)$	**0.147 (1.172)**	**0.014 (1.974)**	**-0.086 (1.284)**	**-0.010 (2.952)**	**-0.033 (1.595)**	**0.024 (3.774)**

MMRI-W

Acquisition (Reference acquisition)	medial-lateral migration (mm)	distal-proximal migration (mm)	posterior-anterior migration (mm)	flexion-extension migration (deg)	external-internal migration (deg)	varus-valgus migration (deg)
1 (2)	-0.326	-0.173	1.702	1.725	-0.779	-0.735
2 (3)	1.315	-0.736	-1.071	-0.359	1.727	0.665
3 (4)	0.094	0.356	-0.081	2.417	0.516	-0.291
4 (5)	0.467	-0.804	0.716	-0.789	-0.416	0.502
5 (6)	-0.432	2.489	-1.456	-2.723	-0.360	-0.305
6 (7)	1.229	-3.267	0.182	4.319	0.750	0.416
7 (8)	0.196	0.690	-0.240	-2.665	0.295	0.291
8 (9)	0.369	1.619	-0.062	2.500	0.206	-0.068
9 (10)	-2.113	1.378	0.618	-3.284	-2.317	-1.114
10 (11)	0.577	-1.102	-0.718	0.452	0.553	0.383
11 (12)	1.669	0.119	-1.792	1.847	1.364	2.007
12 (1)	-1.414	-0.956	0.746	-2.623	-1.781	-1.790
$\mu(\sigma)$	**0.136 (1.100)**	**-0.032 (1.518)**	**-0.121 (1.012)**	**0.068 (2.527)**	**-0.020 (1.189)**	**-0.003 (0.967)**

This table shows the migration calculated using the MRI data of each acquisition with respect to the previous acquisition. A perfect registration result would be zero migration.
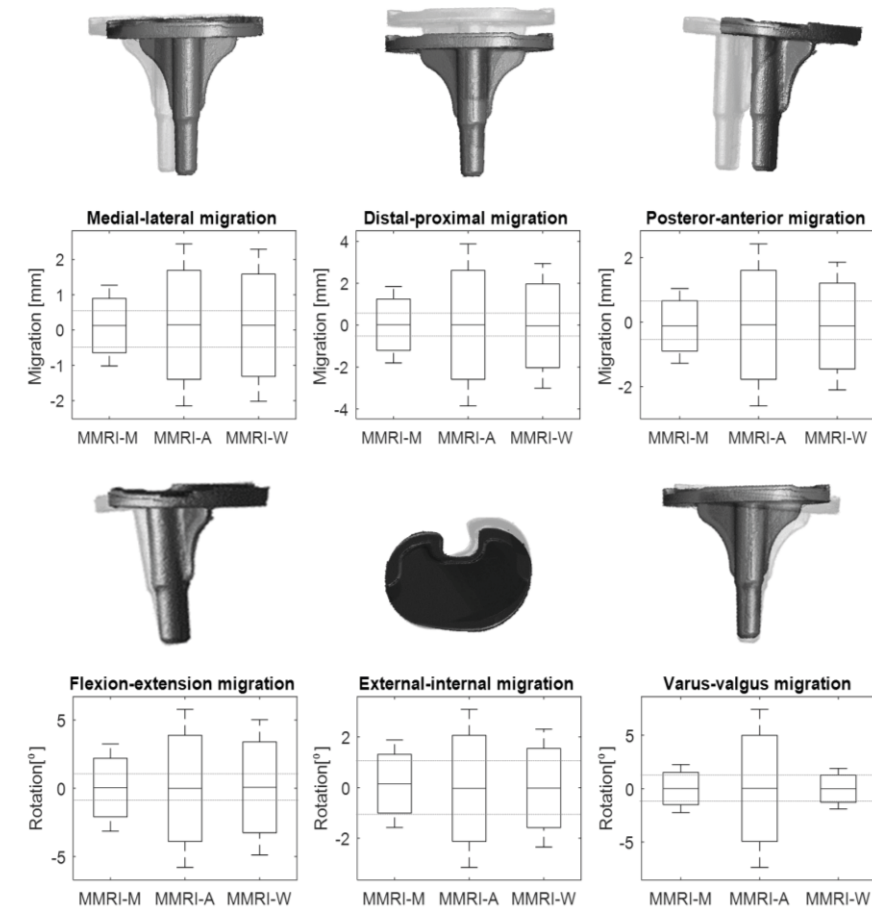
Figure 5.4. Boxplots for the six degrees of freedom, three for translation and three for rotation, for MMRI-M, MMRI-A and MMRI-W (95% CI; μ±2σ). The dashed horizontal lines indicate bounding range of RSA accuracy reported in literature.

5.4 Discussion

The most important finding of the present study is that the low-field MRI method as utilized in this study is not yet as precise as the golden standard RSA. However, low-field MRI is feasible of measuring the relative position of bone and implant with an error of $\mu \leq 0.13$ mm ($\sigma \leq 0.931$ mm) for translation and $\mu \leq 0.15°$ ($\sigma \leq 1.63°$) for rotation when the manual registration algorithm is used, which indicates that with some improvements this technique could reach adequate precision.

5.4.1 Precision of zero motion

The values for the precision of zero motion for rotation are more precise than those in recent marker-free RSA studies from Seehaus et al. (147) μ≤ 1.64° (σ ≤ 3.17°) and de Bruin et al. (150) μ≤ 0.21° (σ ≤ 3.26°). However, in these studies, the values obtained for translation were comparable (μ≤ -0.363 mm (σ ≤ 0.876 mm)) and more accurate (μ≤ -0.083 mm (σ ≤ 0.295 mm)) than the values obtained in this study. In this study, the largest measurement error for translation is in the distal-proximal direction. An explanation for this is that only 2D metal artefact reducing sequences were available on the low-field MRI system, which resulted in a 3 mm through-plane resolution in the distal proximal direction compared to a resolution of 0.4 mm in the medial-lateral and posterior-anterior direction. An improvement in the through-plane resolution is expected to result in a more detailed segmentation and thereby to contribute to a smaller standard deviation for translation. To have a similar through-plane resolution in all directions further research should focus on improving 3D sequences. Another option which could reduce the measurement error in the proximal-distal direction is by changing the scan direction to sagittal or coronal.

Nevertheless, neither the results obtained in this study nor those from marker-free RSA research are as accurate as the golden standard. (143, 147)
To reflect on the precision of the low-field MRI method, reference values for RSA were obtained from the literature. It should be noted that these reported values are subject to variations of the exact methods and implants used. These reference values should therefore be used with caution and can only serve as an indication of the 'overall precision' of marker based and marker-free RSA techniques.

5.4.2 Registration method

Marker-free MRI with manual registration (MMRI-M) had the smallest registration error. Manually, it was possible to match according to specific landmarks such as the posterior notch of the proximal plate or on the distal stem, which explains the favourable results. However, contrary to automatic registration, manual registration is susceptible to observer variation. It is also more time-consuming.

Despite its lower accuracy, the registration method that does not use a 3D reference model (MMRI-W) remains interesting. MMRI-W is an automatic method and is not susceptible to observer variation. Because it omits reference to a 3D reference model, the MMRI-W method makes it possible to determine the position of any prosthesis implanted in a patient, and would thus be the most accessible method when applied in daily practice. This makes it worthwhile to

work on improvements of this method which is a somewhat less accurate automatic registration method.

5.4.3 Strengths and limitations of the technique and the study

In addition to its potential to measure prosthetic migration, low-field MRI is excellently suited for judging the soft tissue structures surrounding the implants. Future research should investigate the added clinical benefit of being able to assess soft tissue structures as well as prosthetic positioning and migration. If low-field MRI is capable of these combined evaluations, the technique could be beneficial for individual patients who have recurrent or persisting symptoms after total knee arthroplasty. Low-field MRI could aid to diagnose whether this is caused by migration of the prosthesis and/or by other issues such as malpositioning or soft tissue impingement problems. Furthermore, it should be noted that compared to high-field MRI, low-field MRI is considerably less expensive and could therefore be a relatively cost-effective manner to assess soft tissue aspects as well as prosthetic migration.

Obviously, this study has some limitations. Firstly, since it is a feasibility study, only one porcine tibia with a tibial component without insert and femoral component was used, and results were analysed by one imaging specialist. For further validation more subjects should be analysed by more than one imaging specialist. An additional shortcoming is that a phantom will always be a limited representation of the human knee. In this study a gelation solution was used to mimic the soft tissue. (154) Gelatine is a more homogeneous substance than human tissue, and while it does mimic globally soft tissue imaging properties, it lacks the variety of soft tissues in the human knee. If the low-field MRI's accuracy is tested in the human knee, the knee's reduced homogeneity will influence the size of the metal artefacts, which could affect the accuracy of the measurements. Moreover, the phantom was at room temperature (21°C). The higher temperature of the human knee could also affect the image quality. (156)

Secondly, during the acquisitions available sequences on the low-field MRI system, and during the automatic registration procedure the registration algorithm available in Mimics were used. Although these methods can be considered as state of the art, further improvements on these aspects can be made in order to further reduce the registration errors. From these two aspects, it is proposed to first focus on improving the MRI sequences on the low-field system. When metal artefacts are reduced even more, segmentations become more similar and registration more accurate. Subsequently, research could focus on further improving the registration methods. Other registration options such as rigid image registration techniques should be further explored. This method allows

scans to be directly registered to each other, without the necessity of any segmentation. (157)

Thirdly, this study focuses on the accuracy of zero motion of low-field MRI. For further validation, it is necessary to generate true migrations with a micromanipulator in order to evaluate low-field MRI's ability to measure prosthetic migration in a multiple human cadaver study with a total knee prosthesis. This should be followed by a clinical validation. If low-field MRI is used in clinical practice movement artefacts may occur. In today's practice, patients are instructed before they are scanned in a high-field MRI scanner to minimize movement artefacts. Since the low-field MRI protocol for measuring migration is shorter than a clinical high-field MRI we expect that when the patient is well instructed movement artefacts can be negligible.

In conclusion low-field MRI as utilized in this study appeared not yet to be as precise as the golden standard RSA. However, RSA has a history of over 50 years. Interestingly, results of the present study showed that low-field MRI is feasible of measuring the relative position of bone and implant with a precision which is comparable to marker-free RSA techniques.
 Of the three tested registration methods, manual registration was most accurate. However, manual registration is susceptible to observer variation and is more time-consuming.

Further research is necessary and should focus on improving scan sequences and registration algorithms, in order to further improve the precision and thereby working towards clinical validation. Consequently, once this technique is validated within a patient cohort, low-field MRI is suggested to be a marker free and radiation free alternative for RSA.

Low-field weight-
bearing MRI to diagnose

PATHOLOGIES ASSOCIATED WITH A PROBLEMATIC TOTAL KNEE ARTHROPLASTY

– a feasibility study.

6

Femke Schröder
Corine Post
Sjoerd van Raak
Frank Simonis
Frank-Christiaan Wagenaar
Rianne Huis in 't Veld
Nico Verdonschot

6.0 Abstract

Introduction: Low-field MRI, allowing imaging in supine and weight-bearing position, may be utilized as a non-invasive and affordable tool to differentiate between causes of dissatisfaction after TKA ('problematic TKA'). However, it remains unclear whether low-field MRI results in sufficient image quality with limited metal artefacts. Therefore, this feasibility study explored the diagnostic value of low-field MRI concerning pathologies associated with problematic TKA's' by comparing low-field MRI findings with CT and surgical findings. Secondly, differences in patellofemoral parameters between supine and weight-bearing low-field MRI were evaluated.

Methods: Eight patients with a problematic TKA were scanned using low-field MRI in weight-bearing and supine conditions. Six of these patients underwent revision surgery. Scans were analysed by a radiologist for pathologies associated with a problematic TKA. Additional patellofemoral and alignment parameters were measured by an imaging expert. MRI observations were compared to those obtained with CT, the diagnosis based on the clinical work-up, and findings during revision surgery.

Results: MRI observations of rotational malalignment, component loosening and patellofemoral arthrosis were comparable with the clinical diagnosis (six out of eight) and were confirmed during surgery (four out of six). All MRI observations were in line with CT findings (seven out of seven). Clinical diagnosis and surgical findings of collateral excessive laxity could not be confirmed with MRI (two out of eight).

Conclusion: Low-field MRI shows comparable diagnostic value as CT and might be a future low cost and ionizing radiation free alternative. Differences between supine and weight-bearing MRI did not yield clinically relevant information.

6.1 Introduction

Total knee arthroplasty (TKA) is a highly successful procedure usually performed on patients with end-stage osteoarthritis to improve long-term function and reduce pain (158). Each year, more than 700,000 TKA procedures are performed in the US, and that figure has been increasing annually (158, 159). Despite the increase, approximately 20% of the patients are dissatisfied after TKA; these patients' cases are referred to as the problematic TKA (158). Pathologies related to this dissatisfaction include intra-articular, peri-articular and extra-articular causes. The classical described pathologies for which revision is performed include loosening, infection, instability, and malalignment (158, 160-163). Medical imaging of the TKA plays an important role in identifying the cause(s) of dissatisfaction. During the past decade, several differential diagnostic algorithms for the problematic TKA have been developed as a result of a multitude of studies (161, 164-166). In all these differential diagnostic algorithms several additional imaging investigations such as CT, SPECT-CT, stress radiographs or other are used. Unfortunately, none of these imaging techniques are solely able to diagnose all probable causes of the problematic TKA simultaneously.

In the native knee, MRI has become the standard to evaluate the joint and surrounding soft tissue (8). MRI is considered to be of limited diagnostic value after TKA, primarily due to metallic susceptibility artefacts caused by the metal implant (167). Recent review articles have described how it is possible to evaluate a TKA with MRI using optimized sequences and advanced metal artefact reduction techniques (159, 168). However, despite these efforts, susceptibility artefacts are still present. Another method to reduce these artefacts is to decrease the main magnetic field, i.e. use low-field MRI (40). Although low-field MRI (≤ 1 T) was previously regarded as having inferior imaging quality, systems have improved through the years (53, 169). Together with the possibility to reduce susceptibility artefacts, low-field MRI is hypothesized to be a potential solution to evaluate the problematic TKA and its surrounding soft tissue.

The majority of medical imaging is performed with the patient in a supine position, except the conventional weight-bearing long-leg view. The knee is a dynamic joint acting in a load-bearing capacity during the day. Therefore, evaluation of the knee in a load-bearing situation may offer improved and more relevant insight in some pathologies. For example, in the native knee, deviated patellar height in the weight-bearing position might be associated with lateral displacement and patellar tilt (30). Patellofemoral maltracking is considered to be diagnosed more effectively in the weight-bearing position (27), whereby the tibial

tubercle-trochlear groove distance (TT-TG) has been reported to decrease (28); whether this also applies after TKA is currently unknown.

Taken together, the absence of a single imaging technique that can simultaneously differentially diagnose a problematic TKA and the potential weight-bearing MRI might offer call for exploration of low-field weight-bearing MRI to diagnose the problematic TKA. Consequently, the aim of this feasibility study was twofold. First, to compare the diagnostic value of low-field weight-bearing MRI concerning pathologies associated with a problematic TKA with CT and surgical findings during revision surgery. Secondly, to evaluate differences between supine and weight-bearing low-field MRI for patellofemoral parameters after TKA.

6.2 Methods

6.2.1 Patient selection criteria

A prospective feasibility study was conducted between November 2018 and June 2019 and eight patients with a problematic TKA (three male and five females, median age 67 years (range 55–72), two left and six right knees) were consecutively included at OCON Centre for Orthopaedic Surgery (Hengelo, The Netherlands) (Figure 6.1). In six out of eight patients the complaints started between the first and third year after TKA. In two patients, the complaints started nine and ten years after TKA. Given there is no available data on the diagnostic value of low-field weight-bearing MRI, a proper sample size calculation could not be conducted. The number of eight patients has been found to be the minimum required in both public and industry-funded pilot and feasibility trials (135). Inclusion criteria comprised patients dissatisfied after primary TKA (NexGen, posterior stabilized, BiometZimmer) and patients considered eligible for revision surgery based on the standard clinical work-up. Exclusion criteria were a body mass index of over 35 kg/m², other implanted devices that could interact with the magnetic field, and the inability to stand for the duration of the MRI experiment. Informed consent was obtained from all patients.

All patients were scheduled for revision surgery within six months after the low-field MRI experiment. For one of the patients, the complaints disappeared before surgery, while a second patient encountered other health problems (Figure 6.1). Therefore, six patients underwent revision surgery, performed by an experienced orthopaedic knee revision surgeon. The revisions were an insert change (two patients, + 4 mm thicker liner), patella resurfacing (one patient), tibia component revision (one patient), and full component revision to a rotating hinge

(two patients) implant. During the revision surgery, the causative findings relating to the revision indication were recorded.
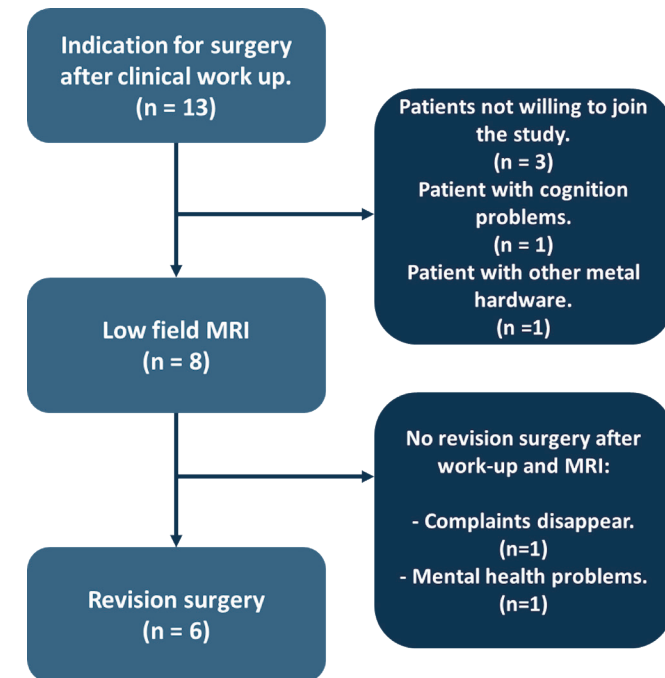

Figure 6.1. Patients selection flowchart

6.2.2 Image acquisition

Patients were scanned at the University of Twente (Enschede, The Netherlands) on a low-field 0.25T MRI system (G-scan brio; Esaote SpA, Genova, Italy) in the weight-bearing and supine conditions (Figure 6.2), using a dedicated knee coil Spin echo (SE), fast spin-echo (FSE), and X-MAR sequences (based on the view angle tilt (VAT) technique). The sequences used were T1, T2, and PD weighted (TR/TE 1160-7060 ms/12-72 ms) in the sagittal, coronal and transversal directions. Slice thickness was 4 mm, with a gap of 0.4 mm. The field of view was between 200 mm and 260 mm, with an acquisition matrix of either 256 x 256 or 512 x 512. The weight-bearing examinations were performed first, with the patient table at an angle of 81⁰. Both knees were under physiological load during the weight-bearing examination. Thereafter, supine examination was performed. The total duration of the imaging protocol was approximately 30 minutes (five minutes for positioning and rotation, 12 minutes for weight-bearing MRI, one minute for rotation and repositioning, 12 minutes for supine MRI).

Figure 5.2. Scanning position in weight-bearing condition in a low-field MRI-scanner. *(Adapted with permission from Esaote (esaote.com)).*

6.2.3 Measurements

The MRI scans were assessed by a radiologist with 10 years' musculoskeletal experience, who was unaware of the clinical diagnosis and findings during surgery. His MRI report described the status of prosthetic fixation and (pathologies of) the surrounding structures, including bone, tendons, ligaments, and muscles. Moreover, patellofemoral alignment parameters and rotational alignment parameters were measured by an imaging expert, who was also kept blind to patient characteristics.

The measurements were performed as shown in figure 6.3. The Insall-Salvati ratio (IS, normal value in the native knee 0.8–1.2 (27)) and the Caton-Deschamps ratio (CD, normal value in the native knee 0.6–1.2) were used to evaluate the patellar height (129). Patellar tilt was evaluated based on the patellar tilt angle (PTA, normal value in the native knee 3^0–7^0)(27). Moreover, the tibial tubercle-trochlear groove distance (TT-TG)) was measured (10–15 mm in the native knee) (130). The rotational alignment was evaluated through tibial component rotation (TCR) using the Berger angle and via femoral component rotation (FCR) measuring the posterior condylar axis (PCA)(170). The images were evaluated semi-automatically using Matlab software that was developed in house (R2018a, The Mathworks, Natick, USA).
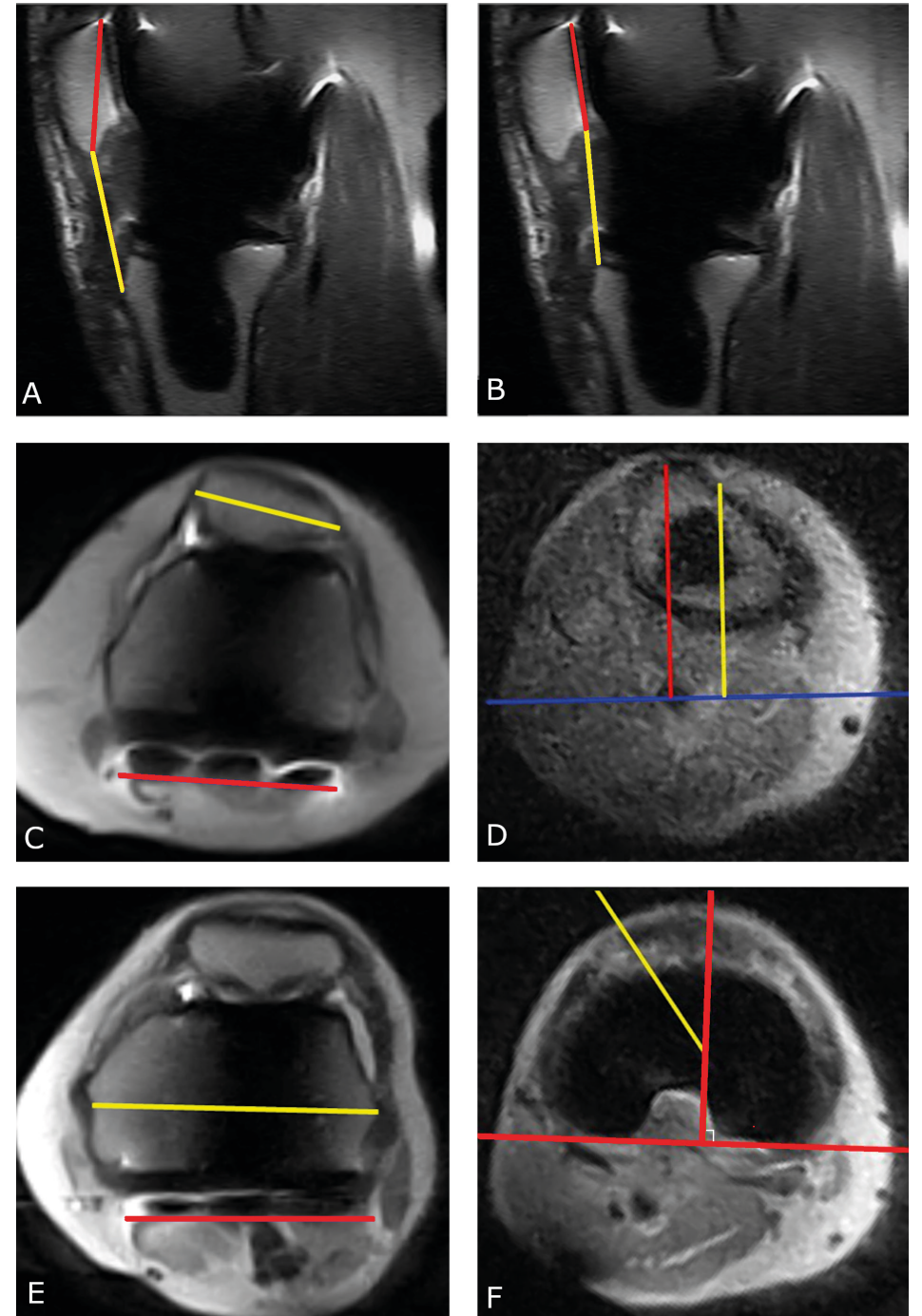
Figure 6.3. The patellar height was measured with the Insall-Salvati ratio (A), the length of the patellar tendon (yellow line) is divided by the diagonal length of the patella (red line), and with the Caton-Deschamps ratio (B), the distance between the distal pole of the patella and the tibial plateau (yellow line) is divided by the posterior length of the patella (red line). The patellar tilt angle (C) was measured as the angle between the maximum width of the patella (yellow line) and the posterior condylar axis (red line). The tibial tubercle- trochlear groove distance was measured on three levels, at the first level a line through the posterior epicondyle (blue) was drawn, at the second level a line through the deepest point of the trochlear groove (yellow) perpendicular to the posterior epicondyle was drawn, then on the third level a line (red) through the most anterior portion of the tibial tuberosity is drawn (D). The distance between the red and yellow line is the TT-TG distance. The femoral component rotation (E) is measured on two levels as the angle between the posterior condylar axis (red line) and the surgical transepicondylar axis (yellow line). The tibial component rotation (F) is measured on three levels, on the first level the centre of the tibia is determined, then on the second level the centre of the tibia is connected to the top of the tibial tuberosity (yellow line), next the angle between the yellow line and the line perpendicular on the tangent of the tibia plateau of the tibial component (red) is calculated.

To be able to compare the MRI observations with the clinical diagnosis, the standard clinical work-up results and the surgical findings during revision surgery were extracted from the patients' medical records. Standard clinical work-up included a diagnosis based on anamnesis, clinical examination, radiological reports made by a musculoskeletal radiologist based on conventional knee radiographs and an indicative CT or other additional investigations, such as stress radiographs or bone scintigraphy.

The study was approved by the Medical Research Ethics Committees of Twente (Netherlands Trial Register: Trial NL7009 (NTR7207). Registered 5 March 2018, https://www.trialregister.nl/trial/7009).

6.2.4 Analysis

MRI observations were descriptively compared with the diagnosis based on CT results, clinical diagnosis, and findings during surgery. The results of these comparisons were scored in consultation between the radiologist and the image expert. When the diagnoses based on MRI was comparable with CT results, clinical diagnosis or findings during surgery, it was scored as excellent agreement (++). If the diagnoses based on MRI was partly comparable with CT, clinical diagnosis or surgery, it was scored as a moderate agreement (+).

When the diagnoses based on MRI was not comparable at all it was scored as no agreement (--). If CT, clinical findings or surgery were not available the agreement was scored as not applicable (n/a). Based on the comparison of the clinical diagnosis and findings during surgery with the low-field MRI observations, several pathologies were discussed. For the patellofemoral alignment parameters of each patient, weight-bearing and supine values were plotted together with their normal ranges for the native knee, as reported in the literature. Due to the small

sample size, statistical paired differences for each of the eight patients' patellofemoral parameters, in both the weight-bearing MRI and supine MRI conditions, were evaluated utilizing the non-parametric Wilcoxon signed-rank test. The statistical analyses were performed using SPSS (version 25, IBM Corp., Armonk, NY, USA). The level of significance was set at $p < 0.05$.

6.3 Results

In all six patients who underwent revision surgery, the diagnosis based on the clinical work-up was comparable with the findings during surgery. Table 6.1 describes the results from the clinical work-up i.e. the diagnosis, the low-field MRI observations, and the findings during surgery.

As can be seen in Table 6.1, in the majority of the cases (four out of six), low-field MRI observations were roughly the same as the findings during surgery. For six of the eight patients, the diagnosis based on the clinical work-up was in line with low-field MRI observations. Interestingly, all MRI observations were comparable with the CT results. However, the additional weight-bearing MRI did not reveal additional information regarding the diagnosis based on low-field MRI.
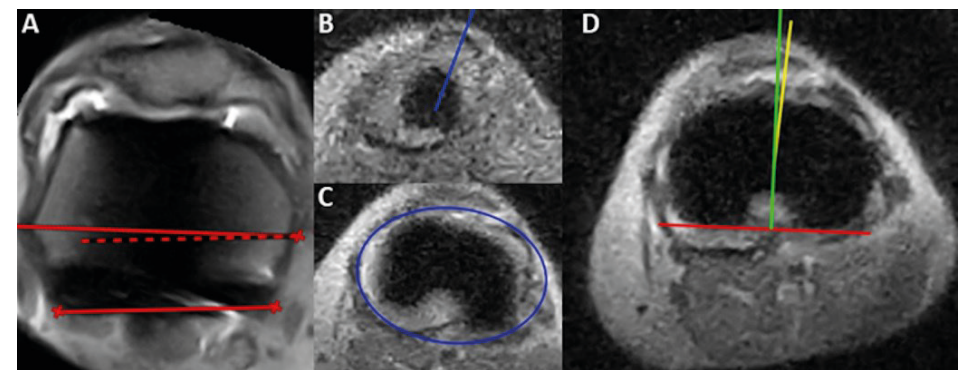
Figure 6.4. Rototional malalignment of the TKA. A) shows 3.3⁰ of internal rotation of the femoral component of patient 3, measured as the angle between the posterior condylar axis and the surgical transepicondylar axis. B-D) show 4.4⁰ tibial component rotation, measured in accordance with the Berger protocol, wherefore B shows the top of the tibia tuberosity, which is connected with the centre of the tibia determined in C. In D, the angle between the yellow line and the green line perpendicular on the tangent of the tibia plateau of the tibial component (red) was calculated as 4.4⁰ tibial component rotation.

Malalignment was measured and confirmed with CT in three cases. Figures 6.4 shows a typical example of prosthetic component malalignment measured on the low-field MRI of two different patients (patients three and four).

Table 6.1: Clinical diagnosis with additional imaging results + low-field MRI observations + findings during surgery per patient

Patient	Clinical work-up				Clinical diagnosis	Low-field MRI	Findings during surgery	Agreement		
	Anamnesis	Conventional radiographs	CT	Other				D & OR & CT & MRI	OR & MRI	D & MRI
1	Instability and diffuse pain	Negative	Negative	Varus & valgus stress films, positive	Collateral laxity	Negative	Collateral laxity	-	-	-
2	Pain anterolateral and swelling	Negative	9° internal rotation of the tibial component	Varus & valgus stress films, positive	Collateral laxity, no clinical	11° internal tibial component rotation	Collateral laxity	++	++	++
3	Instability and pain anterolateral	Negative	4° internal rotation of the femoral component	Valgus stress films, positive	Malalignment of the femoral component	3° internal rotation of the femoral component	Malalignment of the femoral component	++	++	++
4	Pain anterolateral, medial and swelling	Negative	6° internal rotation of the tibial component	Varus stress films, positive	Malalignment and asymmetric laxity	5° internal tibial component rotation	Malalignment of the tibial component	++	++	++
5	Anterior knee pain	Tibial component loosening	Lucency around tibial component suspected for loosening	Negative punction and lab	Tibial component loosening	Effusion around the medial side of the tibial component and the MCL	Partial tibial component loosening,	+	+	+
6	Medial knee pain	Tibial component loosening	Lucency around tibial stem suspected for loosening	Negative punction and lab	Tibial component loosening	Effusion around the tibial stem	n/a	+	n/a	+
7	Diffuse pain and swelling	Negative	Lucency around the tibial component. Possible early loosening	Not applicable	Early tibial component loosening	Joint effusion	n/a	+	+	n/a
8	Pain anterolateral and during stair climbing	Negative	n/a	Bone scintigraphy showing patellofemoral activity	Patellofemoral arthroses	Patellofemoral arthroses	Patellofemoral arthroses	++	++	n/a

D = diagnosis, OR = findings during surgery, ++ = excellent agreement, + = moderate agreement, -- = no agreement, n/a. not applicable.

Prosthetic loosening (tibial component) was the clinical diagnosis for patient six. Figure 6.5 shows the low-field MRI, which showed high signal on the T2-weighted images surrounding the tibial stem. Over time, the patient indicated that complaints had considerably reduced and the revision surgery was consequently cancelled, making it impossible to compare the data with the findings during surgery. Patellofemoral arthrosis was found on the MRI of patient eight (Figure 6.6), which was analogous to the clinical diagnosis and surgical findings. Signs of laxity could not be diagnosed based on low-field MRI (case one and two). In case of ligament instability, stress radiographs remains the superior diagnostic modality.
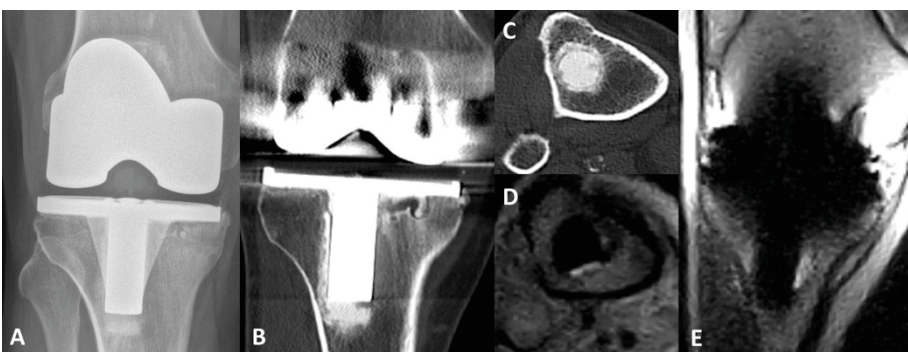
Figure 6.5. Loosening of the tibial component. The conventional radiograph (A) of patient 6 shows tibial component loosening around the medial plate and stem. CT (B and C) and low-field MRI (D and E) show images of the same knee, where images C and D are the transversal views of B and E at the most distal point of the tibial stem. The CT shows lucency (B-C) and MRI effusion (D-E) around the tibial stem, which are elements suspected of loosening the tibial component.
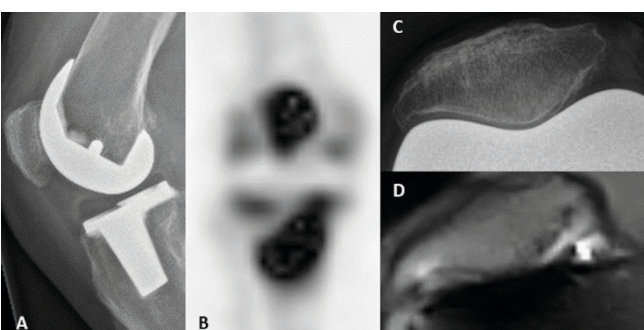
Figure 6.6. Patellofemoral arthrosis. The conventional radiograph (A) of patient 8, together with the bone scintigraphy (B), the additional patellofemoral radiograph (C) and the low-field MRI (D). Except for the conventional radiographs (A), all other images (B-D) show patellofemoral arthrosis.

For all patients, patellofemoral parameters were measured in weight-bearing and supine conditions. Figure 6.7 illustrates the patellofemoral

parameters per patient, per condition. Interestingly, the TT-TG distance significantly decreased in weight-bearing condition (p = 0.012). For the other parameters, no significant differences between supine and weight-bearing conditions were found (IS (p = 0.575), CD (p = 0.068), PTA (p = 0.161)). However, there seemed to be a trend in the decrease of CD and PTA in the weight-bearing condition.
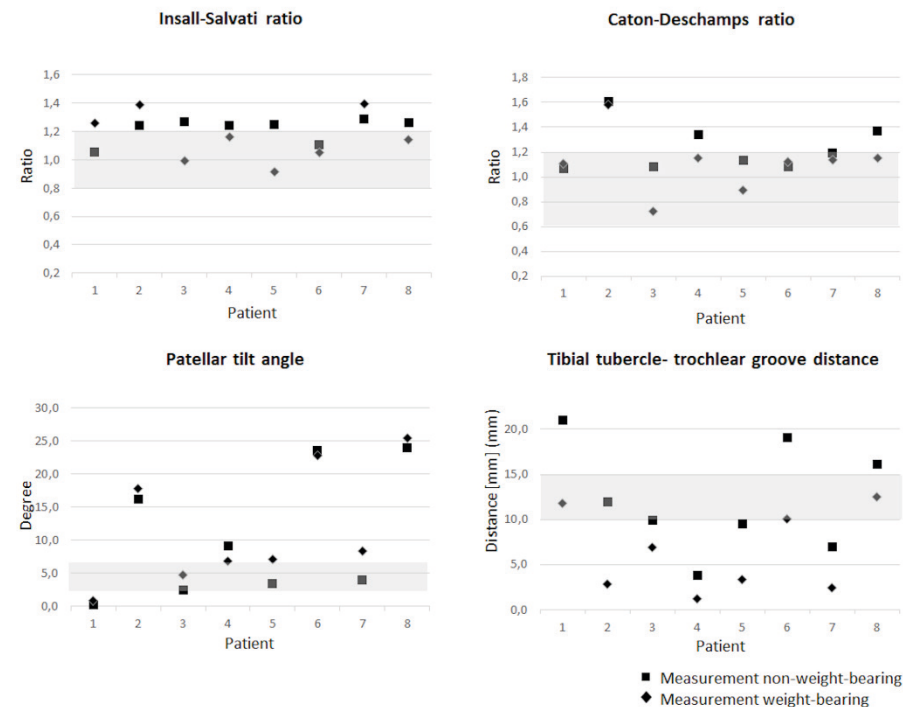
Figure 6.7. Results of the patellofemoral measurements of eight patients with a problematic TKA, scanned in weight-bearing and non-weight-bearing conditions using low-field MRI to measure the IS and CD ratios, the PTA and the TT-TG distance. The grey areas are the ranges given in the literature for the native knee: Insall-Salvati ratio (0.8–1.2)(27) , Caton-Deschamps ratio (0.6–1.2)(129), Patellar tilt angle (3⁰–7⁰)(27), tibial tubercle-trochlear groove distance (10-15 mm)(130)

6.4 Discussion

Identifying the underlying pathologies that cause a problematic TKA is often challenging. This is the first study attempting to explore the diagnostic potential of low-field weight-bearing MRI for imaging pathologies associated with a problematic TKA and compare MRI findings with clinical diagnosis, CT findings and surgical findings. In six out of the eight cases included in this study, the MRI

observations were in line with the diagnosis based on the clinical work-up, and in four out of six cases, the MRI observations of malalignment, suspected loosening, and patellofemoral arthrosis were confirmed with findings during revision surgery. Only collateral laxity could not be confirmed with low-field MRI. Importantly, all MRI observations were comparable with CT or scintigraphy results. Weight-bearing MRI significantly decreased TT-TG distance measurements when compared to supine MRI. In addition, the other patellofemoral parameters showed a decreasing trend when measured in the weight-bearing condition. However, the added value of weight-bearing low-field MRI to evaluate the problematic knee could not be proven yet. Based on our study results, low-field MRI shows a comparable diagnostic value to CT regarding evaluation of the problematic TKA, but currently cannot replace the entire clinical work-up and solely diagnose all pathologies associated with the problematic TKA.

In the cases described in our study, rotational component malalignment could be diagnosed with low-field MRI. As demonstrated in the extant literature, rotational malalignment has been possible to diagnosed by means of high-field MRI (16, 171). In this study, CT or MRI results for component malalignment were not always supported by the clinical diagnosis. This was due to the fact that not all patients with measured component malalignment had clinical complaints related to malalignment. During the evaluation of synovitis, which is related to aseptic loosening (99, 172, 173), the assessed low-field MRI images did show increased signal in T2 scans surrounding the tibial component, which has been associated with aseptic loosening in several high-field MRI studies (99, 172, 173). However, as only one of these patients with observations of synovitis on low-field MRI underwent surgery, the clinical evidence is scarce, and more cases are needed to reach a definitive conclusion. Patellofemoral arthrosis could also be visualised with low-field MRI, as the observations were in line with the clinical diagnosis based on the bone scintigraphy and the findings during surgery. Pathologies only causing laxity could not be diagnosed based on the low-field MRI scans and were only visible on the stress radiographs. It was expected that low-field MRI would provide additional diagnostic information concerning soft-tissue problems, as MRI is the superior imaging modality to diagnose these kind of problems in the native knee (8). Unfortunately, this could not be confirmed in the current study due to the fact that no patients with soft tissue problems, such as a tendinopathy, could be included. Results show that it is possible with low-field MRI to image the soft tissue structures surrounding the prosthetic components, which made it of potential added value when soft tissue problems are present.

When comparing the results of weight-bearing versus supine MRI, as

expected, a significant decrease of the TT-TG distance was found in the weight-bearing condition. This result is in line with findings in the native knee (174) and satisfied knee after TKA, and can be explained by quadriceps loading (141). Moreover, the results suggest a decreasing trend in patellofemoral parameters between the weight-bearing and supine conditions for the CD and the PTA. When evaluating all four patellofemoral measurements, there is a notable deviation between the measurements performed in this study and the normal values in the native knee (27, 129, 130). However, the clinical relevance of these differences is unknown; as there are no reference values for patellofemoral parameters after TKA, no firm conclusions can be drawn between the measured patellofemoral parameters and the patients' complaints yet. In the future, measurement and collection of patellofemoral parameters after TKA would be a possible area of study. When more data is available, normal values can be determined and perhaps patellofemoral measurement outliers in the weight-bearing condition can be related to the cause of the problematic TKA, thereby improving diagnostics.

Although the current study is the first to explore the diagnostic feasibility of low-field MRI regarding pathologies associated with the problematic knee, there are some obvious limitations. First, given the explorative character of the current study the sample size was kept limited and heterogeneous to represent the variety of reasons for the problematic TKA. If considerable differences would exist between patellofemoral measurements based on weight-bearing MRI and supine MRI, they would have been found even with a small sample size. However, in this feasibility study it is less important whether the difference found is statistically significant but much more about whether it could be of clinically relevance to the patient. Although small differences were found between patellofemoral parameters in weight-bearing and supine conditions, differences of clinical relevance were not perceived. Therefore, to be more certain about the diagnostic value of low-field MRI and the added value of weight-bearing MRI, more patients need to be scanned. The current study reveals an estimate of variability between the weight-bearing and supine positions for patellofemoral parameters, which can be used to conduct proper sample size calculations to set up clinically relevant studies in future research. Second, as radiologists are trained to assess high-field MRI scans, it was more difficult to evaluate images made on a lower field strength. Soft tissue structures, such as the popliteus tendon and the semi-membranous tendon, which are close to the posterior part of the prosthetic components, were especially challenging to distinguish. This is likely caused mainly by the reduced signal-to-noise ratio (SNR) of low-field MRI, and partly due to susceptibility artefacts caused by the TKA. Since, malalignment of the tibial

component affects posterior tendon tension (175), and MRI (in contrast to CT) offers the ability to image soft tissue, it would be beneficial if those structures can be visualised.

In clinical practice, a CT scan is often made when additional imaging is needed. In this study, diagnostic findings considering the problematic TKA based on the low-field MRI were interchangeable with the diagnostic findings based on CT. When comparing these two imaging modalities low-field MRI does not use any ionizing radiation, and offers the possibility to image soft tissues surrounding the prosthetic components. Since soft tissue problems are difficult to diagnose with CT, it can be expected that if soft tissue problems are present low-field MRI might make a difference. Moreover, when comparing purchasing and maintenance costs with high-field MRI, low-field MRI is just as CT by a rough estimation 3 times less expensive (176). Hence, from a cost perspective, low-field MRI may be a realistic competitor for CT. These factors made it relevant to study whether low-field MRI could be used as a cost- efficient and effective alternative in diagnosing problems around a problematic TKA.

Currently, there is not one imaging technique capable of differential diagnosis in the problematic knee after TKA. This study focused on the diagnostic value of low-field MRI. However, when evaluating the standard clinical work-up, it is remarkable that the conventional radiographs were of added value in only two out of the eight cases. In all other cases, additional imaging by CT, bone scintigraphy or stress radiographs was needed to further diagnose the problematic TKA. Low-field MRI is an addition to the diagnostic arsenal. Low-field MRI is capable of simultaneously diagnosing different pathologies, such as malalignment, loosening and patellofemoral arthrosis. In our study, low-field MRI could not diagnose laxity and other pathologies such as soft tissue problems. Infection was not present in our population and, therefore, the efficacy of low-field MRI on these subjects remains unknown. Further research is warranted to determine the clinical and cost-effective value of low-field MRI among the current imaging arsenal in patients who are dissatisfied with their TKA.

In conclusion, this feasibility study showed the potential of low-field MRI to image pathologies associated with a problematic total knee arthroplasty. The, diagnoses based on low-field MRI were comparable to the diagnoses based on CT. Our hypothesis of the added value of weight-bearing MRI to diagnose patellofemoral problems associated after primary TKA could not be supported in this feasibility study.

7

The pros and cons of
high field and low-field MRI

TO ASSESS CLINICAL PARAMETERS ASSOCIATED WITH TKA FAILURE.

7.0 Abstract

Introduction: There is a growing demand for a single diagnostic imaging modality that is able to diagnose the problematic knee after total knee arthroplasty (TKA). Magnetic resonance imaging (MRI) has proven to be an accurate imaging modality for diagnosing pathologies in native knees. However, after arthroplasty, a trade-off is required between metal artefact reducing capacities and image quality. Low-field MRI (0.25T) results in fewer metal artefacts and lower image quality compared with high-field MRI (1.5T). Technological developments such as metal artefact reducing sequences (MARS) have continued to improve high-field MRI over the years. In this context, the aim of the present study is to perform a qualitative evaluation of the performance of low- and high-field MRI, with and without MARS, in two case studies after TKA.

Method: A case study was performed. Two patients with a primary TKA were consecutively scanned using low-field and high-field MRI. The scans were performed in 2017 without metal artefact reducing sequences (MARS) and in 2019 with MARS. Scans were analysed for parameters associated with the causes of the problematic TKA, such as loosening and wear, instability, malalignment and patellofemoral problems. Hence, the prosthetic components were segmented, and an evaluation was performed focussing on soft tissue visibility, the measurement of rotational alignment parameters and quantification of patellofemoral parameters.

Results: In 2017 low-field MRI was less hampered by metal artefacts than high-field MRI without MARS. In 2019 MARS sequences became available, and high-field MRI outperformed low-field MRI, which seems especially beneficial for soft-tissue evaluation.

Conclusion: When the two imaging modalities are compared, it seems that high-field MRI offers superior image quality, whereas low-field MRI offers usability at low cost. Particularly since 2019, when high-end MARS sequences became available, high-field MRI has shown the potential to diagnose most of the essential causes of problematic knees. Perhaps these high-end MARS sequences could also be implemented in low-field MRI in the near future to enhance the clinical significance of low-field MRI for the analysis of TKA patients.

7.1 Introduction

Although the studies presented in the foregoing chapters (Chapter 4–6) show low-field MRI to be a promising image modality near total knee arthroplasty (TKA), low-field MRI, to be an attractive clinical alternative, must compete with the clinically available system of high-field MRI (Chapter 2 & 3).

As stated in Chapter 1, traditionally high-field MRI is hampered by susceptibly artefacts caused by metal implants and not capable of adequately imaging bone and its surrounding structures. Fortunately, over the past years, MRI sequences for high-field MRI have undergone vast improvements (177). In part, this is the result of the introduction of metal artefact reducing sequences (MARS), such as view-angle tilting (VAT), slice encoding for metal artefact correction (SEMAC) and multi-acquisition variable resonance image combination (MAVRIC) (123, 124, 178). Recent research shows that when SEMAC is used, distortions caused by metal artefacts are significantly reduced. This results in a more reliable evaluation of soft tissue structures (110, 179). In addition, when SEMAC is used, increased sensitivity and specificity values are found when diagnosing loosening of the prosthesis (110). However, high-end MARS sequences are not always available in hospitals. In our hospital (ZGT), SEMAC was added to the high-field system in 2019.

Parallel to these developments, low-field MRI (0.25 T) shows potential as a low-cost alternative for imaging orthopaedic hardware and its surroundings (Chapter 4 & 6). Low-field MRI might even be able to evaluate prosthetic loosening (Chapter 5) and patellofemoral and rotational alignment problems (Chapter 4 & 6). Compared to high-field MRI (1.5 T), low-field MRI shows advantages including reduction in the number of susceptibility artefacts, reduced purchase and maintaining costs and improved patient safety due to lower absorption of radio-frequency energy. On the downside, low-field MRI has a decreased SNR and resolution (180, 181).

Taken together, both field strengths have their specific advantages and both show potential to diagnose the problematic TKA (168) (Chapter 6). However, a direct comparison in terms of diagnostic performance between these imaging modalities does not yet exist for the specific case of the (problematic) TKA and its surrounding structures. Therefore, the aim of this study is to perform a qualitative evaluation of the performance of low- and high-field MRI, with and without MARS, in two case studies after TKA.

7.2 Method

7.2.1 Cases

To perform a qualitative evaluation of the performance of low- and high-field MRI after TKA, a comparative case study was performed. Two patients who were satisfied with their TKAs volunteered – patient 1 (female, 61 years, right knee, with a primary TKA + patella (NexGen, posterior stabilized, BiometZimmer), in August 2017) and patient 2 (male, 73 years, left knee, primary TKA (NexGen, posterior stabilized, ZimmerBiomet), in January 2019) – and informed consent was obtained. For this case study satisfied TKA patients were chosen because the study focusses primarily on the comparison between high- and low-field MRI for measuring several diagnostic parameters and not on the direct diagnostic value for one specific clinical problem.

7.2.2 Scan protocol

Patients were scanned on a low-field 0.25 Tesla MRI system (G-scan brio; Esaote SpA, Genova, Italy) at the University of Twente and high-field MRI (Magnetom Avanto; Siemens, Erlangen, Germany) at Hospital Group Twente (ZGT). Patients were scanned in supine positions using a dedicated knee coil and sequences according to the MRI scan protocol (table 7.1). In agreement with clinical practise at that time, the 2017 protocol for high-field MRI called for high bandwidth and short repetition times in order to reduce the artefact due to ferromagnetic material. In 2019 SEMAC sequences became available on the high-field system and were used instead. Since the systems were not at the same location, scans on low- and high-field MRI were performed within 14 days of each other.

7.2.3 Parameters

The MRI scans were assessed and analysed for parameters associated with TKA failure; loosening and wear, instability, malalignment and patellofemoral complaints (Figure 7.1) (6, 182).

Loosening and wear can be quantified by determining the position of the prosthesis with respect to its surroundings. If there is a relative movement between the prosthesis and the bony structures, loosening is suspected. Therefore, the possibility of segmenting the prosthetic 3D shape is chosen as a measure to determine the possibility offered by low- and high-field MRI for detecting loosening and wear.

Table 7.1: MRI scan protocol

MRI	Sequence	Plane	TR (ms)	TE (ms)	ST (mm)	FOV (mm²)	Time (min:sec)	Matrix	Pixel size (mm)
Low-field Patient 1 2017	SE, T1	Sagittal	1030	12	4.0	260x260	04:00	256 x 256	1.01
	FSE, PD-XMAR	Transversal	8570	12	4.0	230x230	04:17	256 x 256	0.90
	FSE, PD-XMAR	Coronal	6560	12	4.0	230x230	03:16	256 x 256	0.90
Low-field Patient 2 2019	SE, T1	Sagittal	330	18	4.0	200x200	03:00	512 x 512	0.39
	FSE, PD-XMAR	Transversal	7560	12	4.0	260x260	03:46	256 x 256	1.01
	FSE, PD-XMAR	Coronal	6810	12	4.0	260x260	03:24	256 x 256	1.01
High-field Patient 1 2017	TSE, T1-highBW	Sagittal	500	6	4.0	180x180	03:21	320 x 320	0.56
	TIRM, T1-highBW	Transversal	5980	33	4.0	140x140	05:08	256 x 256	0.55
	TSE, T1-hihgBW	Coronal	500	6	4.0	180x180	02:56	320 x 320	0.56
High-field Patient 2 2019	TSE, T1-SEMAC	Sagittal	401	6.3	4.0	180x180	05:35	320 x 320	0.56
	TSE, PD-SEMAC	Transversal	3800	34	4.0	160x160	03:44	256 x 256	0.63
	TSE, PD-SEMAC	Coronal	3000	34	4.0	180x180	04:09	384 x 384	0.47

SE = spin echo, FSE = fast spin echo, PD = proton density, X-MAR = metal artefact reduction based on view angle tilting, TSE = turbo spin echo, highBW = scanning with a high bandwidth, SEMAC = slice encoding for metal artefact correction, TR = repetition time, TE= echo time, ST = slice thickness, FOV = field of view
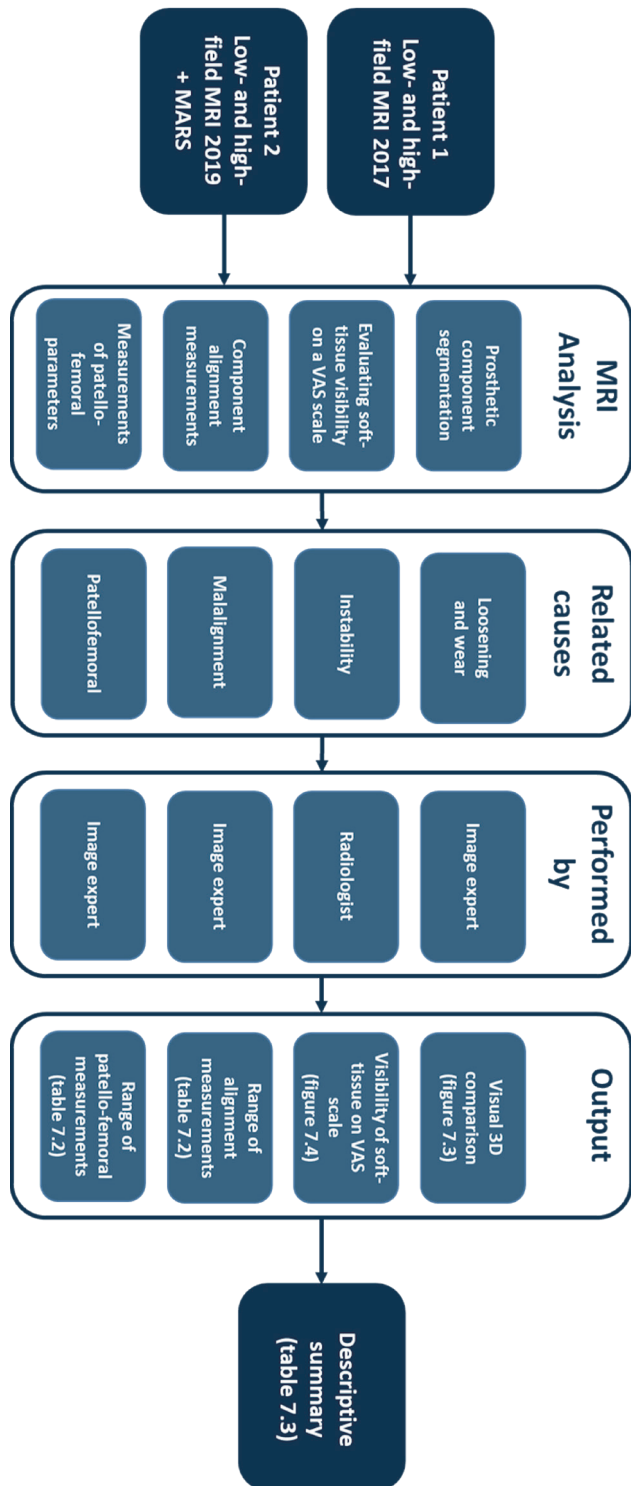
Moreover, loosening and wear result in fibrous membrane formation between the bone and the implant or cement (3), which can be visualized with MRI as hypertrophied synovitis (17) and is not expected to be found in satisfied patients.

Instability can be caused by soft tissue problems, such as tendon abnormalities, tendinosis or tendon rupture, or ligament deficiency (182). Therefore, the visibility of the tendon and ligament structures was assessed. Femoral and tibial component rotation of the prosthetic components was assessed by measuring rotational alignment parameters (91, 171).

Patellofemoral problems are associated with patellar (m)alignment. Therefore, four patellofemoral parameters were assessed.

7.2.4 Measurements and analysis

All measurements and analysis are summarized in Figure 7.1. To segment the prosthesis, the sagittal images of patients 1 and 2 on low-field and high-field MRI were selected and segmented by an image expert with over four years of experience in image analysis. Segmentation of the TKA was performed semi-automatically in Mimics (Mimics Research 21.0, Materialise NV) with the following procedure. First, a suitable threshold was determined by applying a profile line. Second, a region growing algorithm was applied. Third, abundant voxels were manually erased, and missing voxels were filled. Fourth, a 3D model was constructed from the connected voxels. Segmentation of the four scans was visually compared along with the total segmentation time.

To evaluated tendon and ligament visibility, the tendon and ligament structures were assessed by a radiologist with over 10 years of experience in musculoskeletal imaging. The visibility of the popliteus tendon, iliotibial tract, Hoffa's fat pad, patellar tendon, quadriceps tendon, medial collateral ligament, and lateral collateral ligament were rated on a 10-point visual analogue scale (VAS). Zero meant not visible and not accessible and 10 meant excellently visible and excellently accessible. An overview of the results per imaging modality was made.

To evaluate prosthetic component rotation, first the femoral component rotation was measured by the posterior condylar angle, the angle between the posterior condylar line and the surgical epicondylar axis (normal $3.5 \pm 1.2°$ for males or $0.3 \pm 1.2°$ for females (131)). Second, the tibial component rotation was measured by the angle between the geometric centre of the proximal tibial plateau, the distal level of the tibial tubercle and the posterior axis of the tibial plateau (normal 18^0 internal rotation (170)). These measurements were performed by the image analysis expert. Patellar alignment was assessed by quantifying the

Insall-Salvati ratio (IS) and Caton-Deschamps ratio (CD) for patellar height, patellar tilt angle (PTA) for patellar tilt and tibial tubercle groove distance (TT-TG) for patellar translation (MRIproI). These were measured in accordance with the protocol published earlier in Chapter 4. Rotational and patellar alignment parameters were determined semi-automatically by the image analysis expert using custom Matlab software (R2018a, The Mathworks, Natick, USA).

Based on the results of the analysis of the MRI images of the two patients, the imaging expert made an overall rating of the acquired results ranging from very poor (--) to excellent (++) for the following parameters: segmentation, visibility and alignment.

7.3 Results

With low- and high-field MRI, it was possible to image the TKA and the surrounding soft-tissue structures for both patients. Figure 7.2 shows an overview of the obtained images. All images are, to a certain extent, disturbed by susceptibility artefacts. Although, in general, the artefacts were more pronounced on high-field MRI than on low-field MRI, the images collected with the low-field system were harder to assess due to lower resolution and SNR. Segmentations of the prosthetic components on the sagittal MRI images are visualized in Figure 7.3. Based on visual comparison, the 3D model based on the high-field MRI data scanned in 2019 offered the best representation of the TKA shape. Second best was the 3D model obtained from the low-field MRI data collected in 2017. The 3D model obtained from the low-field image from 2019 was slightly inferior to the low-field 3D model from 2017, possibly due to motion artefacts and general patient variations in fat and fluid. The 3D model obtained from the 2017 high-field MRI data had the lowest scores. It showed a remarkable shift in the sagittal plane due the ferromagnetic artefact, which made the prosthetic shapes of the components harder to define.

When evaluating the total segmentation time, the low-field scans took only approximately 5 minutes, while the high-field high bandwidth of 2017 took 7 minutes and the SEMAC from the 2019 scan took 20 minutes to segment. The longer duration of the latter is due to the high resolution and low contrast difference between the pixels of the SEMAC images. The semi-automatic process underperformed, and many manual corrections were necessary.
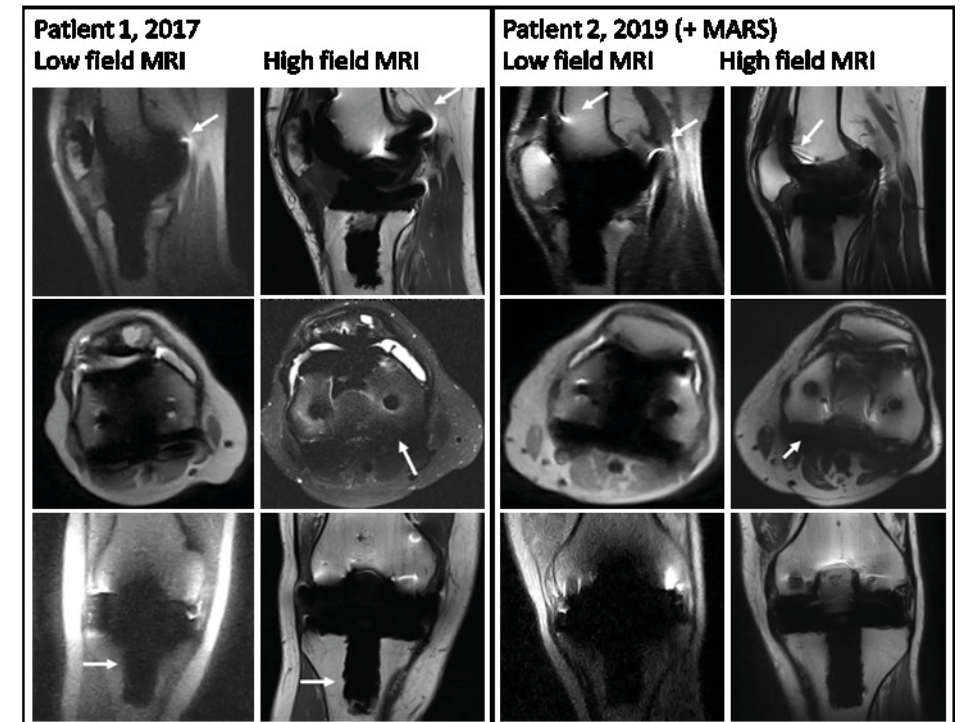
Figure 7.2. Low- and high-field MRI of the knee, images from 2017 & 2019 on both modalities in sagittal, transversal and coronal direction. In the sagittal direction artefacts induced by the prosthesis are most prominent at the borders of the femoral part (white arrows). In the transversal direction, the posterior condylar axis (white arrow) was sometimes hard to differentiate from the surrounding tissues. In the coronal direction, the tibial stem widened due to the artefact (white arrows). Overall the high-field MRI scans out of 2017 have the most prominent artefacts, the low-field scans the least SNR.

The visibility of the tendons and ligaments on the low-field and high-field MRI scans is presented in Figure 7.4. When the two imaging modalities are compared, soft-tissue structures could best be analysed based on high-field MRI. When using SEMAC the structures become even more visible. Only the popliteus tendon and Hoffa's fat pad remain hard to assess on both low-field and high-field MRI (+ SEMAC).

Both low-field and high-field MRI scans can be analysed for component alignment and the four patellofemoral parameters. In Table 7.2 the trend per parameter on low-field and high-field per patient is listed. Results suggest that the dispersion is increased for the measurements performed on the high-field MRI + MARS obtained in 2019 when compared with the high-field MRI analysis of 2017. Although differences between the low- and high-field analyses cannot be quantified, the image expert found it easier to assess the low-field MRI images for

alignment parameters due to the contrast between the prosthetic components and their surroundings, which was relatively better, especially when evaluating the 2017 data.

Patient 1, 2017
Low-field MRI | **High-field MRI** | **Patient 2, 2019 (+ MARS)** **Low-field MRI** | **High-field MRI**
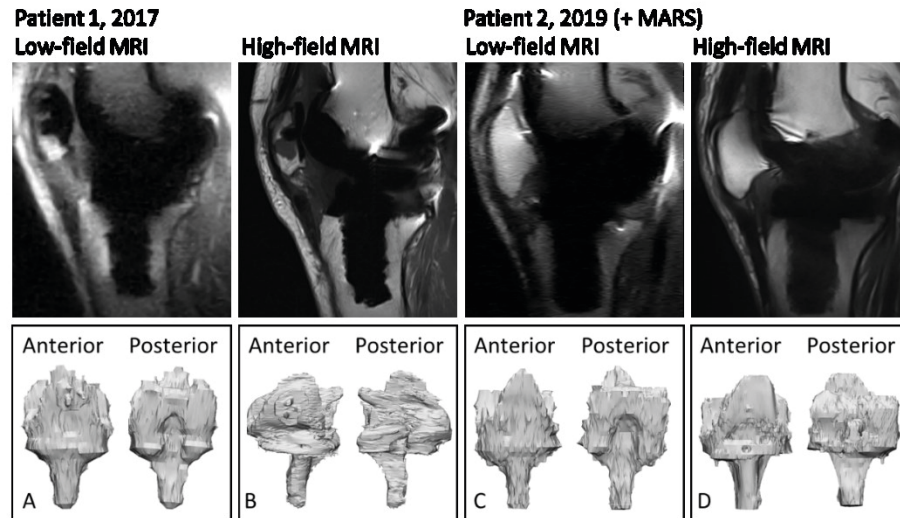
Figure 7.3. Segmentation of the sagittal low- and high-field MRI images. A) low-field MRI segmentation of patient 1, B) high-field MRI segmentation of patient 1, due to the susceptibility artefact the prosthetic are shifted. C) low-field MRI segmentation of patient 2, D) high-field MRI segmentation of patient 2 of a SEMAC acquisition. Even small details such as the cut-out in the anterior part of the tibial component are visible.
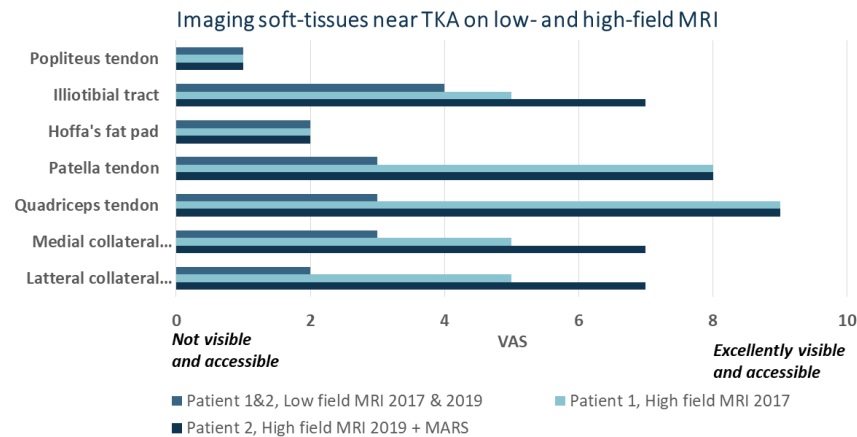
Figure 7.4. Soft-tissue evaluation on low-field and high-field MRI on a 10 point visual analogue scale (VAS).

When summarizing the results for segmentation potential, soft-tissue visibility, alignment and patellofemoral parameters per image modality (Table 7.3), in 2019, high-field MRI with SEMAC outperformed all other MRI setups in terms of resolution and image quality. In 2017, when these high-end sequences were not available, based on the summary of results low-field MRI offered better images.

Table 7.2: Measured component alignment and patellofemoral parameters

	Patient 1, 2017		Patient 2, 2019 (+ MARS)	
	Low-field MRI	High-field MRI	Low-field MRI	High-field MRI
Tibial component rotation (^{0})	24.3–33.9	32.5–34.6	19.2–24.0	20.4–25.7
Femoral component rotation (^{0})	1.2–4.7	2.5–5.9	0.1–1.7	0.0–1.4
Insall-Salvati ratio	0.86–0.99	0.89–1.12	0.38–0.50	0.41–0.53
Caton-Deschamps ratio	0.70–0.89	0.73–0.81	0.89–1.03	0.99–1.11
Patellar tilt angle (^{0})	2.1–2.8	2.4–7.6	5.8–6.7	6.2–7.3
Tibial tubercle groove distance (mm)	11.2–15.9	12.8–21.5	12.3–14.8	11.8–13.9

Table 7.3: Descriptive summary of the analysis results

	Patient 1, 2017		Patient 2, 2019 (+ MARS)	
	Low-field MRI	High-field MRI	Low-field MRI	High-field MRI
Segmentation	+	-	+/-	++ & -
Soft-tissue	-	+/-	-	+
Component Alignment	+	+	+	+
Patellofemoral	++	+	+	+

++ excellent, + good, +/- moderate, - poor, -- very poor.

7.4 Discussion

In this case study, a qualitative evaluation was performed in order to compare the performance of low- and high-field MRI, with and without MARS, in two satisfied TKA patients. Both modalities were capable of imaging the knee after TKA. Whereas in 2017 low-field MRI performed slightly better than high-field MRI, in 2019 high-field MRI outperformed low-field MRI when a SEMAC sequence was added. Both modalities were to some extent hampered by susceptibility artefacts due to the prosthetic components, which made the four evaluations –

segmentation, visualisation of tissues, measuring alignment parameters and measuring patellofemoral parameters – more challenging.

For prosthetic component segmentation, depending on the purpose, both field strengths have their advantages. High-field MRI is recommended when high accuracy is essential for the case and the time and financial aspects are acceptable for the purpose. The segmentation based on the high-field MRI data of patient 2 in 2019 gave the most accurate 3D representation of the prosthetic components, followed by the segmentation based on the low-field MRI data of patient 1 in 2017. Interestingly, low-field MRI segmentations were three times faster and could be executed using a more automated manner of analysis, which was a consequence of the greater homogeneity of pixel contrast values of the prosthetic components. When time and costs are important factors and many scans need to be segmented, low-field MRI might be the expedient choice. In current clinical practice, CT is the first choice to scan bony structures when an 3D model is needed. Current findings suggest that it would be interesting to explore low-field MRI for that specific purpose as a radiation-free alternative.

Soft-tissue structures could be better visualized with high-field MRI compared to low-field MRI. More specifically, high-field MRI with SEMAC performed best. This finding corresponds to previous literature in which SEMAC sequences were compared with high-bandwidth protocols, and images made with SEMAC had a superior visibility of soft-tissue structures when compared with the high-bandwidth protocol (110, 179). However, the question of whether the ability to visualise soft tissue will improve the ability to diagnose soft-tissue pathologies (i.e. tendon ruptures, ligament tears, muscle problems) remains to be answered. To diagnose soft-tissue pathologies, fat suppression is important. Regular fat suppression will increase the metal artefact, for which short tau inversion recovery (STIR) or turbo inversion recovery magnitude (TIRM) sequences are used in the presence of metal hardware (183). Unfortunately, these kinds of sequence reduce the SNR and, as a consequence, result in inferior image quality. Therefore, visualisation of the anatomical soft tissues around the prosthetic component is the first step, the second step being to image soft-tissue pathologies.

Rotational component alignment and patellofemoral parameters could be measured on both MRI modalities for the two cases included. This is in line with the findings in our earlier low-field study (Chapter 4) and for rotational alignment comparable to high-field MRI findings as presented in Chapter 3. In the present case study, only a subjective difference between the measurements based on low-field and high-field MRI is reported. Low-field MRI has less signal void around the prosthetic components, which made it easier to perform the alignment measurements.

This present study has obvious limitations. Firstly, the low-field MRI images made in 2019 were of lower quality than the images obtained in 2017. When comparing the low-field MRI images of 2019 with other low-field MRI images obtained in 2019 and published in previous studies (Chapter 4 & Chapter 6), it is remarkable that the low-field MRI images of patient 2 were of lower quality, probably due to motion and general patient differences. Secondly, the systems used in this study have their own technological specifications and sequences depending on the manufacturer. Especially for low-field MRI, there are major differences between the available systems (55). This makes it hard to extrapolate the results obtained in this study towards the performance of low-field MRI versus high-field MRI in general.

This case study illustrates that low-field and high-field MRI can image the knee after TKA with an image quality that makes it possible to perform several diagnostic measurements. Based on the results presented in this case study, low-field MRI cannot be regarded a substitute for high-field MRI in terms of image quality and artefact reduction, especially when compared to high-field MRI utilizing SEMAC sequences. At best, low-field MRI could be an alternative at least three times less expensive than high-field MRI when imaging the knee after TKA. Currently, for the low-field MRI system available for the current study a VAT sequence is the best MARS protocol available. Whereas MARS sequences for high-field MRI have improved over time, low-field sequences have not. If similar improvements were achieved in low-field MRI, it would perhaps improve the image quality near orthopaedic hardware in a similar way. The fact that low-field MRI sequences lags behind the high-field sequence in the development of improvements can be explained by the fact that low-field MRI is less often used in clinical practice, making it an inferior business case in which to invest in innovative sequences. As a consequence, the full potential of low-field MRI is not realized and may remain underutilized in the nearby future.

As stated before, the image quality of low-field MRI was rated lower than that of high-field MRI + SEMAC sequences. This can be explained by the technical specification of the systems. Low-field MRI uses a main magnetic field that is six times lower and gradients with a quarter of the force used in a high-field system. Although this will result in scans with fewer susceptibility artefacts, the SNR and the resolution will be reduced too. Image quality and the ability to perform diagnostic measurements are factors that are determinative for clinical relevance of an imaging modality. However, real clinical relevancy can only be proven in a clinical study in which patients with complaints are scanned using both high-field and low-field MRI and compared with the reference standard CT or surgical findings.

In conclusion, high-field MRI utilizing high-end metal artefact reducing sequences showed the greatest potential to image the knee after TKA; low-field MRI is a low-cost alternative. In recent years there have been considerable improvements in high-field MRI. It would be beneficial if the same impulse to innovate could be applied to low-field MRI to maximize its diagnostic capacity.

7

7

This chapter reflects on the work presented in this thesis and discusses challenges and future perspectives related to magnetic resonance imaging (MRI) around orthopaedic hardware. The present thesis aimed to investigate the properties of MRI as a diagnostic modality for various pathologies near orthopaedic hardware and explored the added value of weight-bearing low-field MRI for the diagnosis of several pathologies after total knee arthroplasty (TKA).

8.1 MRI near orthopaedic hardware

This thesis showed that both high- and low-field MRI, although hampered by susceptibility artefacts, are capable of diagnosing several pathologies in the proximity of orthopaedic hardware. With respect to the performance of high-field MRI (1.5 T), it appeared that image quality was sufficient to diagnose pathologies such as prosthetic infection, prosthetic loosening and wear, and prosthetic rotational malalignment (**chapter 3**). However, limited information could be extracted on aspects such as arthrofibrosis and soft tissue and patellofemoral problems after TKA. In addition, when evaluating the ability of high-field MRI to image tendon re-tears near titanium anchors, an adequate diagnosis was not always possible due to metal artefacts (**chapter 2**). These findings led to the investigation of low-field MRI as a possible alternative to high-field MRI (**chapters 4, 5 and 6**). Low-field MRI showed potential to image prosthetic rotational malalignment, prosthetic loosening (migration), and patellofemoral pathologies. In the comparative case study of high-field versus low-field MRI (**chapter 7**), metal artefact reducing sequences, which recently became available in our clinical practice, led to a considerable improvement in the performance of high-field MRI after TKA. Therefore, a re-evaluation of high-field MRI of orthopaedic hardware could be promising. It may be possible to adequately diagnose even more pathologies than described in **chapter 3**, for example patellofemoral and soft tissue problems.

An overview of the comparison between low-field and high-field MRI based on the findings presented in the earlier chapters of this thesis is provided in Figure 8.1. It can be stated that both low- and high-field MRI scans are helpful in the diagnosis of several pathologies. High-field MRI is able to diagnose prosthetic infection, prosthetic loosening and wear, prosthetic rotational alignment problems, and patellofemoral alignment problems (**chapters 3 and 6**).

Low-field MRI showed potential to diagnose prosthetic loosening, prosthetic rotational alignment, and patellofemoral alignment problems (**chapters 4 -7**). The findings presented in the previous chapters suggest that both high- and low-field MRI could be potential replacements of the current diagnostic
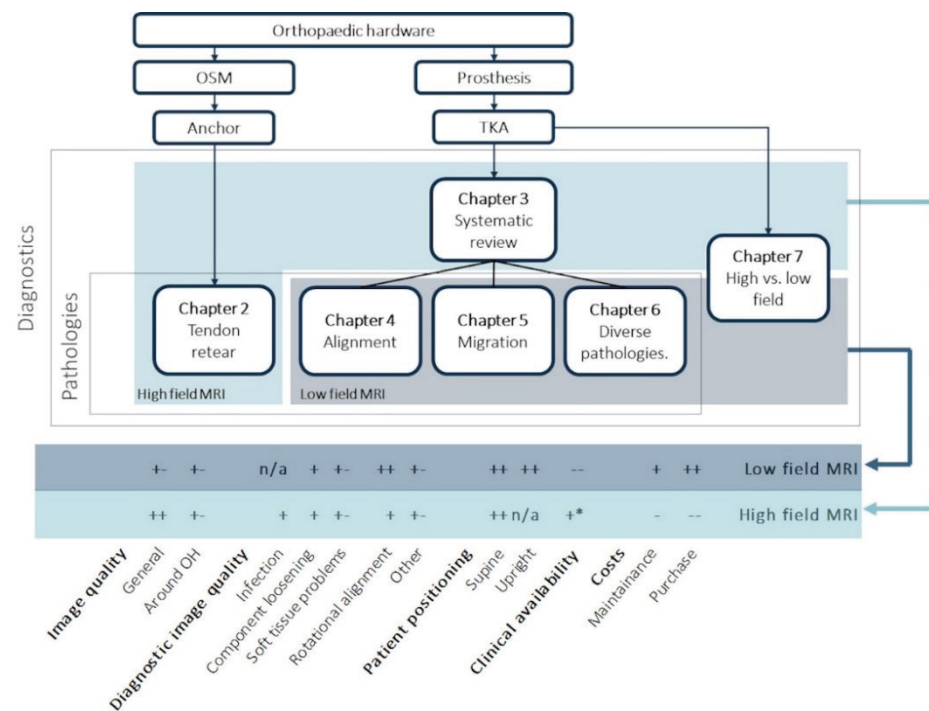
Figure 8.1. The performance of low-field and high-field MRI based on the findings presented in this thesis. OSM = osteosynthesis material, TKA = total knee arthroplasty, ++ outstanding, + good, +- adequate, - moderate, -- poor. *This table considers high-field MRI with state-of-the-art metal artefact reducing sequences (MARS). The availability of high-field MRI with MARS is +; for high-field without MARS, it is ++.

arsenal. If future research confirms the value of MRI near orthopaedic hardware, MRI might serve as a single imaging modality to investigate the probable causes of complaints near orthopaedic hardware (as OSM in general and after TKA in particular).

Even though low- and high-field MRI show potential as diagnostic imaging modalities for patients with complaints following the implementation of orthopaedic hardware, in current clinical practice, plain radiography and computed tomography (CT) are the imaging modalities of choice (184). Although the image quality of CT is disturbed by metal artefacts as well, in the short term it is expected that CT will remain the evaluation technology of choice because it has a high resolution, it is accessible, and it is a time-effective way of visualizing bony structures. CT-based techniques such as SPECT-CT and dual-energy CT might also offer options as differential diagnostic imaging modalities (160, 185).

However, unlike MRI, CT techniques use harmful ionizing radiation and are not capable of imaging soft tissue structures. Therefore, it is expected that

developments to improve imaging near orthopaedic hardware will focus on reducing the ionizing radiation dose of CT or replacing CT with ionizing radiation-free alternatives such as MRI or ultrasound (US). As stated in **chapter 2**, US is still highly operator dependent compared to CT and MRI. Therefore, MRI could be considered the most promising ionizing radiation-free alternative for bone and soft tissue evaluation near orthopaedic hardware (186, 187).

8.2 Weight-bearing MRI

Weight-bearing low-field MRI, which represents the gravitational load in daily activities in the native knee, is described in the literature as presenting the opportunity to add diagnostic value for several knee pathologies, especially when patellofemoral kinematics are assessed in several flexion angles (31, 188). In this thesis, weight-bearing low-field MRI was used to evaluate the knee, and in particular the patellofemoral joint, in a loaded condition after TKA in patients with and without complaints (**chapters 4 and 6**). A hypothesized advantage of low-field MRI compared to high-field MRI was that it offers the opportunity to scan in a weight-bearing condition, which represents the gravitational load during daily activities. It was expected that scanning in a weight-bearing condition after TKA would make available useful information about patellofemoral kinematics and soft tissue problems, which could be used to diagnose the cause of problematic TKA. For comparison, two explorative samples – one with and one without a problematic TKA – were investigated. Patellofemoral problems were present and were assessed by measuring four patellofemoral parameters associated with patellofemoral kinematics. The TT-TG distance decreased in the weight-bearing condition in both studies. This reduction in TT-TG distance is most likely to occur due to quadriceps activation in the weight-bearing condition (141). The Caton-Deschamps ratio and patellar tilt angle decreased in the weight-bearing condition, and differences in deviation between patients with and without complaints were seen (**chapters 4 and 6**). Based on these findings, it can be concluded that after TKA, patellofemoral measurements can be analysed using MRI with good reproducibility. However, only relatively small differences in patellofemoral parameters were found between the weight-bearing and the supine conditions. Because of the design of the study (prospective cohort), the cohort was already filled before pathologies were diagnosed. Therefore, coincidentally, soft tissue problems were not presented and were unfortunately not part of the scope of the study. Within problematic TKA patients, more dispersion between the supine and weight-bearing positions was found in the patellofemoral parameters compared to the group of TKA patients without complaints. However, it should be further explored if this dispersion is of clinical value. If joint movements could

be introduced in addition to weight-bearing during the MRI, enabling knee flexion and extension, clinically relevant differences might be found between flexion and extension in the supine and weight-bearing conditions.

This thesis focused primarily on the knee joint after arthroplasty. During the preliminary research that was conducted before the start of the studies described in **chapters 4-7**, low-field MRI sequences were tested and optimised. These sequences were mostly assessed on the native knees of healthy volunteers, which resulted in images with adequate quality. In the literature, the diagnostic value of low-field MRI of the native joint is also described as adequate (53, 189, 190). This might indicate that weight-bearing MRI could be successfully utilized to assess other (pathological) native joint conditions, for example in the spine, ankle, and foot. It might even offer an opportunity to evaluate the amount of osteoarthrosis after a unilateral knee arthroplasty at the contralateral side (188, 191-194).

An MRI modality with the ability to scan in an upright weight-bearing position remains interesting. Upright MRI is not possible at high field strengths. To mimic an upright weight-bearing condition, mechanical loading jigs are sometimes designed and applied within the MRI scanner to allow for 'physiological' loading conditions in a supine position (195). Various studies have used such a mechanical loading device to image the native knee and have found considerable changes under a loaded condition as compared to an unloaded condition when focusing, for example, on the meniscus and cartilage (196-198). However, mimicking the physiological loading conditions within a high-field MRI scanner is challenging, because the loading conditions from the jigs hardly reproduce the gravitational load, and the limited bore diameter reduces the physiological positions of the extremities. Therefore, such systems are currently mostly used in a research setting, while upright weight-bearing low-field MRI can easily be used in a clinical setting. Although the upright weight-bearing low-field MRI studies presented in this thesis did not improve the diagnosis of problematic TKA, low-field upright weight-bearing MRI itself remains interesting. Therefore, in general, it is recommended that further upright low-field MRI research should primarily focus on the abovementioned promising applications related to the native joint in a gravitational loaded condition.

8.3 Clinical implications and future perspectives

High-field MRI with state-of-the-art metal artefact reducing sequences can be used more often instead of CT or SPECT in the differential diagnosis of the problematic knee. **Chapter 3** showed the diagnostic accuracy of high-field MRI in diagnosing the problematic knee. Although the literature indicates that high-field

MRI is a promising means of diagnosing prosthetic infection, prosthetic loosening and wear, prosthetic alignment problems, and patellofemoral alignment problems, it is presently not often used in clinical practice. Based on the findings of this thesis, high-field MRI should be considered as a potential replacement of parts of the current diagnostic arsenal to diagnose problematic TKA. This is comparable with findings in the literature describing the clinical applicability of MRI near arthroplasty in general (49, 182, 199, 200). Once sequences have improved further, MRI might become a viable substitute for CT in the diagnostic process.

Low-field MRI also shows potential for this application. **Chapter 6** described the first feasibility study of the use of low-field MRI to diagnose patients with problematic TKA. Although the image quality was lower than expected, the images were of adequate quality to diagnose several pathologies. Since the low-field studies described in this thesis were small-cohort pilot and feasibility studies, further clinical research is needed to confirm the diagnostic capacity of low-field MRI of problematic TKA.

When comparing the advantages of the field strengths, low-field MRI seems to have an adequate image quality (**chapter 6 and 7**) with lower estimated purchase (± €450.000,-) and maintenance (± €15.000,-) costs[1]. On the other hand, high-field MRI has better clinical accessibility, since it is available in almost all Western hospitals and has a superior image quality due to the increased SNR (**chapter 7**). However, a potential disadvantage of high-field MRI is that its purchase (± €1.500.000,-) and yearly maintenance (± €75.000,-) costs[1] are at least three times higher than those of low-field MRI. It is known that susceptibility artefacts due to metal implants vary depending on the magnetic field strength (183). However, the balance needs to be found between the most adequate magnetic field strength to reduce artefacts and the desired field strength to retain sufficient image quality. Therefore, **Chapter 7** presented a typical example of the performance of high-field and low-field MRI when metal artefact reducing sequences were used and showed that high-field MRI improved significantly with the use of Slice Encoding for Metal Artefact Correction (SEMAC).

Over the past few years, the use of high-end metal artefact reducing sequences has expanded from the research setting to be introduced in clinical practice (183). Since low-field MRI is less frequently used in clinical practice, the software and hardware developments mostly focus on high-field MRI (169, 201). Unfortunately, these high-end sequences are only available on high-field MRI systems. Moreover, these sequences are expensive and are therefore sometimes not available in regional hospitals. Today, clinical MRI is mostly performed at 1.5 T or 3 T, and for research purposes, even 7 T is used (169). A higher field strength

offers increased SNR and resolution. However, the increased SNR and resolution do not necessarily improve clinical relevance.

That a higher field strength is not directly linked to increased clinical relevance is demonstrated in a study by Campbell et al. (169), which focused on improving low-field MRI. These authors modified a 1.5T Siemens MRI system such that it functioned as a low-field 0.55T MRI scanner. In this approach, the low field strength is combined with the high-performance hardware in order to retain the gradient performance and the receiver system. Images of high susceptibility regions of the lung were improved compared to conventional 1.5T MRI. This resulted in reduced off-resonance spiral blurring and reduced signal distortion caused by field inhomogeneities. Since imaging around orthopaedic hardware and soft tissue also involves high susceptibility regions, these techniques may be interesting to explore and to further improve imaging near orthopaedic hardware. Moreover, Campbell et al. used a prototype spiral spin-echo sequence which, on average, recovered the SNR to 57%, which is typical for the 1.5 T system. This technique made it possible to image high susceptibility regions, which also indicates the possibility to use low-field MRI to ionize radiation-free operative guidance and guiding during radiation therapy (201, 202). This illustrates the high potential of a combination of high-end hardware, low field strength and specifically tailored sequences. At the moment, Siemens™ (Siemens, Erlangen, Germany) is even planning to make this high-end, low-field system commercially available. Future research should explore whether such high-end, low-field MRI systems will also reduce susceptibility artefacts in the proximity of orthopaedic hardware.

These kinds of recent developments in MRI technology (including hardware and software) show that the trend of ever-increasing field strengths is returning for some applications and that low-field MRI may attract renewed interest for some applications (203). These examples show the broader applicability of low-field MRI, which makes the purchase of such a system more attractive. Taken together with its limited costs, lack of ionizing radiation, and usability in several environments (**chapter 7**), low-field MRI remains an imaging modality to keep in mind.

Alongside MRI development, other aspects that affect the image quality of orthopaedic hardware can be considered. Within the orthopaedic field, there is a trend to generate metal-free implants to reduce the chances of negative metal allergy reactions and to produce lower cost solutions. Currently, orthopaedic hardware is mostly made out of titanium and cobalt chrome alloys (204). However, alternative (metal-free) materials are considered for TKA components. Recent research has explored the viability of a knee arthroplasty made out of PEEK

(49, 205-208), a material that will not cause susceptibility artefacts. If in the future orthopaedic hardware is made out of PEEK, the imaging problem described in the current thesis might be solved. However, metal-free implants still have a long development path ahead. Currently, more than 450,000 people in the Netherlands have a metal arthroplasty (209). If these people present with complaints in the near future, an imaging modality that can image near metal will be indispensable.

As described above, technology in the imaging field is evolving at a rapid pace, which risks that research performed on a specific system may become outdated within a short period of time. This was, to some extent, also the case for some of the research presented in this thesis, for example the sequences used to image the rotator cuff re-tear described in **chapter 2** and the first case described in **chapter 7**. With 2020 MRI systems, imaging near orthopaedic hardware should be less hampered by metal artefacts, and scans should be more reliable for diagnostic purposes than described in the discussion of **chapter 2**.

Therefore, there is a need for study designs that incorporate rapid technological developments and remain reliable in obtaining evidence regarding treatment and diagnosis. Hospitals aim to work according to evidence-based practice. However, the large controlled studies that are considered to be the most reliable evaluation in medical science are time consuming, and it can take several years before such studies are reported on. This period will only increase due to the new medical device regulations (32). Closer collaboration between manufacturers, hospitals, and universities might solve part of this challenge, for example where manufacturers share their software, sequences and so on so that researchers can improve them, and where hospitals can continuously evaluate their healthcare improvements with short clinical trials in close collaboration with manufacturers and researchers to maintain continuous innovation and validation. Once the hardware and software of the hospitals' current MRI systems (1.5T) have been updated, their performance in the proximity of orthopaedic hardware will be improved.

When considering the cost aspects of most newly introduced imaging modalities such as high-field MRI, it is clear that these innovations come at a price. According to the Dutch government's general clinical mission, medical providers are obliged to deliver effective care (210). Low-field MRI is a more compact system and has lower purchase and maintenance costs, which offers the opportunity to reorganize care as we know it and bring it closer to the patient's home. As stated in the Dutch Scientific Agenda, medical providers should focus on prevention, personalised care, and the right allocation of care (210). The usability of low-field MRI aligns perfectly with this statement. From this perspective, it would be interesting to reconsider the organization of the healthcare system. What if every

city had its low-field systems at a health centre, where general practitioners together with physiotherapists, podiatrists, and other health professionals with the right indication or suspicion could request MRIs for their clients? Patients who report joint complaints could get a low-field MRI scan of the problematic joint, which could be remotely assessed by a radiologist or computer algorithm. In the near future, machine learning or deep learning techniques can be used to develop an automatic detection algorithm for osteoarthritis, meniscus problems, anterior cruciate ligament tears, or other pathologies. Such artificial intelligence algorithms would provide a rapid and inexpensive way to diagnose several musculoskeletal problems. With these innovative developments, the general practitioner can remain in charge of patient treatment. As a consequence, this might reduce the referrals to (the more expensive) second line of care. Furthermore, it would introduce an accessible imaging modality in the first line of care, which might lead to earlier diagnoses, in turn reducing the use of more expensive future treatments. This would bring healthcare closer to home, reduce the burden on the hospitals, and offer an option for pre-scan, prevention and early monitoring for some diseases at a reduced cost.

8.4 Conclusion

The current thesis demonstrated the ability of both low- and high-field MRI to diagnose prosthetic loosening and wear, prosthetic rotational alignment, and patellofemoral alignment. Based on the results, it can be concluded that MRI in general could be a useful imaging modality for patients with orthopaedic hardware implants (e.g. titanium suture anchors, TKA). The hypothesized added value of weight-bearing in low-field MRI for TKA patients could not be confirmed, and more research on this subject is needed. In recent years, high-field MRI sequences have improved, which has made imaging modality near orthopaedic hardware more interesting. When high-end sequences are used, high-field MRI is less hampered by metal artefacts and is a promising modality to visualize the soft tissue structures around the prosthetic component.

8

8

References

1. Roberts T, M Prummer C, N Papaliodis D, Uhl R, A Wagner T. History of the Orthopedic Screw. Orthopedics. 2013;36:12-4.

2. Thiele K, Fussi J, Perka C, Pfitzner T. [The Berlin diagnostic algorithm for painful knee TKA]. Orthopade. 2016;45(1):38-46.

3. Beltran LS, Bencardino JT, Steinbach LS. Postoperative MRI of the shoulder. Journal of magnetic resonance imaging : JMRI. 2014;40(6):1280-97.

4. Endo Y, Geannette C, Chang WT. Imaging evaluation of polyethylene liner dissociation in total hip arthroplasty. Skeletal Radiology. 2019;48(12):1933-9.

5. Van den Wyngaert T, Palli SR, Imhoff RJ, Hirschmann MT. Cost-Effectiveness of Bone SPECT/CT in Painful Total Knee Arthroplasty. J Nucl Med. 2018;59(11):1742-50.

6. Hirschmann MT, Henckel J, Rasch H. SPECT/CT in patients with painful knee arthroplasty-what is the evidence? Skeletal Radiol. 2013;42(9):1201-7.

7. Fritz J, Lurie B, Potter HG. MR Imaging of Knee Arthroplasty Implants. RadioGraphics. 2015;35(5):1483-501.

8. Dean Deyle G. The role of MRI in musculoskeletal practice: a clinical perspective. The Journal of manual & manipulative therapy. 2011;19(3):152-61.

9. Schenck JF. The role of magnetic susceptibility in magnetic resonance imaging: MRI magnetic compatibility of the first and second kinds. Medical physics. 1996;23(6):815-50.

10. Kumar NM, de Cesar Netto C, Schon LC, Fritz J. Metal Artifact Reduction Magnetic Resonance Imaging Around Arthroplasty Implants: The Negative Effect of Long Echo Trains on the Implant-Related Artifact. Investigative radiology. 2017;52(5):310-6.

11. Vandevenne JE, Vanhoenacker F, Parizel P, Butts Pauly K, Lang RK. Reduction of metal artifacts in musculoskeletal MR imaging. 90(5):345-9 ed: JBR-BTR; 2007.

12. Heyse TJ, Figiel J, Hähnlein U, Timmesfeld N, Schofer MD, Fuchs-Winkelmann S, et al. MRI after patellofemoral replacement: the component-bone interface and rotational alignment. HSS J. 2013;9(2):108-12.

13. Sofka CM, Potter HG, Figgie M, Laskin R. Magnetic resonance imaging of total knee arthroplasty. Clinical orthopaedics and related research. 2003(406):129-35.

14. Price AJ, Alvand A, Troelsen A, Katz JN, Hooper G, Gray A, et al. Knee replacement. The Lancet. 2018;392(10158):1672-82.

15. Kahlenberg CA, Nwachukwu BU, McLawhorn AS, Cross MB, Cornell CN, Padgett DE. Patient Satisfaction After Total Knee Replacement: A Systematic Review. HSS J. 2018;14(2):192-201.

16. Sgroi M, Faschingbauer M, Javaheripour-Otto K, Reichel H, Kappe T. Can rotational alignment of total knee arthroplasty be measured on MRI? Arch Orthop Trauma Surg. 2015;135(11):1589-94.

17. Motsis EK, Paschos N, Pakos EE, Georgoulis AD. Review article: Patellar instability after total knee arthroplasty. Journal of orthopaedic surgery (Hong Kong). 2009;17(3):351-7.

18. Hirschmann MT, Konala P, Iranpour F, Kerner A, Rasch H, Friederich NF. Clinical value of SPECT/CT for evaluation of patients with painful knees after total knee arthroplasty--a new dimension of diagnostics? BMC Musculoskelet Disord. 2011;12:36-.

19.   Cyteval C. Imaging of knee implants and related complications. Diagnostic and Interventional Imaging. 2016;97(7):809-21.

20.   Li AE, Sneag DB, Greditzer HGt, Johnson CC, Miller TT, Potter HG. Total Knee Arthroplasty: Diagnostic Accuracy of Patterns of Synovitis at MR Imaging. Radiology. 2016;281(2):499-506.

21.   Li AE, Sneag DB, Miller TT, Lipman JD, Padgett DE, Potter HG. MRI of polyethylene tibial inserts in total knee arthroplasty: Normal and abnormal appearances. American Journal of Roentgenology. 2016;206(6):1264-71.

22.   Chang MJ, Lim H, Lee NR, Moon Y-W. Diagnosis, causes and treatments of instability following total knee arthroplasty. Knee Surg Relat Res. 2014;26(2):61-7.

23.   Plodkowski AJ, Hayter CL, Miller TT, Nguyen JT, Potter HG. Lamellated hyperintense synovitis: Potential MR imaging sign of an infected knee arthroplasty. Radiology. 2013;266(1):256-60.

24.   Hirschmann A, Hirschmann MT. Chronic Knee Pain: Clinical Value of MRI versus SPECT/CT. Semin Musculoskelet Radiol. 2016;20(1):3-11.

25.   Thakkar RS, Thakkar SC, Srikumaran U, McFarland EG, Fayad LM. Complications of rotator cuff surgery-the role of post-operative imaging in patient care. The British journal of radiology. 2014;87(1039):20130630.

26.   Zlatkin MB. MRI of the postoperative shoulder. Skeletal Radiol. 2002;31(2):63-80.

27.   Mariani S, La Marra A, Arrigoni F, Necozione S, Splendiani A, Di Cesare E, et al. Dynamic measurement of patello-femoral joint alignment using weight-bearing magnetic resonance imaging (WB-MRI). Eur J Radiol. 2015;84(12):2571-8.

28.   Izadpanah K, Weitzel E, Vicari M, Hennig J, Weigel M, Sudkamp NP, et al. Influence of knee flexion angle and weight bearing on the Tibial Tuberosity-Trochlear Groove (TTTG) distance for evaluation of patellofemoral alignment. Knee Surg Sports Traumatol Arthrosc. 2014;22(11):2655-61.

29.   Becher C, Fleischer B, Rase M, Schumacher T, Ettinger M, Ostermeier S, et al. Effects of upright weight bearing and the knee flexion angle on patellofemoral indices using magnetic resonance imaging in patients with patellofemoral instability. Knee Surg Sports Traumatol Arthrosc. 2017;25(8):2405-13.

30.   Teng HL, Chen YJ, Powers CM. Predictors of patellar alignment during weight bearing: an examination of patellar height and trochlear geometry. Knee. 2014;21(1):142-6.

31.   Bruno F, Barile A, Arrigoni F, Laporta A, Russo A, Carotti M, et al. Weight-bearing MRI of the knee: a review of advantages and limits. Acta Biomed. 2018;89(1-S):78-88.

32.   Edelman RR. The history of MR imaging as seen through the pages of radiology. Radiology. 2014;273(2 Suppl):S181-200.

33.   Lauterbur PC. Image Formation by Induced Local Interactions: Examples Employing Nuclear Magnetic Resonance. Nature. 1973;242(5394):190-1.

34.   Berquist TH. Magnetic resonance imaging: preliminary experience in orthopedic radiology. Magnetic resonance imaging. 1984;2(1):41-52.

35.   Li KC, Henkelman RM, Poon PY, Rubenstein J. MR imaging of the normal knee. Journal of computer assisted tomography. 1984;8(6):1147-54.

36.   Kieft GJ, Bloem JL, Obermann WR, Verbout AJ, Rozing PM, Doornbos J. Normal shoulder: MR imaging. Radiology. 1986;159(3):741-5.

37.   Marques JP, Simonis FFJ, Webb AG. Low-field MRI: An MR physics perspective. Journal of Magnetic Resonance Imaging. 2019;49(6):1528-42.

38.   Radzi S, Cowin G, Robinson M, Pratap J, Volp A, Schuetz MA, et al. Metal artifacts from titanium and steel screws in CT, 1.5T and 3T MR images of the tibial Pilon: a quantitative assessment in 3D. Quant Imaging Med Surg. 2014;4(3):163-72.

39.   Lee CS, Davis SM, McGroder C, Stetson WB, Powell SE. Analysis of Low-Field Magnetic Resonance Imaging Scanners for Evaluation of Knee Pathology Based on Arthroscopy. Orthop J Sports Med. 2013;1(7):2325967113513423-.

40.   Vandevenne JE, Vanhoenacker FM, Parizel PM, Butts Pauly K, Lang RK. Reduction of metal artefacts in musculoskeletal MR imaging. JBR-BTR : organe de la Societe royale belge de radiologie (SRBR) = orgaan van de Koninklijke Belgische Vereniging voor Radiologie (KBVR). 2007;90(5):345-9.

41.   Ai T, Padua A, Goerner F, Nittka M, Gugala Z, Jadhav S, et al. SEMAC-VAT and MSVAT-SPACE sequence strategies for metal artifact reduction in 1.5T magnetic resonance imaging. Investigative radiology. 2012;47(5):267-76.

42.   Lu W, Pauly KB, Gold GE, Pauly JM, Hargreaves BA. SEMAC: Slice Encoding for Metal Artifact Correction in MRI. Magn Reson Med. 2009;62(1):66-76.

43.   Carl M, Koch K, Du J. MR imaging near metal with undersampled 3D radial UTE-MAVRIC sequences. Magn Reson Med. 2013;69(1):27-36.

44.   Reichert M, Ai T, Morelli JN, Nittka M, Attenberger U, Runge VM. Metal artefact reduction in MRI at both 1.5 and 3.0 T using slice encoding for metal artefact correction and view angle tilting. The British journal of radiology. 2015;88(1048):20140601-.

45.   Chen CA, Chen W, Goodman SB, Hargreaves BA, Koch KM, Lu W, et al. New MR imaging methods for metallic implants in the knee: artifact correction and clinical impact. Journal of magnetic resonance imaging : JMRI. 2011;33(5):1121-7.

46.   Hayter CL, Koff MF, Shah P, Koch KM, Miller TT, Potter HG. MRI After Arthroplasty: Comparison of MAVRIC and Conventional Fast Spin-Echo Techniques. American Journal of Roentgenology. 2011;197(3):W405-W11.

47.   den Harder JC, van Yperen GH, Blume UA, Bos C. Off-resonance suppression for multispectral MR imaging near metallic implants. Magn Reson Med. 2015;73(1):233-43.

48.   Lee MJ, Kim S, Lee SA, Song HT, Huh YM, Kim DH, et al. Overcoming artifacts from metallic orthopedic implants at high-field-strength MR imaging and multi-detector CT. Radiographics. 2007;27(3):791-803.

49.   Mushtaq N, To K, Gooding C, Khan W. Radiological Imaging Evaluation of the Failing Total Hip Replacement. Front Surg. 2019;6:35.

50.   Talbot BS, Weinberg EP. MR Imaging with Metal-suppression Sequences for Evaluation of Total Joint Arthroplasty. RadioGraphics. 2015;36(1):209-25.

51.   Magee T, Shapiro M, Williams D. Comparison of high-field-strength versus low-field-strength MRI of the shoulder. AJR American journal of roentgenology. 2003;181(5):1211-5.

52.   Thomsen HS, Larsen L, Chabanova E, Moller JM. Open low-field-strength MRI of the shoulder is not so bad. AJR American journal of roentgenology. 2004;182(6):1601-2.

53.   Ghazinoor S, Crues JV, 3rd, Crowley C. Low-field musculoskeletal MRI. Journal of magnetic resonance imaging : JMRI. 2007;25(2):234-44.

54.   Lee CS, Davis SM, McGroder C, Kouk S, Sung RM, Stetson WB, et al. Analysis of Low-Field MRI Scanners for Evaluation of Shoulder Pathology Based on Arthroscopy. Orthop J Sports Med. 2014;2(7):2325967114540407-.

55. Marques JP, Simonis FFJ, Webb AG. Low-field MRI: An MR physics perspective. Journal of magnetic resonance imaging : JMRI. 2019;49(6):1528-42.

56. Le BTN, Wu XL, Lam PH, Murrell GAC. Factors predicting rotator cuff retears: An analysis of 1000 consecutive rotator cuff repairs. American Journal of Sports Medicine. 2014;42(5):1134-42.

57. Thakkar RS, Thakkar SC, Srikumaran U, McFarland EG, Fayad LM. Complications of rotator cuff surgery-the role of post-operative imaging in patient care. British Journal of Radiology. 2014;87(1039).

58. Zlatkin MB. MRI of the postoperative shoulder. Skeletal Radiology. 2002;31(2):63-80.

59. Beltran LS, Bencardino JT, Steinbach LS. Postoperative MRI of the shoulder. Journal of Magnetic Resonance Imaging. 2014;40(6):1280-97.

60. Bancroft LW, Wasyliw C, Pettis C, Farley T. Postoperative Shoulder Magnetic Resonance Imaging. Magnetic Resonance Imaging Clinics of North America. 2012;20(2):313-25.

61. Knudsen HB, Gelineck J, Søjbjerg JO, Olsen BS, Johannsen HV, Sneppen O. Functional and magnetic resonance imaging evaluation after single-tendon rotator cuff reconstruction. Journal of Shoulder and Elbow Surgery. 1999;8(3):242-6.

62. Vandevenne JE, Vanhoenacker FM, Parizel PM, ButtsPauly K, Lang PK. Reduction of metal artefacts in musculoskeletal MR imaging. Journal Belge de Radiologie. 2007;90(5):345-9.

63. Owen RS, Iannotti JP, Kneeland JB, Dalinka MK, Deren JA, Oleaga L. Shoulder after surgery: MR imaging with surgical validation. Radiology. 1993;186(2):443-7.

64. Motamedi AR, Urrea LH, Hancock RE, Hawkins RJ, Ho C. Accuracy of magnetic resonance imaging in determining the presence and size of recurrent rotator cuff tears. Journal of Shoulder and Elbow Surgery. 2002;11(1):6-10.

65. Khazzam M, Kuhn JE, Mulligan E, Abboud JA, Baumgarten KM, Brophy RH, et al. Magnetic resonance imaging identification of rotator cuff retears after repair: Interobserver and intraobserver agreement. American Journal of Sports Medicine. 2012;40(8):1722-7.

66. Goutallier D, Postel JM, Bernageau J, Lavau L, Voisin MC. Fatty muscle degeneration in cuff ruptures: Pre- and postoperative evaluation by CT scan. Clinical orthopaedics and related research. 1994(304):78-83.

67. Warner JJP, Higgins L, Parsons Iv IM, Dowdy P. Diagnosis and treatment of anterosuperior rotator cuff tears. Journal of Shoulder and Elbow Surgery. 2001;10(1):37-46.

68. Svanholm H, Starklint H, Gundersen HJG, Fabricius J, Barlebo H, Olsen S. Reproducibility of histomorphologic diagnoses with special reference to the kappa statistic. APMIS. 1989;97(8):689-98.

69. Pawaskar AC, Kekatpure A, Cho NS, Rhee YG, Jeon IH. Magnetic resonance appearance of bioabsorbable anchor screws for double row arthroscopic rotator cuff repairs. Indian Journal of Orthopaedics. 2015;49(2):164-70.

70. Dhawan A, Ghodadra N, Karas V, Salata MJ, Cole BJ. Complications of bioabsorbable suture anchors in the shoulder. American Journal of Sports Medicine. 2012;40(6):1424-30.

71. Ai T, Padua A, Goerner F, Nittka M, Gugala Z, Jadhav S, et al. SEMAC-VAT and MSVAT-SPACE sequence strategies for metal artifact reduction in 1.5T magnetic resonance imaging. Investigative Radiology. 2012;47(5):267-76.

72. De Jesus JO, Parker L, Frangos AJ, Nazarian LN. Accuracy of MRI, MR arthrography, and ultrasound in the diagnosis of rotator cuff tears: A meta-analysis. American Journal of Roentgenology. 2009;192(6):1701-7.

73. Adler RS. Postoperative rotator cuff. Seminars in Musculoskeletal Radiology. 2013;17(1):12-9.

74. Charousset C, Bellaïche L, Duranthon LD, Grimberg J. Accuracy of CT arthrography in the assessment of tears of the rotator cuff. Journal of Bone and Joint Surgery - Series B. 2005;87(6):824-8.

75. Roy JS, BraÃn C, Leblond J, Desmeules F, Dionne CE, MacDermid JC, et al. Diagnostic accuracy of ultrasonography, MRI and MR arthrography in the characterisation of rotator cuff disorders: A systematic review and meta-analysis. British Journal of Sports Medicine. 2015;49(20):1316-28.

76. Mohana-Borges AVR, Chung CB, Resnick D. MR Imaging and MR Arthrography of the Postoperative Shoulder: Spectrum of Normal and Abnormal Findings. Radiographics. 2004;24(1):69-85.

77. Chung CB, Steinbach LS. MRI of the upper extremity: shoulder, elbow, wrist and hand 2010.

78. Ghazinoor S, Crues Iii JV, Crowley C. Low-field musculoskeletal MRI. Journal of Magnetic Resonance Imaging. 2007;25(2):234-44.

79. Lee CS, Davis SM, McGroder C, Stetson WB, Powell SE. Analysis of low-field magnetic resonance imaging scanners for evaluation of knee pathology based on arthroscopy. Orthopaedic Journal of Sports Medicine. 2013;1(7).

80. Radzi S, Cowin G, Robinson M. Metal artifacts from titanium and steel screws in CT, 1. 5T and 3T MR images of the tibial Pilon: A quantitative assessment in 3D. Quant Imaging Med Surg. 2014;4(3):163-72.

81. Burn E, Liddle AD, Hamilton TW, Pai S, Pandit HG, Murray DW, et al. Choosing Between Unicompartmental and Total Knee Replacement: What Can Economic Evaluations Tell Us? A Systematic Review. Pharmacoecon Open. 2017;1(4):241-53.

82. Kurtz S, Mowat F, Ong K, Chan N, Lau E, Halpern M. Prevalence of primary and revision total hip and knee arthroplasty in the United States from 1990 through 2002. The Journal of bone and joint surgery American volume. 2005;87(7):1487-97.

83. Lum ZC, Shieh AK, Dorr LD. Why total knees fail-A modern perspective review. World J Orthop. 2018;9(4):60-4.

84. Seil R, Pape D. Causes of failure and etiology of painful primary total knee arthroplasty. Knee Surg Sports Traumatol Arthrosc. 2011;19(9):1418-32.

85. Signore A, Sconfienza LM, Borens O, Glaudemans A, Cassar-Pullicino V, Trampuz A, et al. Consensus document for the diagnosis of prosthetic joint infections: a joint paper by the EANM, EBJIS, and ESR (with ESCMID endorsement). European journal of nuclear medicine and molecular imaging. 2019;46(4):971-88.

86. Sofka CM, Potter HG, Figgie M, Laskin R. Magnetic resonance imaging of total knee arthroplasty. Clinical orthopaedics and related research. 2003(406):129-35.

87. Heyse TJ, Figiel J, Hähnlein U, Timmesfeld N, Schmitt J, Schofer MD, et al. MRI after unicondylar knee arthroplasty: The preserved compartments. Knee. 2012;19(6):923-6.

R

R

88. Moher D, Liberati A, Tetzlaff J, Altman DG. Preferred reporting items for systematic reviews and meta-analyses: the PRISMA statement. BMJ. 2009;339:b2535.

89. Potter HG, Foo LF. Magnetic Resonance Imaging of Joint Arthroplasty. Orthopedic Clinics. 2006;37(3):361-73.

90. Murakami AM, Hash TW, Hepinstall MS, Lyman S, Nestor BJ, Potter HG. MRI evaluation of rotational alignment and synovitis in patients with pain after total knee replacement. Journal of Bone and Joint Surgery - Series B. 2012;94 B(9):1209-15.

91. Panni AS, Ascione F, Rossini M, Braile A, Corona K, Vasso M, et al. Tibial internal rotation negatively affects clinical outcomes in total knee arthroplasty: a systematic review. Knee Surg Sports Traumatol Arthrosc. 2018;26(6):1636-44.

92. Kurosaka M, Yoshiya S, Mizuno K, Yamamoto T. Maximizing flexion after total knee arthroplasty: the need and the pitfalls. The Journal of arthroplasty. 2002;17(4 Suppl 1):59-62.

93. Lee KY, Slavinsky JP, Ries MD, Blumenkrantz G, Majumdar S. Magnetic resonance imaging of in vivo kinematics after total knee arthroplasty. Journal of Magnetic Resonance Imaging. 2005;21(2):172-8.

94. Prinsen CAC, Mokkink LB, Bouter LM, Alonso J, Patrick DL, de Vet HCW, et al. COSMIN guideline for systematic reviews of patient-reported outcome measures. Quality of life research : an international journal of quality of life aspects of treatment, care and rehabilitation. 2018;27(5):1147-57.

95. Koo TK, Li MY. A Guideline of Selecting and Reporting Intraclass Correlation Coefficients for Reliability Research. J Chiropr Med. 2016;15(2):155-63.

96. McHugh ML. Interrater reliability: the kappa statistic. Biochemia medica. 2012;22(3):276-82.

97. Whiting PF, Rutjes AW, Westwood ME, Mallett S, Deeks JJ, Reitsma JB, et al. QUADAS-2: a revised tool for the quality assessment of diagnostic accuracy studies. Annals of internal medicine. 2011;155(8):529-36.

98. Heyse TJ, Chong LR, Davis J, Boettner F, Haas SB, Potter HG. MRI analysis for rotation of total knee components. Knee. 2012;19(5):571-5.

99. Li AE, Sneag DB, Greditzer HG, Johnson CC, Miller TT, Potter HG. Total knee arthroplasty: Diagnostic accuracy of patterns of synovitis at MR imaging. Radiology. 2016;281(2):499-506.

100. Raphael B, Haims AH, Wu JS, Katz LD, White LM, Lynch K. MRI comparison of periprosthetic structures around zirconium knee prostheses and cobalt chrome prostheses. American Journal of Roentgenology. 2006;186(6):1771-7.

101. Heyse TJ, Chong LR, Davis J, Boettner F, Haas SB, Potter HG. MRI analysis of the component-bone interface after TKA. Knee. 2012;19(4):290-4.

102. Heyse TJ, Chong LR, Davis J, Haas SB, Figgie MP, Potter HG. MRI Diagnosis of Patellar Clunk Syndrome Following Total Knee Arthroplasty. HSS Journal. 2012;8(2):92-5.

103. Heyse TJ, Figiel J, Hähnlein U, Schmitt J, Timmesfeld N, Fuchs-Winkelmann S, et al. MRI after unicondylar knee arthroplasty: Rotational alignment of components. Archives of Orthopaedic and Trauma Surgery. 2013;133(11):1579-86.

104. Heyse TJ, Stiehl JB, Tibesku CO. Measuring tibial component rotation of TKA in MRI: What is reproducible? Knee. 2015;22(6):604-8.

105. Li AE, Johnson CC, Sneag DB, Koch CN, Fields K, Miller TT, et al. Frondlike synovitis on MRI and correlation with polyethylene surface damage of total knee arthroplasty. American Journal of Roentgenology. 2017;209(4):W231-W7.

106. Jawhar A, Reichert M, Kostrzewa M, Nittka M, Attenberger U, Roehl H, et al. Usefulness of slice encoding for metal artifact correction (SEMAC) technique for reducing metal artifacts after total knee arthroplasty. European Journal of Orthopaedic Surgery and Traumatology. 2018.

107. Malcherczyk D, Figiel J, Hähnlein U, Susanne FW, Efe T, Heyse TJ. Mri following uka?:The component-bone interface. Acta Orthopaedica Belgica. 2015;81(1):84-9.

108. Sgroi M, Faschingbauer M, Javaheripour-Otto K, Reichel H, Kappe T. Can rotational alignment of total knee arthroplasty be measured on MRI? Archives of Orthopaedic and Trauma Surgery. 2015;135(11):1589-94.

109. Meftah M, Potter HG, Gold S, Ranawat AS, Ranawat AS, Ranawat CS. Assessment of reactive synovitis in rotating-platform posterior-stabilized design: A 10-year prospective matched-pair mri study. Journal of Arthroplasty. 2013;28(9):1551-5.

110. Sutter R, Hodek R, Fucentese SF, Nittka M, Pfirrmann CW. Total knee arthroplasty MRI featuring slice-encoding for metal artifact correction: reduction of artifacts for STIR and proton density-weighted sequences. AJR American journal of roentgenology. 2013;201(6):1315-24.

111. Vessely MB, Frick MA, Oakes D, Wenger DE, Berry DJ. Magnetic Resonance Imaging With Metal Suppression for Evaluation of Periprosthetic Osteolysis After Total Knee Arthroplasty. Journal of Arthroplasty. 2006;21(6):826-31.

112. Park CN, Zuiderbaan HA, Chang A, Khamaisy S, Pearle AD, Ranawat AS. Role of magnetic resonance imaging in the diagnosis of the painful unicompartmental knee arthroplasty. Knee. 2015;22(4):341-6.

113. Minoda Y, Yoshida T, Sugimoto K, Baba S, Ikebuchi M, Nakamura H. Detection of small periprosthetic bone defects after total knee arthroplasty. Journal of Arthroplasty. 2014;29(12):2280-4.

114. Minoda Y, Yamamura K, Sugimoto K, Mizokawa S, Baba S, Nakamura H. Detection of bone defects around zirconium component after total knee arthroplasty. Knee. 2017;24(4):844-50.

115. Solomon LB, Stamenkov RB, MacDonald AJ, Yaikwavong N, Neale SD, Moss MJ, et al. Imaging periprosthetic osteolysis around total knee arthroplasties using a human cadaver model. Journal of Arthroplasty. 2012;27(6):1069-74.

116. Atkins BL, Athanasou N, Deeks JJ, Crook DW, Simpson H, Peto TE, et al. Prospective evaluation of criteria for microbiological diagnosis of prosthetic-joint infection at revision arthroplasty. The OSIRIS Collaborative Study Group. Journal of clinical microbiology. 1998;36(10):2932-9.

117. Pakos EE, Trikalinos TA, Fotopoulos AD, Ioannidis JP. Prosthesis infection: diagnosis after total joint arthroplasty with antigranulocyte scintigraphy with 99mTc-labeled monoclonal antibodies--a meta-analysis. Radiology. 2007;242(1):101-8.

118. Koff MF, Esposito C, Shah P, Miranda M, Baral E, Fields K, et al. MRI of THA Correlates With Implant Wear and Tissue Reactions: A Cross-sectional Study. Clinical orthopaedics and related research. 2019;477(1):159-74.

119. Higuera C, Parvizi J. 18 Causes and Diagnosis of Aseptic Loosening After Total Knee Replacement. 2015. p. 225-37.

R

120.   Victor J. Rotational alignment of the distal femur: a literature review. Orthopaedics & traumatology, surgery & research : OTSR. 2009;95(5):365-72.

121.   Thompson R, Novikov D, Cizmic Z, Feng JE, Fideler K, Sayeed Z, et al. Arthrofibrosis After Total Knee Arthroplasty: Pathophysiology, Diagnosis, and Management. The Orthopedic clinics of North America. 2019;50(3):269-79.

122.   Wendt RE, 3rd, Wilcott MR, 3rd, Nitz W, Murphy PH, Bryan RN. MR imaging of susceptibility-induced magnetic field inhomogeneities. Radiology. 1988;168(3):837-41.

123.   Koch KM, Lorbiecki JE, Hinks RS, King KF. A multispectral three-dimensional acquisition technique for imaging near metal implants. Magn Reson Med. 2009;61(2):381-90.

124.   Lu W, Pauly KB, Gold GE, Pauly JM, Hargreaves BA. SEMAC: Slice Encoding for Metal Artifact Correction in MRI. Magnetic resonance in medicine. 2009;62(1):66-76.

125.   Bourne RB, Chesworth BM, Davis AM, Mahomed NN, Charron KDJ. Patient Satisfaction after Total Knee Arthroplasty: Who is Satisfied and Who is Not? Clinical Orthopaedics and Related Research®. 2010;468(1):57-63.

126.   Scott CEH, Howie CR, MacDonald D, Biant LC. Predicting dissatisfaction following total knee replacement. The Journal of Bone and Joint Surgery British volume. 2010;92-B(9):1253-8.

127.   Khan M, Osman K, Green G, Haddad FS. The epidemiology of failure in total knee arthroplasty: avoiding your next revision. The bone & joint journal. 2016;98-b(1 Suppl A):105-12.

128.   (LROI) DAR. Online LROI annual report 2018. 2018.

129.   Prudhon JL, Caton JH, Aslanian T, Verdier R. How is patella height modified after total knee arthroplasty? Int Orthop. 2018;42(2):311-6.

130.   Hinckel BB, Gobbi RG, Filho EN, Pecora JR, Camanho GL, Rodrigues MB, et al. Are the osseous and tendinous-cartilaginous tibial tuberosity-trochlear groove distances the same on CT and MRI? Skeletal Radiol. 2015;44(8):1085-93.

131.   Berger RA, Rubash HE, Seel MJ, Thompson WH, Crossett LS. Determining the rotational alignment of the femoral component in total knee arthroplasty using the epicondylar axis. Clinical orthopaedics and related research. 1993(286):40-7.

132.   Schoettle PB, Zanetti M, Seifert B, Pfirrmann CW, Fucentese SF, Romero J. The tibial tuberosity-trochlear groove distance; a comparative study between CT and MRI scanning. Knee. 2006;13(1):26-31.

133.   Chhabra A, Subhawong TK, Carrino JA. A systematised MRI approach to evaluating the patellofemoral joint. Skeletal radiology. 2011;40(4):375-87.

134.   Macri EM, Crossley KM, d'Entremont AG, Hart HF, Forster BB, Wilson DR, et al. Patellofemoral and tibiofemoral alignment in a fully weight-bearing upright MR: Implementation and repeatability. Journal of magnetic resonance imaging : JMRI. 2018;47(3):841-7.

135.   Billingham SA, Whitehead AL, Julious SA. An audit of sample sizes for pilot and feasibility trials being undertaken in the United Kingdom registered in the United Kingdom Clinical Research Network database. BMC medical research methodology. 2013;13:104.

136.   Ali SA, Helmer R, Terk MR. Patella alta: lack of correlation between patellotrochlear cartilage congruence and commonly used patellar height ratios. AJR American journal of roentgenology. 2009;193(5):1361-6.

137.   Caton JH, Prudhon JL, Aslanian T, Verdier R. Patellar height assessment in total knee arthroplasty: a new method. Int Orthop. 2016;40(12):2527-31.

138.   Draper CE, Besier TF, Santos JM, Jennings F, Fredericson M, Gold GE, et al. Using real-time MRI to quantify altered joint kinematics in subjects with patellofemoral pain and to evaluate the effects of a patellar brace or sleeve on joint motion. J Orthop Res. 2009;27(5):571-7.

139.   Berger RA, Crossett LS, Jacobs JJ, Rubash HE. Malrotation causing patellofemoral complications after total knee arthroplasty. Clinical orthopaedics and related research. 1998(356):144-53.

140.   Carpenter RD, Brilhault J, Majumdar S, Ries MD. Magnetic resonance imaging of in vivo patellofemoral kinematics after total knee arthroplasty. Knee. 2009;16(5):332-6.

141.   Wünschel M, Leichtle U, Obloh C, Wülker N, Müller O. The effect of different quadriceps loading patterns on tibiofemoral joint kinematics and patellofemoral contact pressure during simulated partial weight-bearing knee flexion. Knee Surg Sports Traumatol Arthrosc. 2011;19(7):1099-106.

142.   Schröder FF, Verdonschot NJJ, ten Haken B, Peters A, Vochteloo AJH, Pakvis DFM, et al. Low-field magnetic resonance imaging offers potential for measuring tibial component migration. Journal of Experimental Orthopaedics. 2018;5(1).

143.   Valstar ER, Nelissen RGHH, Reiber JHC, Rozing PM. The use of Roentgen stereophotogrammetry to study micromotion of orthopaedic implants. ISPRS Journal of Photogrammetry and Remote Sensing. 2002;56(5-6):376-89.

144.   Kärrholm J, Gill RHS, Valstar ER. The history and future of radiostereometric analysis. Clinical orthopaedics and related research. 2006(448):10-21.

145.   Kärrholm J, Herberts P, Hultmark P, Malchau H, Nivbrant B, Thanner J. Radiostereometry of hip prostheses: Review of methodology and clinical results. Clinical orthopaedics and related research. 1997(344):94-110.

146.   Vrooman HA, Valstar ER, Brand GJ, Admiraal DR, Rozing PM, Reiber JHC. Fast and accurate automated measurements in digitized stereophotogrammetric radiographs. Journal of Biomechanics. 1998;31(5):491-8.

147.   Seehaus F, Olender GD, Kaptein BL, Ostermeier S, Hurschler C. Markerless Roentgen Stereophotogrammetric Analysis for in vivo implant migration measurement using three dimensional surface models to represent bone. Journal of Biomechanics. 2012;45(8):1540-5.

148.   Kaptein BL, Valstar ER, Stoel BC, Rozing PM, Reiber JHC. A new model-based RSA method validated using CAD models and models from reversed engineering. Journal of Biomechanics. 2003;36(6):873-82.

149.   Otten V, Maguire GQ, Jr., Noz ME, Zeleznik MP, Nilsson KG, Olivecrona H. Are CT Scans a Satisfactory Substitute for the Follow-Up of RSA Migration Studies of Uncemented Cups? A Comparison of RSA Double Examinations and CT Datasets of 46 Total Hip Arthroplasties. BioMed Research International. 2017;2017.

150.   de Bruin PW, Kaptein BL, Stoel BC, Reiber JHC, Rozing PM, Valstar ER. Image-based RSA: Roentgen stereophotogrammetric analysis based on 2D-3D image registration. Journal of Biomechanics. 2008;41(1):155-64.

151.   Moro-Oka TA, Hamai S, Miura H, Shimoto T, Higaki H, Fregly BJ, et al. Can magnetic resonance imaging-derived bone models be used for accurate motion measurement

with single-plane three-dimensional shape registration? Journal of Orthopaedic Research. 2007;25(7):867-72.

152. Doran SJ, Charles-Edwards L, Reinsberg SA, Leach MO. A complete distortion correction for MR images: I. Gradient warp correction. Physics in Medicine and Biology. 2005;50(7):1343-61.

153. Robertsson O, Annette WD, Lars L, Martin S. Annual Report 2017, Swedisch Knee Arthroplasty Register., 2017Th Edn. Lund. 2017.

154. Madsen EL, Blechinaer JC, Frank GR. Low-contrast focal lesion detectability phantom for 1H MR imaging. Medical physics. 1991;18(3):549-54.

155. ISO 16087:2013 Implants for surgery—roentgen stereophotogrammetric analysis for the assessment of migration of orthopaedic implants. 2013.

156. Petrén-mallmin m, Ericsson A, Rauschning W, Hemmingsson A. The effect of temperature on MR relaxation times and signal intensities for human tissues. MAGMA Magnetic Resonance Materials in Physics, Biology, and Medicine. 1993;1(3-4):176-84.

157. Vandemeulebroucke J, Deklerck R, Temmermans F, Van Gompel G, Buls N, Scheerlinck T, et al., editors. Automated estimation of hip prosthesis migration: A feasibility study. Proceedings of SPIE - The International Society for Optical Engineering; 2013.

158. Price AJ, Alvand A, Troelsen A, Katz JN, Hooper G, Gray A, et al. Knee replacement. Lancet. 2018;392(10158):1672-82.

159. Khodarahmi I, Fishman EK, Fritz J. Dedicated CT and MRI Techniques for the Evaluation of the Postoperative Knee. Semin Musculoskelet Radiol. 2018;22(4):444-56.

160. van der Bruggen W, Hirschmann MT, Strobel K, Kampen WU, Kuwert T, Gnanasegaran G, et al. SPECT/CT in the Postoperative Painful Knee. Semin Nucl Med. 2018;48(5):439-53.

161. Flierl MA, Sobh AH, Culp BM, Baker EA, Sporer SM. Evaluation of the Painful Total Knee Arthroplasty. The Journal of the American Academy of Orthopaedic Surgeons. 2019;27(20):743-51.

162. Rivière C, Iranpour F, Auvinet E, Howell S, Vendittoli PA, Cobb J, et al. Alignment options for total knee arthroplasty: A systematic review. Orthopaedics & Traumatology: Surgery & Research. 2017;103(7):1047-56.

163. Oussedik S, Abdel MP, Victor J, Pagnano MW, Haddad FS. Alignment in total knee arthroplasty. The bone & joint journal. 2020;102-B(3):276-9.

164. Hirschmann MT, Amsler F, Rasch H. Clinical value of SPECT/CT in the painful total knee arthroplasty (TKA): a prospective study in a consecutive series of 100 TKA. European journal of nuclear medicine and molecular imaging. 2015;42(12):1869-82.

165. Thiele K, Fussi J, Perka C, Pfitzner T. The Berlin diagnostic algorithm for painful knee TKA. Orthopade. 2016;45(1):38-46.

166. Hofmann S, Seitlinger G, Djahani O, Pietsch M. The painful knee after TKA: a diagnostic algorithm for failure analysis. Knee Surg Sports Traumatol Arthrosc. 2011;19(9):1442-52.

167. Sofka CM, Potter HG, Figgie M, Laskin R. Magnetic resonance imaging of total knee arthroplasty. Clinical orthopaedics and related research. 2003;406(406):129-35.

168. Schroder FF, Post CE, Wagenaar FBM, Verdonschot N, Huis In't Veld R. MRI as Diagnostic Modality for Analyzing the Problematic Knee Arthroplasty: A Systematic Review. Journal of magnetic resonance imaging : JMRI. 2020;51(2):446-58.

169. Campbell-Washburn AE, Ramasawmy R, Restivo MC, Bhattacharya I, Basar B, Herzka DA, et al. Opportunities in Interventional and Diagnostic Imaging by Using High-Performance Low-Field-Strength MRI. Radiology. 2019;293(2):384-93.

170. Berger RA, Crossett LS, Jacobs JJ, Rubash HE. Malrotation causing patellofemoral complications after total knee arthroplasty. Clinical orthopaedics and related research. 1998;356(356):144-53.

171. Murakami AM, Hash TW, Hepinstall MS, Lyman S, Nestor BJ, Potter HG. MRI evaluation of rotational alignment and synovitis in patients with pain after total knee replacement. J Bone Joint Surg Br. 2012;94(9):1209-15.

172. Meftah M, Potter HG, Gold S, Ranawat AS, Ranawat AS, Ranawat CS. Assessment of reactive synovitis in rotating-platform posterior-stabilized design: a 10-year prospective matched-pair MRI study. J Arthroplasty. 2013;28(9):1551-5.

173. Li AE, Johnson CC, Sneag DB, Koch CN, Fields K, Miller TT, et al. Frondlike Synovitis on MRI and Correlation With Polyethylene Surface Damage of Total Knee Arthroplasty. AJR Am J Roentgenol. 2017;209(4):W231-W7.

174. Scott CE, Howie CR, MacDonald D, Biant LC. Predicting dissatisfaction following total knee replacement: a prospective study of 1217 patients. J Bone Joint Surg Br. 2010;92(9):1253-8.

175. Fottner A, Woiczinski M, Schröder C, Schmidutz F, Weber P, Müller PE, et al. Impact of tibial baseplate malposition on kinematics, contact forces and ligament tensions in TKA: A numerical analysis. Journal of the Mechanical Behavior of Biomedical Materials. 2020;103:103564.

176. Ibrahim R, Samian Sd, Mazli MZ, Amrizal MN, Aljunid SM. Cost of Magnetic Resonance Imaging (MRI) and Computed Tomography (CT) scan in UKMMC. BMC Health Serv Res. 2012;12(Suppl 1):P11-P.

177. Jungmann PM, Agten CA, Pfirrmann CW, Sutter R. Advances in MRI around metal. Journal of magnetic resonance imaging : JMRI. 2017;46(4):972-91.

178. Jungmann PM, Ganter C, Schaeffeler CJ, Bauer JS, Baum T, Meier R, et al. View-Angle Tilting and Slice-Encoding Metal Artifact Correction for Artifact Reduction in MRI: Experimental Sequence Optimization for Orthopaedic Tumor Endoprostheses and Clinical Application. PLoS One. 2015;10(4):e0124922.

179. Jawhar A, Reichert M, Kostrzewa M, Nittka M, Attenberger U, Roehl H, et al. Usefulness of slice encoding for metal artifact correction (SEMAC) technique for reducing metal artifacts after total knee arthroplasty. Eur J Orthop Surg Traumatol. 2019;29(3):659-66.

180. Bendix T, Sorensen JS, Henriksson GA, Bolstad JE, Narvestad EK, Jensen TS. Lumbar modic changes-a comparison between findings at low- and high-field magnetic resonance imaging. Spine. 2012;37(20):1756-62.

181. Coffey AM, Truong ML, Chekmenev EY. Low-field MRI can be more sensitive than high-field MRI. Journal of magnetic resonance (San Diego, Calif : 1997). 2013;237:169-74.

182. Fritz J, Lurie B, Potter HG. MR Imaging of Knee Arthroplasty Implants. Radiographics. 2015;35(5):1483-501.

183. Talbot BS, Weinberg EP. MR Imaging with Metal-suppression Sequences for Evaluation of Total Joint Arthroplasty. Radiographics. 2016;36(1):209-25.

R

R

184. Fayad LM, Bluemke DA, Fishman EK. Musculoskeletal imaging with computed tomography and magnetic resonance imaging: when is computed tomography the study of choice? Current problems in diagnostic radiology. 2005;34(6):220-37.

185. Kasparek MF, Töpker M, Lazar M, Weber M, Kasparek M, Mang T, et al. Dual-energy CT and ceramic or titanium prostheses material reduce CT artifacts and provide superior image quality of total knee arthroplasty. Knee Surgery, Sports Traumatology, Arthroscopy. 2019;27(5):1552-61.

186. Lerch TD, Degonda C, Schmaranzer F, Todorski I, Cullmann-Bastian J, Zheng G, et al. Patient-Specific 3-D Magnetic Resonance Imaging-Based Dynamic Simulation of Hip Impingement and Range of Motion Can Replace 3-D Computed Tomography-Based Simulation for Patients With Femoroacetabular Impingement: Implications for Planning Open Hip Preservation Surgery and Hip Arthroscopy. The American journal of sports medicine. 2019;47(12):2966-77.

187. Ahn JM, El-Khoury GY. Role of magnetic resonance imaging in musculoskeletal trauma. Topics in magnetic resonance imaging : TMRI. 2007;18(3):155-68.

188. Bruno F, Arrigoni F, Palumbo P, Natella R, Splendiani A, Di Cesare E, et al. Weight-bearing MR Imaging of Knee, Ankle and Foot. Semin Musculoskelet Radiol. 2019;23(06):594-602.

189. Ghazinoor S, Crues JV, 3rd. Low field MRI: a review of the literature and our experience in upper extremity imaging. Clinics in sports medicine. 2006;25(3):591-606, viii.

190. Leigheb M, Guzzardi G, Barini M, Abruzzese M, Riva S, Pasche A, et al. Role of low field MRI in detecting knee lesions. Acta Biomed. 2018;90(1-s):116-22.

191. Bruno F, Smaldone F, Varrassi M, Arrigoni F, Barile A, Di Cesare E, et al. MRI findings in lumbar spine following O2–O3 chemiodiscolysis: A long-term follow-up. Interventional Neuroradiology. 2017;23(4):444-50.

192. Splendiani A, Perri M, Grattacaso G, Di Tunno V, Marsecano C, Panebianco L, et al. Magnetic resonance imaging (MRI) of the lumbar spine with dedicated G-scan machine in the upright position: a retrospective study and our experience in 10 years with 4305 patients. La Radiologia medica. 2016;121(1):38-44.

193. Splendiani A, Ferrari F, Barile A, Masciocchi C, Gallucci M. Occult neural foraminal stenosis caused by association between disc degeneration and facet joint osteoarthritis: demonstration with dedicated upright MRI system. La Radiologia medica. 2014;119(3):164-74.

194. Kleeblad LJ, Zuiderbaan HA, Burge AJ, Amirtharaj MJ, Potter HG, Pearle AD. MRI Findings at the Bone-Component Interface in Symptomatic Unicompartmental Knee Arthroplasty and the Relationship to Radiographic Findings. HSS J. 2018;14(3):286-93.

195. Jerban S, Chang EY, Du J. Magnetic resonance imaging (MRI) studies of knee joint under mechanical loading: Review. Magnetic resonance imaging. 2020;65:27-36.

196. Stehling C, Souza RB, Graverand M-PHL, Wyman BT, Li X, Majumdar S, et al. Loading of the knee during 3.0 T MRI is associated with significantly increased medial meniscus extrusion in mild and moderate osteoarthritis. European Journal of Radiology. 2012;81(8):1839-45.

197. Patel R, Eltgroth M, Souza R, Zhang CA, Majumdar S, Link TM, et al. Loaded versus unloaded magnetic resonance imaging (MRI) of the knee: Effect on meniscus extrusion in healthy volunteers and patients with osteoarthritis. Eur J Radiol Open. 2016;3:100-7.

198. Calixto NE, Kumar D, Subburaj K, Singh J, Schooler J, Nardo L, et al. Zonal differences in meniscus MR relaxation times in response to in vivo static loading in knee osteoarthritis. Journal of Orthopaedic Research. 2016;34(2):249-61.

199. Burge AJ, Konin GP, Berkowitz JL, Lin B, Koff MF, Potter HG. What is the Diagnostic Accuracy of MRI for Component Loosening in THA? Clinical orthopaedics and related research. 2019;477(9):2085-94.

200. Nwawka OK, Konin GP, Sneag DB, Gulotta LV, Potter HG. Magnetic resonance imaging of shoulder arthroplasty: review article. HSS J. 2014;10(3):213-24.

201. Simonetti OP, Ahmad R. Low-Field Cardiac Magnetic Resonance Imaging: A Compelling Case for Cardiac Magnetic Resonance's Future. Circ Cardiovasc Imaging. 2017;10(6):e005446.

202. Spieler B, Samuels SE, Llorente R, Yechieli R, Ford JC, Mellon EA. Advantages of Radiation Therapy Simulation with 0.35 Tesla Magnetic Resonance Imaging for Stereotactic Ablation of Spinal Metastases. Practical radiation oncology. 2020;10(5):339-44.

203. Grist TM. The Next Chapter in MRI: Back to the Future? Radiology. 2019;293(2):394-5.

204. Navarro M, Michiardi A, Castaño O, Planell JA. Biomaterials in orthopaedics. J R Soc Interface. 2008;5(27):1137-58.

205. de Ruiter L, Janssen D, Briscoe A, Verdonschot N. Biomechanical compatibility of a peek-optima femoral total knee arthroplasty implant design during gait. Orthopaedic Proceedings. 2016;98-B(SUPP_3):140-.

206. de Ruiter L, Janssen D, Briscoe A, Verdonschot N. A preclinical numerical assessment of a polyetheretherketone femoral component in total knee arthroplasty during gait. Journal of experimental orthopaedics. 2017;4(1):3-.

207. Meng X, Du Z, Wang Y. Feasibility of Magnetic Resonance Imaging Monitoring of Postoperative Total Knee Arthroplasty without Metal Artifacts: A Preliminary Study of a Novel Implant Model. BioMed research international. 2018;2018:8194670-.

208. Rankin KE, Dickinson AS, Briscoe A, Browne M. Does a PEEK Femoral TKA Implant Preserve Intact Femoral Surface Strains Compared With CoCr? A Preliminary Laboratory Study. Clinical orthopaedics and related research. 2016;474(11):2405-13.

209. LROI. Rapportage Landelijke Registratie Orthopedische Implantaten. 2019.

210. Health~Holland. Kennis- en Innovatieagenda 2020-2023 Gezondheid & Zorg, Vitaal functionerende burgers in een gezonder economie. 2019.

Summary

In orthopaedic surgery, often orthopaedic hardware (e.g. suture anchors, prosthesis, osteosynthesis material) made of metal alloys is implanted. Before the implantation of orthopaedic hardware, magnetic resonance imaging (MRI) is the imaging modality of choice for imaging musculoskeletal structures. After implantation of orthopaedic hardware, MRI is disturbed by susceptibility artefacts due to the metal implants, which reduce the diagnostic value. Lowering the main magnetic field should reduce the size and prominence of susceptibility artefacts.

In clinical practice MRI is performed in supine condition; however, given that during the day our limbs are in weight-bearing position, it seems relevant to image them in similar weight-bearing conditions. Low-field MRI offers the possibility for imaging in upright weight-bearing position.

Therefore, this thesis first investigates the diagnostic properties of MRI near orthopaedic hardware. Second, it explores the added value of weight-bearing low-field MRI after the most frequently performed joint procedure, the total knee arthroplasty (TKA).

In **chapter 2** the diagnostic properties of MRI (1.5T) after rotator cuff tendon surgery with a titanium suture anchor were evaluated. MRI scans of twenty patients, who underwent revision surgery of the rotator cuff as a result of a clinically suspected retear, were retrospectively analysed by four specialized shoulder surgeons and compared with intra-operative findings (gold standard). In 64% of the patients studied an accurate diagnosis with MRI of the rotator cuff retear was possible.

As stated, the most frequently performed total joint procedure is the TKA, although approximately 20% of TKA patients remain dissatisfied postoperatively. The most common causes of complaint are infection, loosening and wear, instability, malalignment, arthrofibrosis, and patellofemoral problems.

Chapter 3 provides a systematic review which critically appraises, summarizes, and compares the literature on the diagnostic properties of MRI (1.5T) to identify the causes of complaint that are directly related to implant failure of TKA or unicompartmental knee arthroplasty (UKA). Whereas studies regarding the diagnosis of instability, arthrofibrosis or patellofemoral complaints using MRI are limited and inconclusive, this review revealed that MRI can be used with reproducible and accurate results for diagnosing infection, loosening and wear, and malalignment after knee arthroplasty.

Chapter 4 presents a pilot study that evaluates the reproducibility of measurements of patellofemoral and component alignment parameters after TKA using low-field MRI (0.25T). Additionally, the study investigates whether there were differences in patellofemoral parameters across supine and weight-bearing conditions. Eight patients without complaints after primary TKA were scanned on low-field MRI in supine and weight-bearing conditions. Patellofemoral parameters and rotational component alignment parameters could be performed with good to excellent reproducibility. The differences in patellofemoral parameters between weight-bearing and supine condition were relatively small. The ability to take reproducible measurements after TKA using low-field WB MRI illustrates the potential of low-field MRI for evaluating post-TKA patients with (patellofemoral) complaints.

Chapter 5 presents a proof-of-concept study conducted to evaluate low-field MRI as an alternative to Roentgen stereophotogrammetric analysis (RSA). RSA is used to measure early prosthetic migration and to predict pending implant failure. However, the need for perioperatively placed tantalum markers and the fact that patients are exposed to additional radiation during longitudinal RSA studies limit the clinical applications. The disadvantages of RSA lead to this feasibility study in which the use of low-field MRI to measure the precision of zero motion is evaluated. Results show that the precision of zero motion for low-field MRI was between 0.584 mm and 1.974 mm for translation and 0.884° and 3.774° for rotation. Currently, these low-field MRI results are not as precise as today's gold standard (marker-based RSA).

A feasibility study which explores the diagnostic value of low-field MRI for pathologies associated with the problematic TKA is presented in **Chapter 6**. Prospectively, eight patients with problematic TKAs were scanned on low-field MRI in weight-bearing and supine conditions. Scans were analysed for pathologies associated with a problematic TKA and compared to those obtained with CT, the diagnosis based on the clinical work-up, and findings during revision surgery. In all cases MRI observations were in line with the diagnosis based on CT. In the majority (six out of eight) of the cases, MRI observations were comparable with the clinical diagnosis. In four out of six cases, MRI observations of malalignment, loosening, and patellofemoral arthrosis were comparable with the findings during surgery. Although differences between supine and weight-bearing MRI images did not yield clinically relevant information, the results of the study suggest that low-field MRI is a feasible method of assessing malalignment, loosening and patellofemoral arthrosis of the problematic TKA.

When using MRI after arthroplasty, a trade-off is required between metal artefact reducing capacities and image quality. Low-field MRI (0.25T) results in fewer metal artefacts and lower image quality compared with high-field MRI (1.5T). However, technological developments like metal artefact reducing sequences (MARS) continued to improve on high-field MRI over the years. Therefore, in **Chapter 7** the performance of low-field and high-field MRI after TKA with and without MARS was compared in two case studies. Results suggest that low-field MRI was less hampered by metal artefacts compared to high-field MRI without MARS. When MARS sequences were used, high-field MRI seemed to outperform low-field MRI, confirming the value of the ongoing technological developments to improve high-field MRI over the years.

Chapter 8 presents a general discussion on the main findings of the studies described in this thesis, proposes future directions and explores the implications for clinical practice. It is concluded that MRI is a useful imaging modality after surgery in which orthopaedic hardware (titanium suture anchors, TKA, or other) is implanted. Although the added value of weight-bearing MRI could not be proven, high-field MRI performs as well as low-field MRI in imaging several pathologies and can be considered as an addition to the current diagnostic arsenal. High-field MRI excels in image quality, low-field in usability at low cost.

Samenvatting

Tijdens orthopedische ingrepen wordt er vaak metalen hardware geïmplanteerd zoals ankers, protheses of osteosynthese materialen. Echter, als een patiënt, na een operatie waarbij metalen hardware geïmplanteerd werd, klachten ontwikkelt, wordt de MRI door de metalen hardware verstoord, wat de diagnostiek bemoeilijkt. In theorie zouden de verstoringen door metalen hardware kleiner moeten worden als het magnetisch veld van de MRI verlaagd wordt.

In de klinische praktijk wordt een MRI scan in liggende positie gemaakt, terwijl in veel gevallen een staande positie meer relevant zou zijn om pathologieën van het musculoskeletale systeem af te beelden. Met laagveld MRI is het mogelijk om scans in staande positie te maken, dit is mogelijk relevant om de oorzaak van klachten, die kunnen ontstaan na het implanteren van metalen hardware, in normaliter belaste delen, te diagnosticeren.

In dit proefschrift worden eerst de diagnostische eigenschappen van MRI in de nabijheid van orthopedische metalen hardware onderzocht. Vervolgens wordt verkend of laagveld MRI in belaste positie van meerwaarde is na een totale knie prothese (TKP).

In **hoofdstuk 2** wordt de diagnostische waarde van 1.5T MRI onderzocht bij 20 patiënten die klachten hebben na een rotator cuff repair, een ingreep waarbij een metalen anker ter fixatie wordt gebruikt. Retrospectief zijn 20 MRI-scans van deze patiënten beoordeeld door vier gespecialiseerde schouderchirurgen. Bevindingen op basis van de beelden zijn vergeleken met de bevindingen tijdens revisiechirurgie (rotator cuff re-repair). Het was in 36% van de gevallen niet mogelijk om op basis van de MRI een cuff re-ruptuur te diagnosticeren.

De TKP behoort tot één van de meest geïmplanteerde orthopedische hardware. Echter na een TKP is 20% van de patiënten ontevreden. De meest voorkomende onderliggende oorzaken van ontevredenheid zijn infectie, loslating en slijtage, instabiliteit, malpositie, arthrofibrose en patellofemorale klachten. In **hoofdstuk 3** worden de diagnostische eigenschappen van 1.5T MRI om de oorzaak van een falende TKP of unilaterale knie prothese te identificeren systematisch beschouwd. De bevindingen ondersteunen dat 1.5T MRI reproduceerbare en accurate resultaten geeft om infectie, loslating, slijtage en malpositie te diagnosticeren. Beperkter en minder doorslaggevend zijn de onderzoeken die 1.5T MRI inzetten om instabiliteit, arthrofibrose en patellofemorale klachten te diagnosticeren.

In **hoofdstuk 4** werd de reproduceerbaarheid van patellofemorale en malpositie metingen na TKP onderzocht. Dit zijn metingen die, wanneer afwijkend, worden geassocieerd met een problematische TKP. Hiervoor werden 8 patiënten zonder klachten na TKP gescand op laagveld MRI (0,25T). Ook werd onderzocht of er verschillen te vinden waren in patellofemorale waarden tussen metingen in staande en liggende positie. De verschillen in patellofemorale waardes tussen staande en liggende positie waren klein. Wel konden de metingen met een excellente reproduceerbaarheid worden uitgevoerd. Dit illustreert dat laagveld MRI potentie biedt om de knie na TKP te evalueren.

Loslating van de prothese is een mogelijke oorzaak van klachten na TKP. Roentgen stereophotogrammetry (RSA) is de gouden standaard om vroegtijdige loslating van een prothese te meten. RSA heeft enkele nadelen zoals de noodzaak voor peroperatief geplaatste markers en het feit dat patiënten gedurende de follow-up metingen blootgesteld worden aan extra röntgenstraling. De nadelen van RSA hebben geleid tot de evaluatie van laagveld MRI als mogelijk alternatief. In **hoofdstuk 5** wordt de precisie van laagveld MRI om de positie van de prothese te meten bepaald. Deze precisie was tussen de 0,584 en 1,974 mm voor translatie en tussen de 0,884 en 3,774 graden voor rotatie. Op basis van deze bevindingen is laagveld MRI nog niet zo precies als RSA.

In **hoofdstuk 6** wordt in een haalbaarheidsstudie de waarde van laagveld MRI om verschillende pathologieën na een TKP te diagnosticeren verkend. In deze prospectieve studie werden 8 patiënten met een problematische TKP geïncludeerd en gescand in liggende en staande positie met laagveld MRI. De scans werden geëvalueerd op de aanwezigheid van pathologieën, die geassocieerd worden met de problematische TKP en de bevindingen werden vergeleken met de bevindingen op basis van CT, de klinische diagnose en revisiechirurgie. In alle gevallen waren de MRI bevindingen in overeenstemming met de diagnose gebaseerd op CT. In de meerderheid van de cases (6 uit 8) waren de MRI bevindingen gelijk met de klinische diagnose. In vier van de zes casussen waren de MRI bevindingen in overeenstemming met de operatieve bevindingen. Alhoewel de staande MRI geen extra diagnostische informatie gaf, suggereren de resultaten van deze studie wel dat laagveld MRI in staat is om malpositie, loslating en patellofemorale artrose als oorzaken van een problematische knie aan te wijzen.

Wanneer bij patiënten met een TKP als beeldvormende modaliteit MRI wordt ingezet moet er een afweging gemaakt worden tussen het belang van voldoende beeldkwaliteit en metaal artefact reductie. Laagveld MRI (0,25T) geeft een kleiner artefact, maar ook een mindere beeldkwaliteit, vergeleken met hoogveld MRI (1,5T). De afgelopen jaren zijn metaal artefact reducerende

sequenties (MARS) geïntroduceerd. Hierdoor is de hinder, veroorzaakt door metaal artefact op hoogveld MRI, verminderd.

Om deze afweging te kunnen maken worden in twee case studies in **hoofdstuk 7** de prestaties van laagveld en hoogveld MRI (+MARS) met elkaar vergeleken. De resultaten van deze cases suggereren dat laagveld MRI minder verstoord wordt door metaal artefacten dan hoogveld MRI zonder MARS. Echter wanneer MARS sequenties gebruikt werden, waren de hoogveld MRI beelden substantieel beter dan laagveld MRI. Dit onderschrijft de waarde van de technologische ontwikkelingen die de afgelopen jaren hoogveld MRI hebben verbeterd.

Tot slot worden in **hoofdstuk 8** de belangrijkste bevindingen uit deze thesis bediscussieerd en worden implicaties voor de klinische praktijk en richtingen voor vervolgonderzoek gegeven. Er wordt geconcludeerd dat MRI een nuttige beeldvormende modaliteit na chirurgie is, waarbij metalen ankers, prothese of osteosynthese materiaal zijn geïmplanteerd. De meerwaarde van staande MRI kon op basis van deze thesis nog niet worden aangetoond. Wel kan gesteld worden dat laag- en hoogveld MRI beiden in staat zijn om diverse pathologieën na een TKP te diagnosticeren, waarbij hoogveld MRI excelleert in beeld kwaliteit en laagveld MRI in lage kosten en bruikbaarheid.

Dankwoord

Het starten, uitvoeren en afronden van het promotietraject was niet mogelijk geweest zonder de hulp van velen. Ik wil iedereen die hieraan heeft bijgedragen hartelijk bedanken, maar een aantal mensen wil ik graag in het bijzonder noemen te beginnen met mijn promotor en copromotor.

Professor dr.ir. N. Verdonschot, beste Nico, bedankt! Dank voor het vertrouwen, ik had mij geen betere promotor kunnen wensen. Tijdens de maandelijkse gesprekken wist je altijd snel de onderwerpen te doorgronden en leverde je waardevolle input. Ik waardeer het enorm dat er altijd, ondanks je drukke schema, tijd voor mij werd vrijgemaakt.

Dr. M.H.A. Huis int' Veld, beste Rianne, bedankt! Dank voor je geloof in mij, de student die een onderzoeksstage liep bij het OCON. Mede door jouw inzet kreeg ik de mogelijkheid om bij OCON aan het werk te gaan en simultaan met mijn promotieonderzoek te starten. Jouw onderzoekvaardigheden en kritische blik hebben dit proefschrift naar een hoger niveau gebracht. Ik heb de afgelopen jaren ontzettend veel van je geleerd.

De onderzoeken, omschreven in de hoofdstukken die u allen in dit proefschrift heeft kunnen lezen, zijn in meerdere fases verricht. Het eerste deel startte al in maart 2015 tijdens mijn 10 weekse stage bij het OCON. Wie mij op dat moment had verteld dat dit zou gaan bijdragen aan mijn latere proefschrift, had ik niet geloofd.

Prof. dr. ir. B ten Haken wist dat vast op dat moment ook nog niet. Beste Bennie, dankjewel voor je bijdrage aan de eerste hoofdstukken van dit proefschrift. Jij hebt mij geënthousiasmeerd voor het onderwerp (laagveld)MRI. Eerst tijdens het onderwijs wat jij gaf gedurende de opleiding TG en later tijdens de stages. Bedankt dat ik mee mocht naar de Dierenkliniek den Ham waar de eerste preliminaire studieresultaten werden verzameld op de veterinaire laagveld MRI. Alhoewel je eigen interesse meer ligt bij de magnetische detectie, nam je altijd de tijd om mij verder te helpen met het laagveld onderzoek.

Dr. ir. F.F.J.Simonis, beste Frank, waar je collega Bennie in de startfase betrokken was bij het onderzoek op de laagveld MRI kwam jij in 2016 het MRI team op de UT versterken. Vanaf dat moment heb jij mij veel geleerd over MRI en was jij altijd

bereid nog een keer uit te leggen hoe die ene setting technisch gezien ook al weer werkte en niet te vergeten hielp jij met het opstellen van de optimale studie protocollen. Vele uren heb jij mij geholpen met de instellingen maar ook het scannen van proefpersonen en patiënten op de laagveld MRI, waarvoor bedankt! Ook nu sta jij nog elke keer klaar om die ene MRI vraag te beantwoorden.

Beste leden van de promotiecommissie, Prof. dr. ir. C.H. Slump, Prof. dr. ir. G.J. Verkerke , Prof. dr. L. Geris, dr. J.M.H. Smolders, dr. A.J.H. Vochteloo, graag wil ik jullie bedanken voor dat jullie zitting hebben willen nemen in de promotiecommissie en voor de tijd die jullie hebben genomen om dit proefschrift te lezen en beoordelen.

Ook wil ik graag alle collega's van het OCON bedanken. Velen hebben op hun eigen manier bijgedragen aan het in dit proefschrift beschreven onderzoek of aan mijn klinische en/of persoonlijke ontwikkeling. In het bijzonder wil ik Frank-Christiaan bedanken, als lid van de knie-revisie-unit deelde jij je kennis t.a.v. de problematische knie. Je leerde me tijdens de klinische fellow hoe een patiënt met knieproblemen te diagnosticeren, dankjewel. Anne Vochteloo, tijdens mijn eerste 10 weekse stage bij OCON was jij mijn begeleider, zoals later ook voor mijn klinische fellow mijn opleider. Klinisch en wetenschappelijk is de knie is niet helemaal jouw onderwerp, maar dat gaan we in de toekomst, zowel klinisch als wetenschappelijk, met 3D in de hand-pols helemaal goedmaken.
OCON, bedankt voor alle steun en mogelijkheden, op naar een mooie toekomst samen!

Graag wil ik ook de afdeling radiologie MRON/ZGT bedanken. De MRI laboranten die altijd wel even een fantoom wilden scannen of mee wilden denken hoe een sequentie vorm te geven. Ook Sjoerd van Raak musculoskeletaal radioloog wil ik bedanken. Zowel betrokken bij de klinische fellow als het onderzoek. Jij leerde mij hoe beelden van de knie en schouder te beoordelen, maar ook was jij t.a.v. de hoogveld MRI een goede gesprekspartner.

Mijn paranimfen Anoek en oud OCON collega Corine. Dank dat jullie vandaag mijn paranimfen willen zijn tijdens de verdediging van mijn proefschrift. Corine je hebt een grote rol in mijn promotietraject gespeeld. Doordat jij als onderzoeker op het MRIpro project kwam werken raakte het onderzoek in een stroomversnelling in plaats van dat het stil kwam te liggen tijdens mijn klinische fellowship. Als collega's konden we het goed met elkaar vinden. Gezellig avondjes met de collega's uit eten, samen op congres, etc. Dank voor alle leuke momenten.

Anoek, wij kennen elkaar al erg lang. Zoals jij mij vaker hebt geholpen met je creativiteit(Ik kan mij nog heel wat teken en handvaardigheid opdrachten herinneren), schoot jij mij ook deze keer te hulp. Het resultaat mag er wezen. Dank voor de hulp bij dit mooie proefschrift, maar het voornaamste, dank dat je al jaren zo'n geweldige vriendin bent!

Lieve vrienden en familie, jullie boden de afgelopen jaren een luisterend oor en zorgden ervoor dat, heel verstandig, niet elke zondag alleen aan paarden en de PhD werd gespendeerd. Etentjes, weekendjesweg (wintersport)vakanties, en meer. Jullie zorg(d)en voor de ontspanning, jullie zijn fantastisch!

Lieve pap en mam, bedankt voor de onvoorwaardelijke steun. Jullie hebben nooit getwijfeld aan alles wat ik weer eens tegelijkertijd wilde doen. Jullie hebben mij altijd gesteund en gemotiveerd het beste uit mijzelf te halen. Elk probleem groot of klein kan besproken worden, de oplossing of hulp staat klaar.

Als laatst, maar wel het allerbelangrijkst. Lieve Steven, enthousiast en met humor wist je aan de PhD uurtjes thuis altijd een vrolijke draai te geven. Je was en bent er voor mij op elk moment.

Wierden, december 2020

List of author's publications & conference contributions.

Publications

Full papers

Schröder FF, Post CE, van Raak SM, Simonis FFJ, Wagenaar FBM, Huis In't Veld MHA, Verdonschot N. The diagnostic potential of low-field MRI in problematic total knee arthroplasties - a feasibility study. J Exp Orthop. 2020 Jul 31;7(1):59. *(this thesis Ch6)*

Schröder FF, Post CE, Wagenaar FBM, Verdonschot N, Huis In't Veld MHA. MRI as Diagnostic Modality for Analyzing the Problematic Knee Arthroplasty: A Systematic Review. J Magn Reson Imaging. 2019 Jul;51(2):446-458. *(this thesis Ch3)*

Schröder FF, Huis In't Veld R, den Otter LA, van Raak SM, Ten Haken B, Vochteloo AJH. Metal artefacts severely hamper magnetic resonance imaging of the rotator cuff tendons after rotator cuff repair with titanium suture anchors. Shoulder Elbow. 2018 Apr;10(2):107-113. *(this thesis Ch2)*

Schröder FF, Verdonschot NJJ, Ten Haken B, Peters A, Vochteloo AJH, Pakvis DFM, Huis In't Veld R. Low-field magnetic resonance imaging offers potential for measuring tibial component migration. J Exp Orthop. 2018 Jan 12;5(1):4. *(this thesis Ch5)*

Schröder FF, de Graaff F, Bouman DE, Brusse-Keizer M, Slump KH, Klaase JM. The Preoperative CT-Scan Can Help to Predict Postoperative Complications after Pancreatoduodenectomy. Biomed Res Int. 2015;824525.

Published abstracts

Schröder FF, Post CE, Simonis FFJ, Wagenaar FBM, Huis In't Veld R, Verdonschot N. Weight-bearing low field MRI after total knee arthroplasty in patient with and without complaints. orthopaedic Proceedings. 2020;102-b(supp_2):99-99.

Schröder FF, Huis In't Veld R, Simonis FFJ, Post C, Vochteloo AJH, Verdonschot N. The precision of low-field MRIto measure prosthetic migration: a cadaver study. Orthopaedic Proceedings. 2019;101-b(supp_5):18-18.

Post C, Schroder FF, Simonis FFJ, Peters A, Huis In't Veld R, Verdonschot N. A guide to diagnose failed total knee arthroplasty: a case study comparing low-field and high-field MRI. Orthopaedic Proceedings. 2019;101-b(supp_5):135-135. *(this thesis Ch7)*

Conference contributions

<u>Schröder FF</u>, Post CE, Simonis FFJ, Wagenaar FBM, Huis In't Veld R, Verdonschot N. Weight-bearing low field MRI after total knee arthroplasty in patient with and without complaints. 27th Annual Meeting of EORS, October 2-5, Maastricht, Netherlands, 2019.

<u>Schröder FF</u>, Post CE, Simonis FFJ, Wagenaar FBM, Huis In't Veld R, Verdonschot N. Weight-bearing low field MRI after total knee arthroplasty in patient with and without complaints. International Society for Technology in Arthroplasty conference, Toronto, Canada, October 2-5, 2019. Awarded with **Young investigator scholarship**.

<u>Schröder FF</u>, Huis In't Veld R, Simonis FFJ, Post C, Vochteloo AJH, Verdonschot N. The precision of low-field mri to measure prosthetic migration: a cadaver study. International Society for Technology in Arthroplasty conference, London, United Kingdom, October 10-13, 2018. Awarded with **Young investigator scholarship.**

Post C, <u>Schroder FF</u>, Simonis FFJ, Peters A, Huis In't Veld R, Verdonschot N. A guide to diagnose failed total knee arthroplasty: a case study comparing low-field and high-field mri. International Society for Technology in Arthroplasty conference, London, United Kingdom, October 10-13, 2018.

<u>Schröder FF</u>, Verdonschot NJJ, Ten Haken B, Peters A, Vochteloo AJH, Pakvis DFM, Huis In't Veld R. A novel approach to measure tibial component migration by low field markerless magnetic resonance imaging. ZGT wetenschapsdag, Almelo, The Netherlands, October 11, 2017. **Best poster award.**

<u>Schröder FF,</u> Huis In't Veld R, van Raak SM, Ten Haken B, Vochteloo AJH. Metal artefacts hamper magnetic resonance imaging of the rotator cuff tendons after rotator cuff repair with titanium suture anchors. 27th SECEC-ESSE, September 13-16, Berlin, Germany, 2017.

<u>Schröder FF</u>, Simonis FFJ, Huis in't Veld R, Pakvis DFM, Peters A, Vochteloo, Ten Haken B. A novel approach to measure tibial component migration by low field markerless magnetic resonance imaging. ISMRM 25th Annual Meeting, April 22-27, Honolulu,HI,USA, 2017.

<u>Schröder FF</u>, Simonis FFJ, Huis in't Veld R, Pakvis DFM, Peters A, Vochteloo, Ten Haken B. A novel approach to measure tibial component migration by low field markerless magnetic resonance imaging. ISMRM Benelux Chapter, 9th annual meeting, January 20, Tilburg, The Netherlands, 2017.

<u>Schröder FF</u>, ten Haken B, Verdonschot NJJ, Pakvis DFM, Peters A, Vochteloo AJH, Huis In't Veld R. Laagveld MRI is een potentieel alternatief voor Roentgen stereophotogrammetry. NOV Najaarscongres, Velthoven, The Netherlands, October 12-13, 2016.

<u>Schröder FF</u>, Huis In't Veld R, den Otter LA, van Raak SM, Ten Haken B, Vochteloo AJH. Metaalartefacten verstoren MRI beelden bij diagnostiek van re-rupturen na een cuffrepair; is laagveld MRI de toekomst? ZGT wetenschapsdag, Almelo, The Netherlands, October 11, 2016.

<u>Schröder FF</u>, de Graaff F, Bouman DE, Brusse-Keizer M, Slump CH, Klaase JM, De preoperatieve CT-scan is behulpzaam bij het voorspellen van postoperatieve complicaties na pancreatoduodenectomie. NvVH chirurgen dagen, May 28-30, Velthoven, The Netherlands, 2015.

<u>Schröder FF</u>, de Graaff F, Bouman DE, Brusse-Keizer M, Slump CH, Klaase JM, The preoperative CT-scan can help to predict postoperative complications after pancreatoduodenectomy. ASGBI 2015 International Surgical Congress, April 22-24, Manchester, United Kingdom, 2015.

P

Curriculum Vitae

Femke Schröder was born in Wierden on 30 December 1991. After finishing high school (Pius-X college, Almelo), she began studying Technical Medicine at the University of Twente, Enschede in 2010. During her studies, in 2015, she undertook a clinical and research internship at OCON centre for orthopaedic surgery in Hengelo. The foundations of her PhD were laid here. She graduated with a master's degree in Technical Medicine in 2016, after which she started working as a technical physician at OCON and partly continued her research. In 2017 she got the opportunity to start with a fellowship for technical physicians, a clinical specialisation programme which educates clinical professionals dedicated to innovating and improving care within orthopaedic surgery. After finishing her fellowship in 2019, she worked as specialised technical physician at OCON, with a focus on patient-specific orthopaedic surgery and image-guided interventions. Since mid-2020 she has combined this work with her function as coordinator external collaboration with hospitals at the Technical Medical Centre in Enschede.

C